MCR-76-11
Contract NAS8-30690

Final
Report

February 1976

Experimental Study Of Transient Liquid Motion In Orbiting Spacecraft

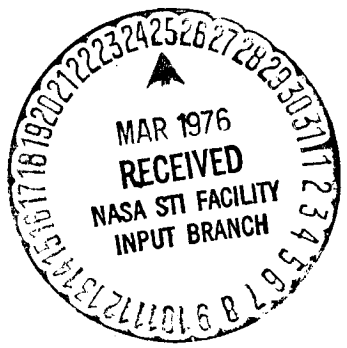

MARTIN MARIETTA

NAS8-30690 February 1976

EXPERIMENTAL STUDY OF TRANSIENT LIQUID MOTION IN ORBITING SPACECRAFT

Authors :

Robert L. Berry
James R. Tegart

MCR-76-11

Approved by:

A. D. Devers
Program Manager

Prepared for:

National Aeronautics and Space Administration
George C. Marshall Space Flight Center
Huntsville, Alabama 35812

MARTIN MARIETTA CORPORATION
Denver Division
Denver, Colorado 80201

FOREWORD

This report, prepared by the Martin Marietta Corporation, Denver Division, under Contract NAS8-30690, presents the results of an analytical and experimental study of transient liquid motion similar to that encountered in orbiting spacecraft. The study was performed from March 1974 to February 1976 and was administered by the National Aeronautics and Space Administration, George C. Marshall Space Flight Center, Huntsville, Alabama, under the direction of Mr. Frank Bugg.

Some of the results of this study were published in an interim report, MCR-75-4, February 1975. In addition, two 16 mm high speed movies have been generated which document the test results.

ABSTRACT

This report presents the results of a two year study of transient liquid motion such as that which will be experienced during orbital maneuvers by Space Tug. A test program was conducted in the Martin Marietta Drop Tower Test Facility involving forty-five drops. Biaxial, low-g accelerations were applied to instrumented, model propellant tanks during free-fall testing, and forces exerted during liquid reorientation were measured and recorded. High speed photographic records of the liquid reorientation were also made. The test data was used to verify a mechanical analog which portrays the liquid as a point mass moving on an ellipsoidal constraint surface. The mechanical analog was coded into two Fortran IV digital computer programs: LAMPS; Large Amplitude Slosh (a two dimensional simulation), and LAMPS3 (a three dimensional simulation, cast in the framework of a general spacecraft simulation program). Results show excellent correlation between test data and analytical predictions of reorientation forces and liquid center of mass motion, verifying the basic analytical approach.

ACKNOWLEDGEMENTS

The authors would like to express their appreciation to several individuals who contributed to the successful completion of this study. Mr. Frank Bugg, NASA MSFC, assisted in laying out the test program and monitored the entire study. Dr. Darrel Devers and Mr. Carl Bodley (Dyanamics and Loads Section, Martin Marietta Corporation, Denver Division) made major contributions to the development of the mechanical analog. Mr. Leonard Demchak, Dynamics and Loads, provided invaluable assistance in data reduction and computer program checkout. Mr. Dave Maytum and Mr. E. R. Wilson, Martin Marietta, Denver, made significant contributions to the design and construction of the test module. Mr. John Smith and Mr. Duane Brown fabricated the test module and performed the drop tower tests.

CONTENTS

LIST OF FIGURES

I. INTRODUCTION

In the near future, vehicles similar to Space Tug will perform orbital maneuvers while carying a large mass of liquid propellant. An indepth understanding of the interaction forces between the propellant and the space vehicle is required to properly assess the dynamics of these maneuvers. During orbital maneuvers, the propellant mass is subjected to small accelerations which can induce large amplitude propellant slosh. Due to the relatively large mass of propellant, the forces exerted on the spacecraft by the moving propellant may have a significant effect on gross vehicle motion. Knowledge of these interaction forces is imparative in the design of spacecraft control systems, propellant management devices and docking mechanisms, in addition to being required for maneuver studies such as deorbit/reentry.

A two year study (Phase I - 1974, Phase II - 1975) has been conducted to develop and verify a mechanical analog to simulate large amplitude liquid motion in a container subjected to low-g acceleration environments. The primary purpose of the model is to simulate the interaction forces between the liquid and its container. The study consisted of both experimental and analytical tasks.

The Martin Marietta (Denver) Drop Tower Test Facility was used in the conduct of the experimental phase of the study. A test module capable of measuring forces generated by large amplitude slosh in a scale model tank was constructed. Dimensional analysis techniques were used to ensure that the model simulations would be representative of reorientation in a full scale liquid oxygen tank. Three model tanks were tested; all three were axisymmetric with cylindrical barrel sections and hemispherical domes. The models consisted of a baseline tank, a half size tank (to increase equivalent reorientation time), and a baseline tank containing three ring baffles. During the study, the test module was dropped in the free-fall tower (simulating low-g) and small biaxial accelerations were applied. The ensuing liquid motion was photographed and two dimensional forces were measured and recorded. A total of forty-five tests were conducted. Various tank fill volumes, tank orientations and acceleration magnitudes were investigated. The test durations (1.5 to 2.0 seconds) correspond to approximately 15 to 20 seconds of liquid motion in a full size tank (10 foot diameter). Chapter II details the test program.

A two dimensional mechanical analog was developed during Phase I to simulate the observed large amplitude slosh. The analog portrays the liquid as a point mass moving on an ellipsoidal constraint surface. The constraint surface is defined by the ellipsoid which best fits the locus of liquid center of mass locations prescribed by slowly rotating the tank in a one-g field. The mechanical analog was implemented in a computer program, LAMPS (Large Amplitude Slosh), which outputs force time histories on the tank due to liquid motion. The Phase I test program and computer program LAMPS were both detailed in an interim report (Reference 1).

During Phase II of the study, the mechanical analog was expanded to three dimensions and integrated into the general spacecraft equations to facilitate its use in subsequent analyses. The three dimensional model was implemented into a computer program LAMPS3, which is in the framework of an existing dynamic simulation program DYNAMO (Dynamic Analysis Multiple Options). Chapter III discusses the implementation of the model; Appendix A presents a users guide for LAMPS3.

Chapter IV presents a discussion of the acquired test data and correlation with analytical results.

II. EXPERIMENTAL INVESTIGATION

The primary objective of the experimental investigation was to generate data for correlation with the computer model developed under the analytical task. The experiments simulated the reorientation of liquid within a propellant tank as it would occur during spacecraft maneuvering. The motion of the propellant in the main tanks of a Space Tug during docking maneuvers was used as an example to define typical environmental conditions. Scaling was used to relate those conditions to a small tank model.

A drop tower, which can simulate a low-g environment, was selected as the means of performing the tests. The testing was conducted in two phases, with 22 tests in Phase I and 23 tests in Phase II. For each test the motion of the liquid was photographed and the forcesexerted by the liquid on the tank were measured. Since the test conditions used have not been experimentally simulated before, the tests add to the basic understanding of the reorientation of propellant within a tank.

A. TEST APPROACH

When the propellant within a tank is reoriented, it is displaced from its initial position and relocated to a new equilibrium position due to an acceleration field acting on the tank. A prior maneuver is assumed to have positioned the liquid at its initial location. Since an attitude control system is defined as the source of the accelerations, the orientation of the acceleration with respect to the initial liquid position is arbitrary. For the test program, the most significant liquid motion and forces were desired, so the reorientation produced by an acceleration essentially opposite in direction to the one that established the initial position of the liquid was considered. An off-axis component was added to the reorienting acceleration to avoid symmetrical liquid motion, which tends to be a special case.

The typical conditions for a test are as shown in Figure II-1. A cylindrical tank with hemispherical end domes and an L/d of 1.28 was tested. A volume of liquid was initially at rest and the liquid surface was positioned with respect to the tank axes as determined by the angle θx. The axial (Aa) and lateral (Al) components of the reorienting acceleration are defined with respect to the initial liquid interface. The axial

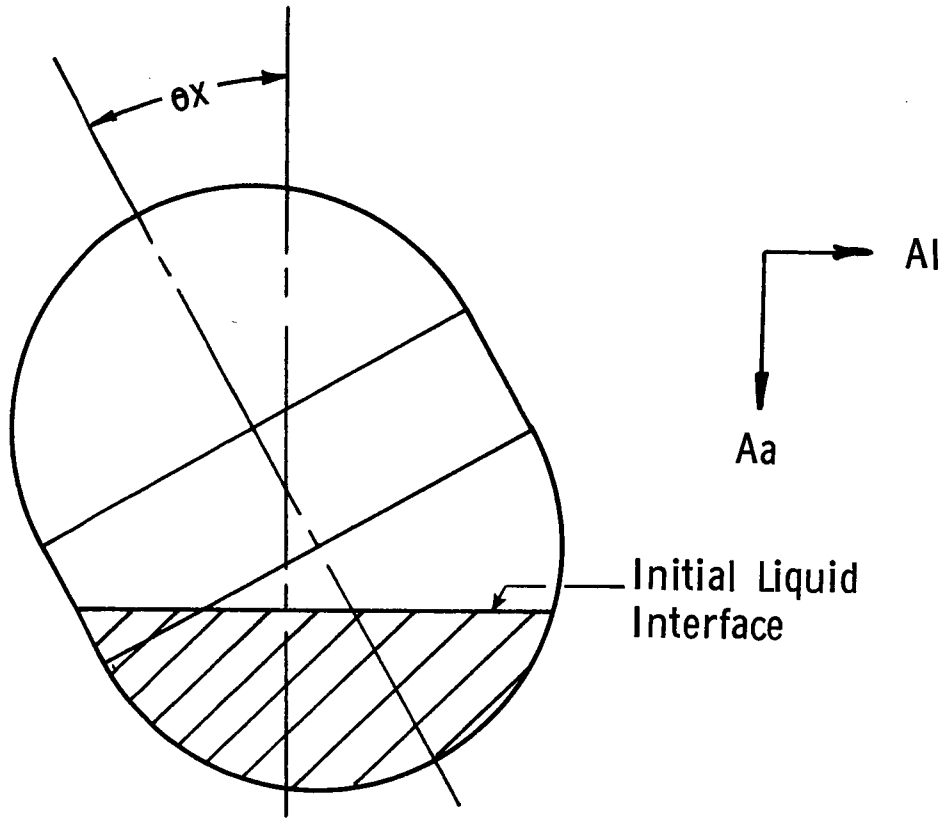

Figure II-1. Initial Conditions

component of the acceleration is always defined as being perpendicular to the liquid interface. The acceleration was continuously applied and the liquid was reoriented to the opposite end of the tank.

A scaling analysis was performed to determine the appropriate test parameters based on a Space Tug tank; 3.1 m (10 ft.) diameter, maneuvering accelerations on the order of 0.02 g to 0.04 g., and liquid oxygen as the propellant. A complete discussion of the scaling approach can be found in the Interim Report (Reference 1); only a brief summary will be presented here.

The following dimensionless parameters characterize the motion of the liquid as it is reoriented.

Froude Number - Ratio of inertia to gravity force
Bond Number - Ratio of gravity to surface tension force
Reynolds Number - Ratio of inertia to viscous force

Froude number has been expressed as a function of the Bond and Reynolds numbers based on the results of numerous reorientation tests. If both the Reynolds and Bond numbers are sufficiently large, which was the case for the selected test conditions, the Froude number is a constant. By equating the Froude number of the full size system and the model, similarity of test conditions is obtained.

This scaling analysis yielded a relation between time (t), acceleration (A), and tank radius (r):

$$\frac{ta}{tm} = \sqrt{\frac{Am}{Aa}\,\frac{r_a}{r_m}} \quad ,$$

where the subscript "a" refers to the full-size system and the subscript "m" refers to the model.

The purpose of the scaling was to make the test conditions representative of the actual operational environment. The test conditions were duplicated in the analytical model so scaling did not enter into the correlation.

A model tank, 12.7 cm (5.0 in) in diameter, was used for the Phase I tests. For Phase II, this tank was again used in addition to a tank of the same size with ring baffles, and also a 4.6 cm (2.5 in) diameter tank. The dimensions of the three model tanks are shown in Figure II-2.

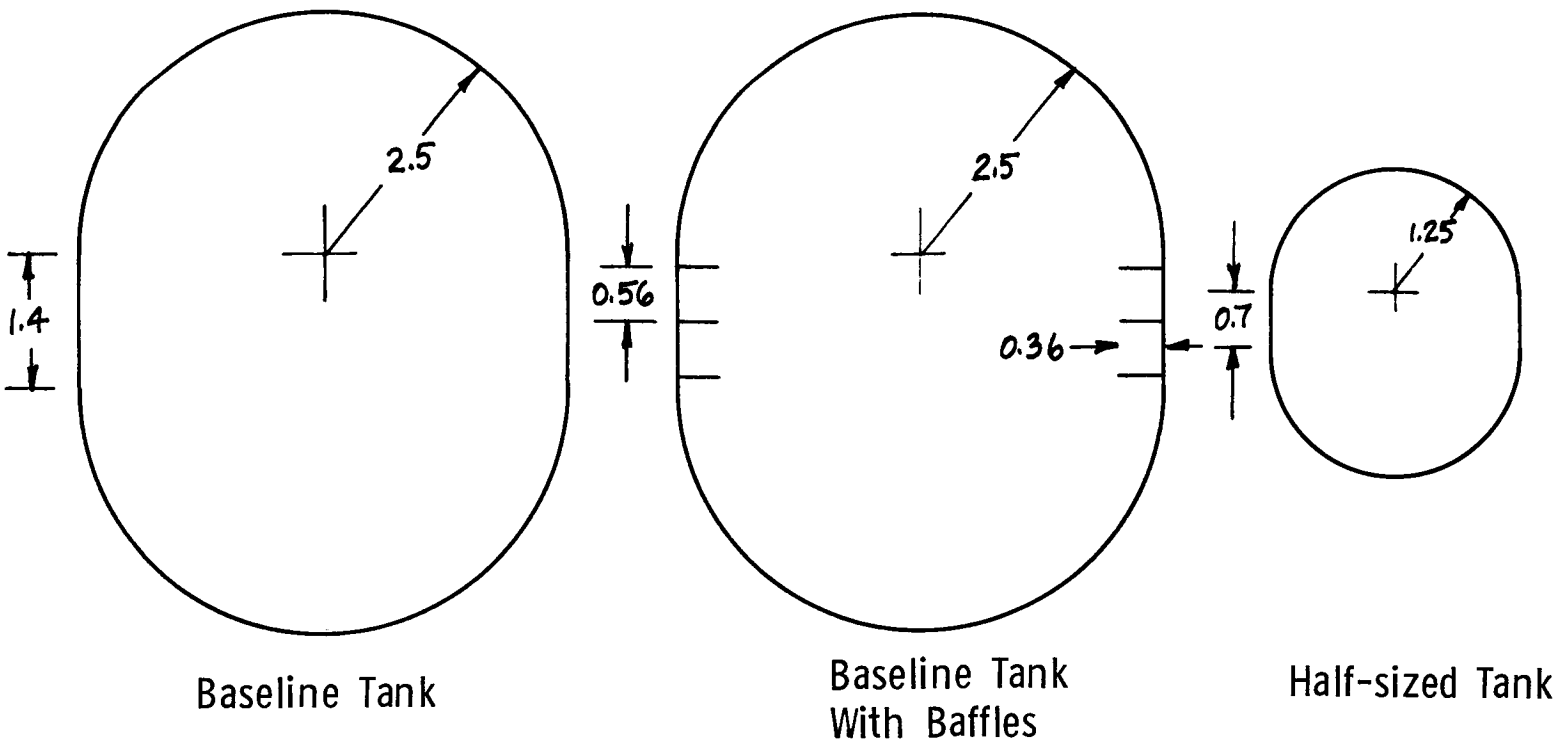

Figure II-2. Model Tank Dimensions (all dimensions are in inches)

The drop tower was selected as the means of simulating the acceleration environment. Following release of the drop capsule, a near zero-g test period of up to 2.1 seconds is available. During the test period, an acceleration can be applied to the model to simulate the reorientation acceleration. Due to physical constraints of the drop tower, the test acceleration cannot be larger than about 0.1 g.

A large model acceleration and a small model radius are desirable, based on the Froude number scaling, to make test time represent as long an actual time period as possible. A maximum model acceleration of 0.1 g was selected and, to consider the effect of acceleration, a smaller value of 0.05 g was also used. The lateral component of the acceleration ranged from a momentary pulse to a value of 50% of the axial acceleration.

Too small a model radius would reduce the magnitude of the liquid forces, hence two tank sizes were considered. The large tanks favored the liquid forces and the small tank provided a longer full-scale test time.

FC-43, a very dense fluorocarbon solvent, was selected as the test liquid. Its properties at $20^{o}C$ ($68^{o}F$) are as follows (Reference 2):

Density	1.905 gm/cc (118.9 lbm/ft^3)
Surface Tension	16.7 dynes/cm (1.14×10^{-3} lbf/ft)
Viscosity	6.5 cp (4.36×10^{-3} lbm/ft-sec)

This choice of test liquid, tank size and accelerations yielded a time scaling ratio (ta/tm) of 7.4 for the larger tank. Hence, 2.1 seconds of test time were equivalent to 15 seconds of real time. For the small tank, the ratio was 10.4 and 2.1 seconds of test time equals 21.8 seconds of real time.

Earth gravity was used to establish the initial position of the liquid in the tank. A flat interface is a realistic initial condition for a large tank in a relatively low-g environment. The acceleration would have to be 10^{-5} g or less with a tank on the order of 3 meters (9.8 feet) in diameter before the interface would have any significant curvature.

The parameters for each of the tests are listed in Table II-1. The tank orientation is the angle Θ x defined on Figure II-1. Spring motors were used to produce the acceleration and the motor force is listed in the table. Elsewhere in this report, the actual acceleration achieved is presented along with the force data (see Appendix B).

TABLE II-1 TEST MATRIX

TEST NO.	LIQUID VOLUME (%)	TANK ORIENTATION (θ_X DEGREES)	SPRING MOTOR FORCE N (LBF) AXIAL	LATERAL	TANK
		PHASE I			
1	25	0	67 (15)	3.3 (0.75)	Large Tank
2	50	0			
3	75	0			
4	25	30			
5	50	30			
6	75	30			
7	25	60			
8	50	60			
9	75	60			
10	25	90			
11	50	90			
12	75	90			
13	25	0	133 (30)		
14	50	0			
15	75	0			
16	25	45			
17	50	45			
18	75	45			
19	25	90			
20	50	90			
21	75	90			
22	10	0			
		PHASE II			
1	25	0	133 (30	0	Large Tank
2	25	45		0	Large Tank
3	10	0		3.3 (0.75)	Large Tank
4	10	45			with Baffles
5	10	90			
6	25	0			
7	25	45			
8	25	90			
9	50	0			
10	50	45			
11	50	90			
12	10	45	67 (15)		
13	25	45			
14	50	45			
15	25	0	133 (30		Small Tank
16	25	45			
17	50	0			
18	50	45			

TABLE II-1 (Cont)

TEST NO.	LIQUID VOLUME (%)	TANK ORIENTATION (θ X DEGREES)	SPRING MOTOR FORCE N (LBF) AXIAL	LATERAL	TANK
			PHASE II (Cont)		
19	25	45	67 (15)	3.3 (0.75)	Small Tank
20	50	45	67 (15)	3.3 (0.75)	↓
21	25	45	133 (30)	6.7 (1.5)	
22	50	45	↓	6.7 (1.5)	
23	25	90		3.3 (0.75)	↓

B. TEST SYSTEM DESCRIPTION

A test system that can produce the required subscale model test conditions and measure the liquid forces was designed and built for Martin Marietta'sDrop Tower Test Facility. Flexibility to duplicate the varied test conditions, and sensitivity to record the small liquid forces, were the key requirements in designing the test system.

1. Test Module - The test module consists of the tank, force measuring links and slider mechanism. This module is shown mounted on the drop capsule in Figure II-3. Figure II-4 and Figure II-5 present front and back views of the box in which the force links and tank are mounted.

The model tanks were made of clear plastic. The flange around the tanks provided structural strength and permitted the tanks to be mounted at the proper angle within the force link yoke.

Three force links, two vertical and one lateral, allowed all forces acting on the tank to be measured. Bearings at each end of the links permitted only forces along the link axis to be measured. The bearings that are mounted on the box are self-aligning.

Three flexures, perpendicular to the plane of the force links, prevented any motion of the tank out of that plane. The spring constant of these flexures is small in comparison to the spring constant of the load cells and force links. Therefore, the effect of these flexures on the force sensed by the load cells was insignificant.

The platform of the slider was attached to the rails with three linear bearings; one under the camera and two under the tank. A constant force spring motor provided the lateral acceleration of the slider. An electric solenoid was used to release the slider at the beginning of the test.

2. Drop Test Facility - The complete drop capsule is shown in Figure II-6. Due to the rather high accelerations being used, evacuation of the drag shield was not necessary. A simple frame was mounted over the test module rather than sealing the drop capsule with its cylindrical cover. The spring motors that provide the axial acceleration of the drop capsule and a crush tube are mounted on the conical base.

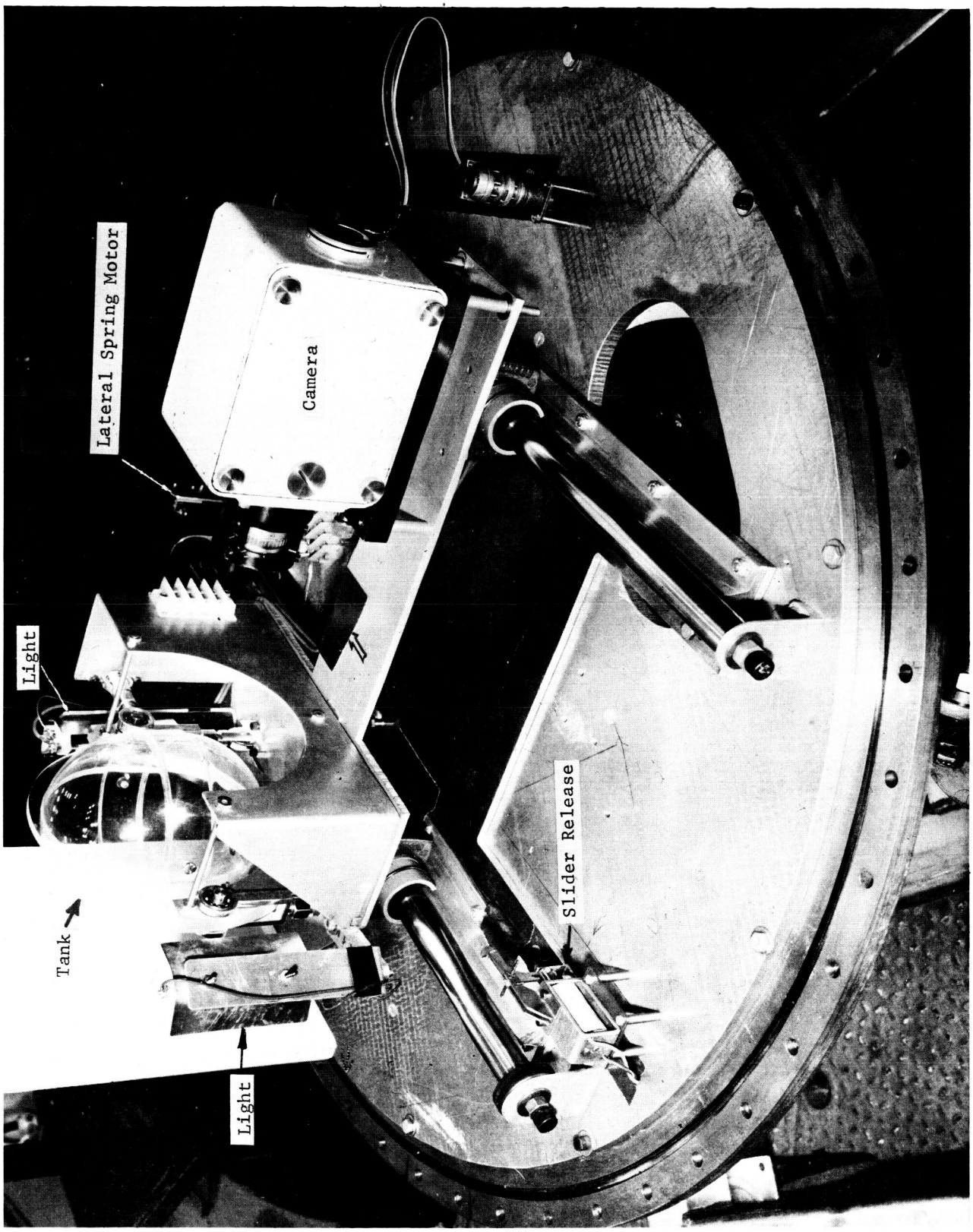

Figure II-3. Test Module Mounted on Drop Capsule

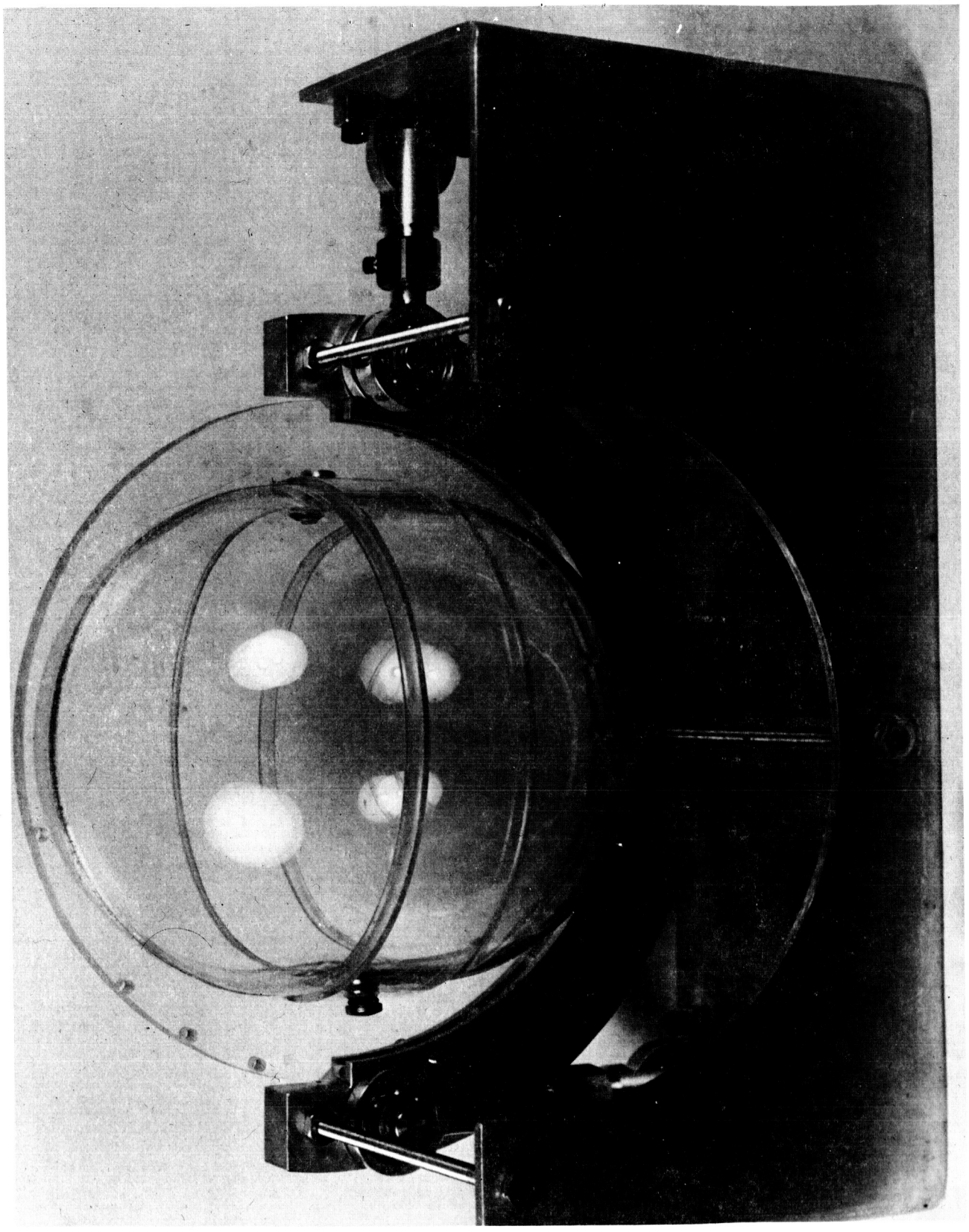

Figure II-4. Camera View of Tank and Force Links

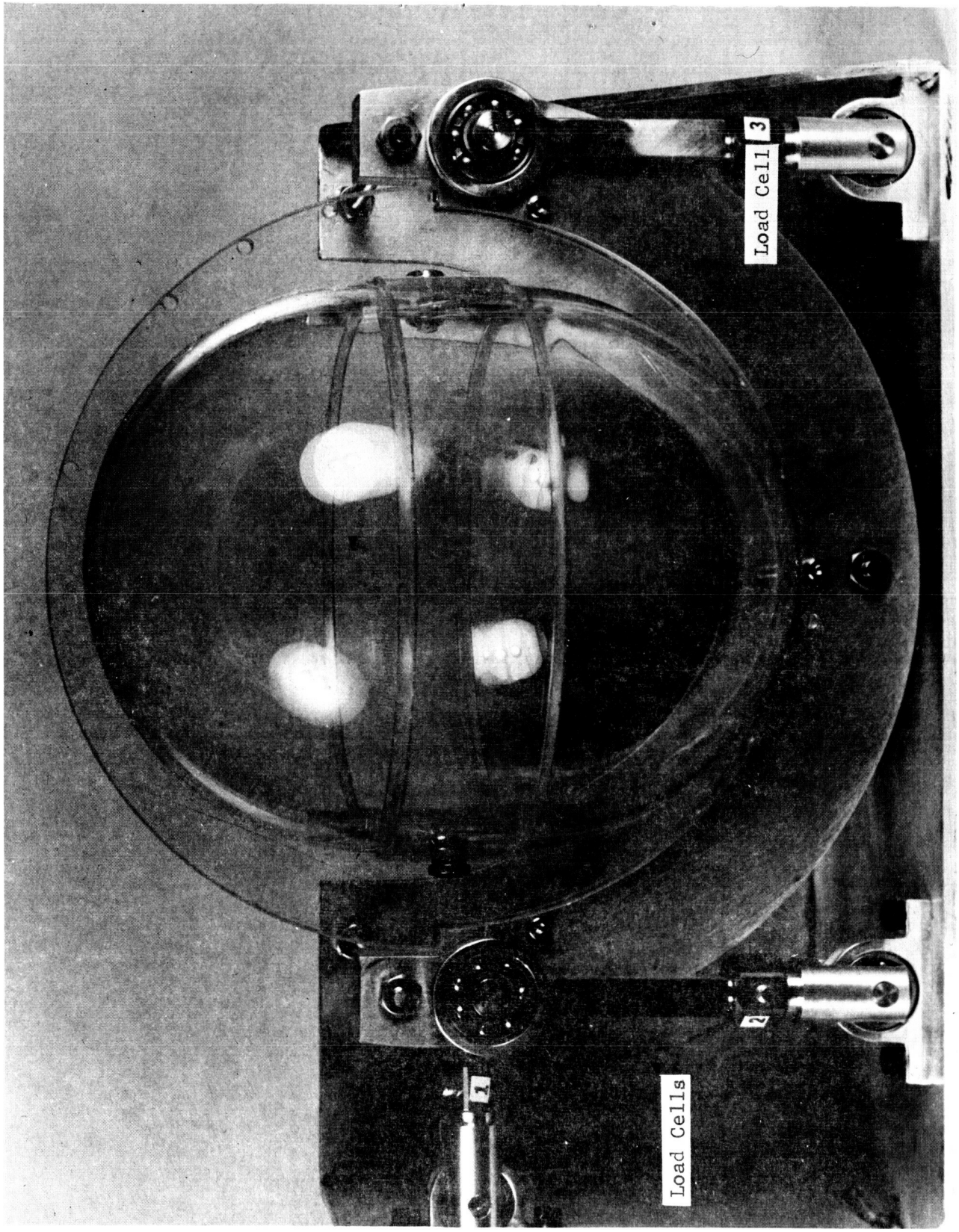

Figure II-5. Back View of Tank and Force Links

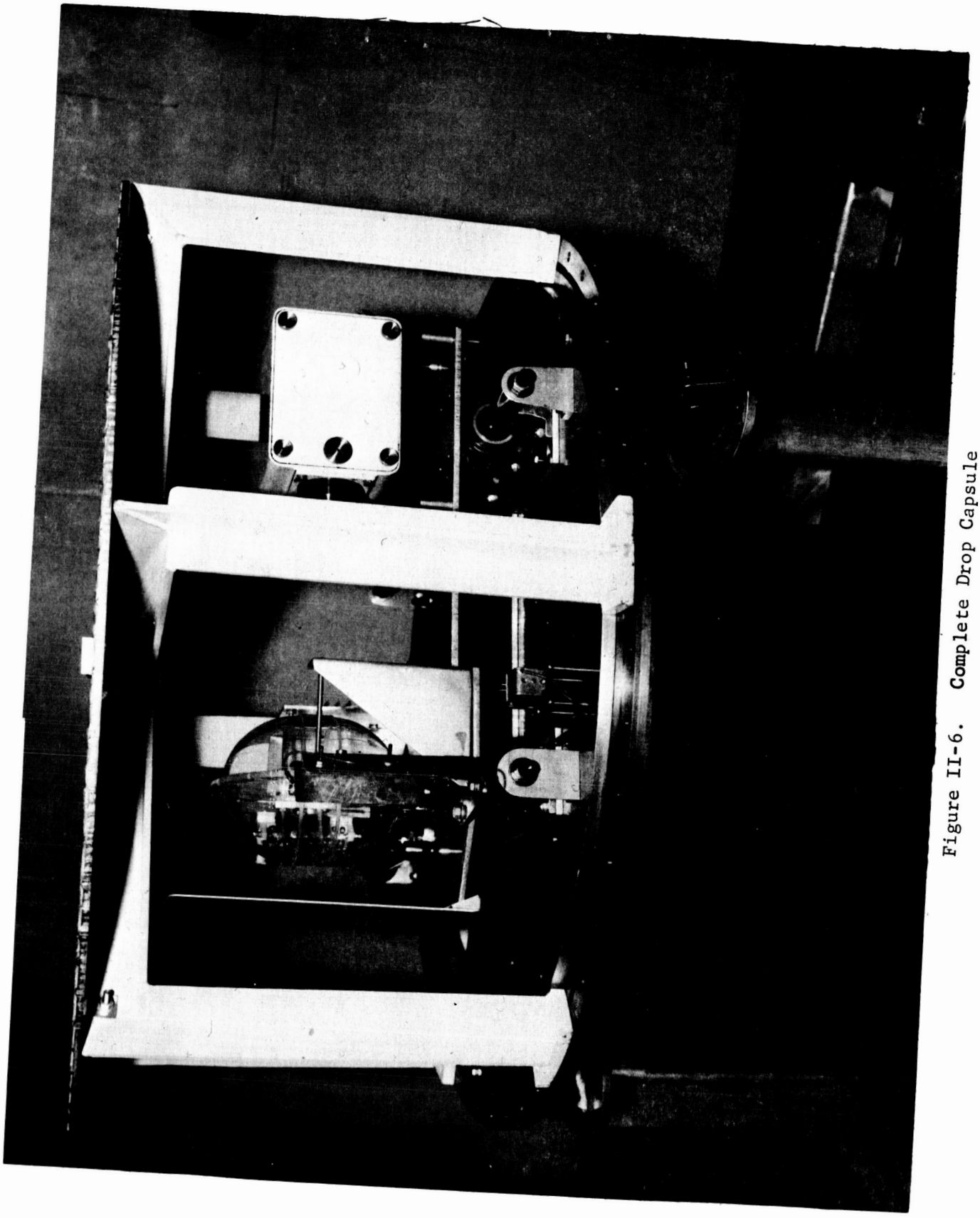

Figure II-6. Complete Drop Capsule

The total drop test system is illustrated in Figure II-7. The cable from the axial spring motor was extended and secured to the bottom of the drag shield. After releasing the drag shield from the top of the 23-meter (75-foot) drop tower, a solenoid was actuated releasing the slider. Both the lateral and axial spring motors accelerated the test module throughout the drop test. The drop capsule impacts the drag shield, with the crush tube absorbing the impact, and the drag shield lands in a bin of wheat at the end of the test.

3. Instrumentation - The motion of the liquid was recorded with a 16-mm Milliken DBM-3a camera mounted on the slider. The film speed was 200 frames per second. Immediately before the drag shield was released, the camera was started and it was automatically stopped when the drag shield impacted the wheat.

Quartz crystal load cells (Kistler Model 912) were used to measure the liquid forces. These load cells have a capacity of 2220N (500 lbf) in tension and 22200N (5000 lbf) in compression, providing the capability of withstanding the impact at the end of the test. Peak, high frequency accelerations of up to 160g have been measured at impact. Due to their high degree of linearity, these load cells are fully capable of measuring the small forces due to the liquid motion.

The load cells were mounted in the force measuring links. Low noise cables were used to feed the output of the load cells to charge amplifiers. The charge amplifiers were located about half way up to the drop tower to minimize the motion of the cable as the drag shield falls. The amplifiers were set on long time constant and the most sensitive scale that could be accommodated, to measure the low amplitude and low frequency forces. Each charge amplifier input was momentarily grounded prior to the test, so all forces were measured with respect to zero at one-g.

The output of the charge amplifiers was fed in parallel to both a tape recorder and a chart recorder. In order to filter out the vibration induced by the camera motor, a 10 Hz low-pass filter was used in the amplifier for the chart recorder. An end-to-end calibration of the force measuring system was accomplished with the fixture shown in Figure II-8. Known weights were suspended from the hook at various positions with respect to the force links, and the charge amplifiers were adjusted to give the proper output.

An accelerometer was mounted on the slider for the Phase I tests, to measure the axial acceleration of the drop capsule. It was found that the acceleration can be readily calculated from the known capsule travel distance, weights and test time. The accelerometer was not used during Phase II. The lateral acceleration can be calculated from the travel versus time obtained from the film data.

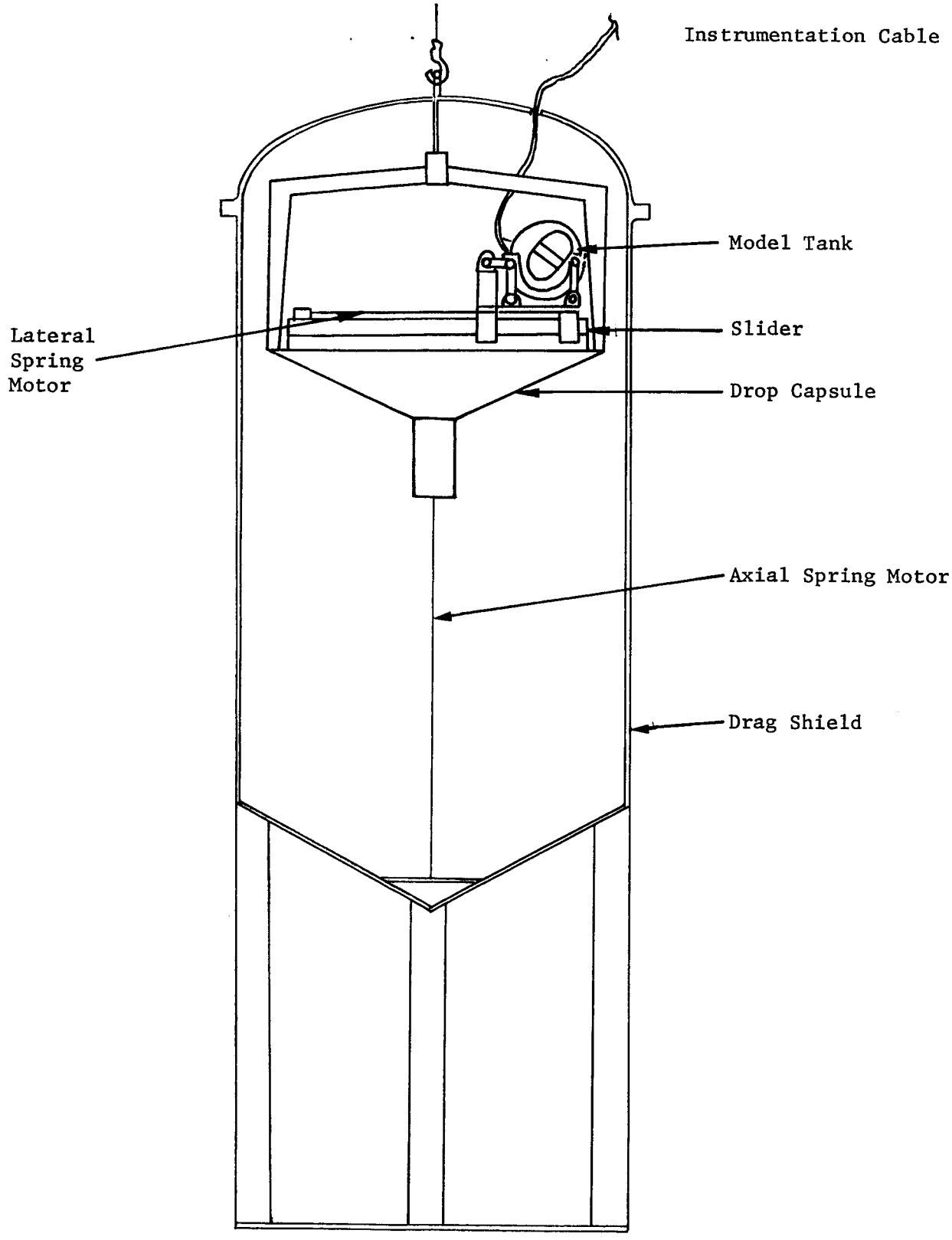

Figure II-7. Complete Drop Test System

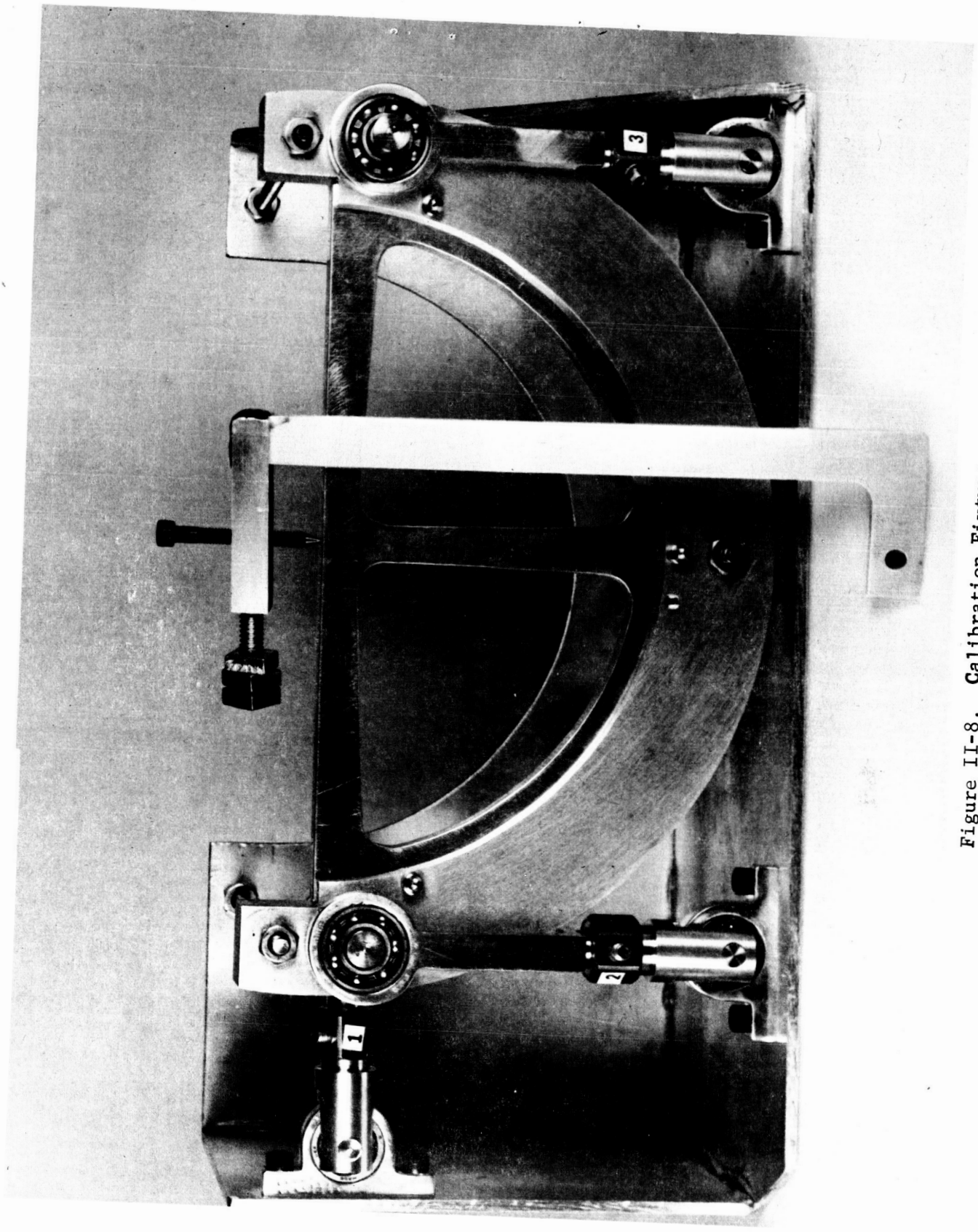

Figure II-8. Calibration Fixture

C. DATA REDUCTION

A lateral force (F_1) and two vertical forces (F_2 and F_3) were measured and recorded during the drop tests (see Figure II-5). The test data was manually scaled from oscillograph records and converted to a punched card data bank. A data reduction computer program was then used to convert the raw data from voltage to engineering force units using appropriate scale factors based on charge amplifier sensitivities. The data was then smoothed to remove test fixture and camera noise by a moving average digital low pass filter set at 10 Hz. Figure II-9 depicts the shape of the filter used. The force triad was then transposed to the tank triad as shown in Figure II-10. The following set of equations was used to perform the transposition.

$$FZ_I = F_2 + F_3$$

$$FY_I = F_1$$

$$MX_I = F_2 b + F_1 c - F_3 a$$

$$FZ_T = FZ_I \cos \theta X - FY_I \sin \theta X$$

$$FY_T = FY_I \cos \theta X - FZ_I \sin \theta X$$

$$MX_T = MX_I$$

where subscript (I) denotes the intertial triad and subscript (T) denotes the tank triad. The results were plotted with time as the ordinate.

To facilitate comparison between the test and analytical results, the test data was further adjusted. As previously mentioned, the force gages registered "0" in 1 g prior to each drop. The analytical model records this one-g force as a negative force in the Z_I direction. To make the analysis and test results compatible, the initial zero test forces were converted to negative Z_I forces. In this conversion, the fluid cm offset was accounted for in the determination of the adjusted F_2 and F_3 values. This conversion allows direct comparison between predicted and measured force time histories.

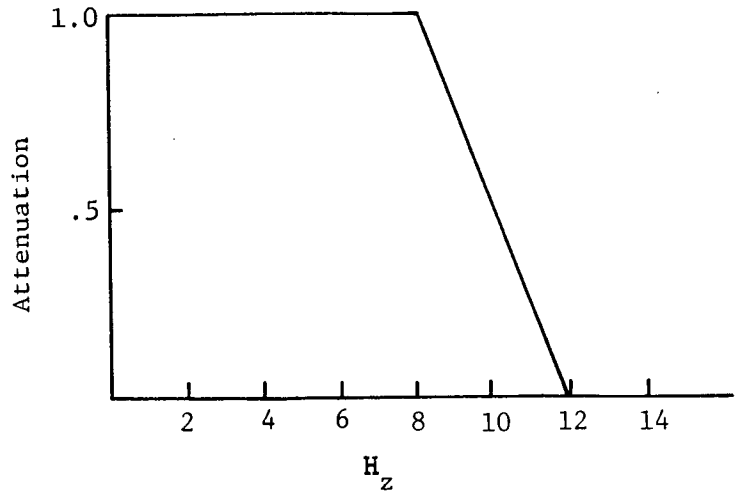

Figure II- 9. Digital Filter Shape

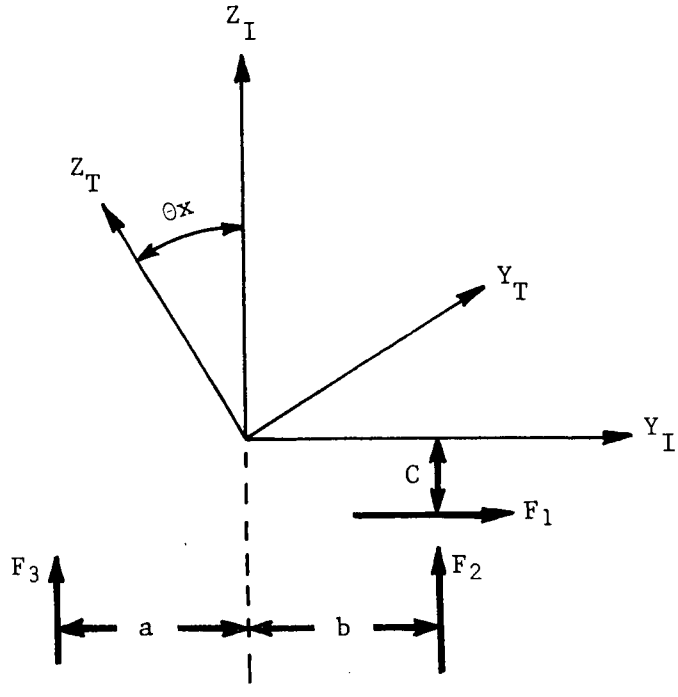

Figure II- 10. Coordinate Systems

III. MECHANICAL ANALOG

This chapter details the approach whereby the tank/liquid mechanical analog is cast into a state space framework that is amenable to accommodation into a typical spacecraft system of governing equations. The basic approach is characterized as a system of interconnected "bodies" subject to certain constraint conditions which restrict the relative motion between the "bodies", one of which represents a typical liquid mass within a container. The ensuing discussion describes some of the particulars relating to the tank/liquid mechanical analog which depicts the fluid mass as moving on a predetermined constraint surface within the tank boundry. An in-depth theoretical development for the general class of spinning, interconnected "bodies" can be found in Reference 3. This discussion will be limited to a cursory overview of the developments contained in the reference and focus on some of the specifics related to the three dimensional tank/liquid mechanical analog developed during Phase II.

A. GOVERNING EQUATIONS - GENERAL

The system of equations governing the dynamics of an interconnected set of bodies undergoing large relative motions is depicted in a state space form that can be readily solved by numerical integration techniques on a digital computer. In terms of the state space, y^i, a canonical, first-order expression of the governing equations appears in a rather general form as:

$$\frac{d}{dt} \quad y^i = f\ (y^i,\ t) \tag{III-1}$$

More specifically, the matrix form for the equations as applied to our class of problems is given as

$$\{\dot{p}\} = \{G\} + [\Omega]\{p\} + [b]^T \{\lambda\} \qquad a$$

$$\{\dot{\beta}\} = [B]\{u\} \qquad b \tag{III-2}$$

$$[b]\{u\} = \{\dot{\alpha}\} \qquad c$$

State variables of the configuration space, y^i, include ordinary momenta, p^i, and relative position and/or attitude coordinates, β^i. The vector, β^i, contains such items as Euler angles and inertial position coordinates. The vector, λ^j, represents the constraint forces and/or moments required to affect the particular constraints for the problem (e.g., hinge constraints between adjacent bodies and/or motion restricted to a constraint surface).

For a typical body, k, of the system, the component ordinary momenta vector, $\{P\}_k$, is

$$\{P\}_k = [M]_k \{u\}_k \tag{III-3}$$

where

$$\{u\}_k = \begin{bmatrix} \omega_x \\ \omega_y \\ \omega_z \\ u \\ v \\ w \end{bmatrix}$$

The matrix, $[b]$, contains kinematical coefficients which are described in further detail in the following subsection. The matrix, $[\Omega]$, (for the kth body) contains three (3 by 3) partitions of skew symmetric submatrices of the body velocity vectors, $\{u\}_k$.

$$[\Omega] = \left[\begin{array}{ccc|ccc} 0 & \omega_z & -\omega_y & 0 & w & -v \\ -\omega_z & 0 & \omega_x & -w & 0 & u \\ \omega_y & -\omega_x & 0 & v & -u & 0 \\ \hline & & & 0 & \omega_z & -\omega_y \\ & & & -\omega_z & 0 & \omega_x \\ & & & \omega_y & -\omega_x & 0 \end{array}\right] \tag{III-4}$$

The matrix, $[B]$, contains kinematical coefficients of the same form as matrix, $[b]$. The vector, $\{\dot{\alpha}\}$, in the last expression of equation III-2 is referred to as a "rhenomic" prescription of relative velocities within the system. Whenever $\{\dot{\alpha}\} = 0$, an ordinary constraint is imposed that fixes certain degrees of freedom with respect to each other within the overall dynamical system. The rhenomic constraint (time dependent) results from prescribing the rhenomic velocities, $\{\dot{\alpha}\}$, as a function of the independent variable, time. This latter situation will be employed to impose the constraint whereby the tank fluid mass is restricted to move on an ellipsoidal surface (taken with respect to the tank axis system). There exists another important transformation that relates the nonholonomic velocities, $\{u\}_k$, to generalized velocities,

$$\{u\}_k = \begin{Bmatrix} \omega_x \\ \omega_y \\ \omega_z \\ u \\ v \\ w \end{Bmatrix} = \left[\begin{array}{c|c} \Pi_k & \\ \hline & \gamma_k \end{array}\right] \begin{Bmatrix} \dot{\Phi} \\ \dot{\Theta} \\ \dot{\Psi} \\ \dot{x} \\ \dot{y} \\ \dot{z} \end{Bmatrix} \quad \text{(III-5)}$$

where in (III-5), the nonholonomic velocities vector, $\{u\}$, contains the three projections $(\omega_x, \omega_y, \omega_z)_k$ of the angular velocity vector $\bar{\omega}_k$ onto the body fixed axis and the three projections of the reference point translational velocity $(u, v, w)_k$ onto the body axes. The elements of γ_{ij_k} $(i, j = 1, 2, 3)$ are direction cosines; the sub-matrix $[\gamma]$ is an orthonormal rotation transformation relating the attitude of the body fixed axis system to the inertial frame. The sub-matrix, $[\Pi]$, is also a rotation transformation; however, it is not orthonormal since it relates vector components based on an orthogonal basis to those of a skew basis; namely, the axes about which Euler rotations are measured.

The mass matrix for body k, appears as

$$[m]_k = \left[\begin{array}{ccc|ccc} J_{xx} & -J_{xy} & -J_{xz} & & -S_z & S_y \\ -J_{xy} & J_{yy} & -J_{yz} & S_z & & -S_x \\ -J_{xz} & -J_{yz} & J_{zz} & -S_y & S_x & \\ \hline & S_z & -S_y & m & & \\ -S_z & & S_x & & m & \\ S_y & -S_x & & & & m \end{array}\right] = \left[\begin{array}{c|c} J & -s \\ \hline s & m \end{array}\right] \qquad \text{(III-6)}$$

The kth component of second part of the right hand side of (III-2a) can be expanded to read as

$$[\Omega]_k \{p\}_k = \left[\begin{array}{ccc|ccc} 0 & \omega_z & -\omega_y & & w & -v \\ -\omega_z & 0 & \omega_x & -w & & u \\ \omega_y & -\omega_x & 0 & v & -u & \\ \hline & & & 0 & \omega_z & -\omega_y \\ & & & -\omega_z & 0 & \omega_x \\ & & & \omega_y & -\omega_x & 0 \end{array}\right] \left[\begin{array}{c} p(\omega_x) \\ p(\omega_y) \\ p(\omega_z) \\ p(u) \\ p(v) \\ p(w) \end{array}\right] \qquad \text{(III-7)}$$

The force/torque vector, $\{G\}_k$, contains the external forces and torques plus any stiffness and damping force that may arise through connections with the other bodies making up the system. Clearly, $\{G\}$ is the implement through which additional system forces/torques are "fed back" to the dynamical system.

The constraint equations (third of III-2) are written in terms of the nonholomic velocities, $\{u\}$, which in turn are expressed in terms of the generalized velocities as in (III-5). The coefficients $[b]$ are obtained from expressions of kinematic constraint and these same $[b]$ coefficients are transposed to premultiply the vector $\{\lambda\}$, providing constraint forces and torques.

B. KINEMATIC COEFFICIENTS

This subsection discusses the aforementioned kinematical relations involving expressions of relative and absolute velocities which lead to the form of the $[b]$ coefficients. The discussion will focus on two adjacent interconnected bodies.

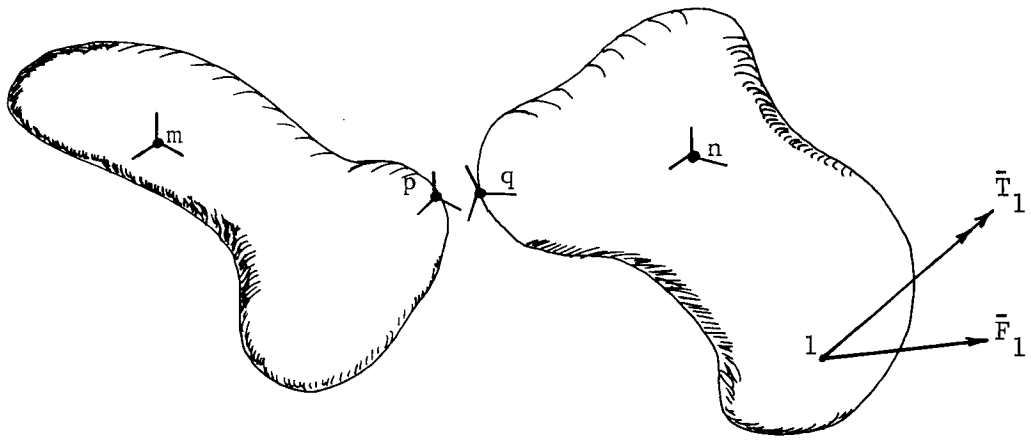

FIGURE III-1 TWO INTERCONNECTED BODY SYSTEM

The origins of the body reference systems are labeled m and n. The portions of the body where the bodies connect are located and labeled p and q.

In general, for each interconnected pair of bodies, there will be five (5) axis systems or coordinate bases. First, there will be an axis system fixed to each of the points, m, p, q, n (see Figure III-1). The fifth axis system is a skew or non-orthogonal basis comprising direction lines or unit vectors about which Euler rotations are measured. The Euler rotations are used to describe relative attitudes between the p and q frames.

At each connection joint, there will be six (6) components of relative velocity (three relative Euler angle rates and three relative translational rates that are measured along the skew axes) to be expressed.

$$\begin{Bmatrix} \Delta\dot{\theta} \\ \dot{\Delta} \end{Bmatrix} = \left[\begin{array}{c|c|c|c} -\Pi^{-1} R^q_p R^p_m & & \Pi^{-1} R^q_n & \\ \hline -R^p_m S_{mp} & -R^p_m & R^p_q R^q_n S_{nq} & R^p_q R^q_n \end{array}\right] \begin{Bmatrix} u_m \\ u_n \end{Bmatrix} \qquad \text{(III-8)}$$

$$= \begin{bmatrix} b_p & b_q \end{bmatrix} \begin{Bmatrix} u_m \\ u_n \end{Bmatrix}$$

In (III-8), R^q_p is a (3 x 3) rotation transformation relating vector components in the p system to components in the q system. It transforms from p to q. The transformation R^p_m is similar, and note that the product ($R^q_p R^p_m = R^q_m$) transforms from m to q. The matrix, $[\Pi]^{-1}$ relates vector components referred to orthogonal axes to those referred to skew axes. The matrix $[S_{mp}]$ is a (3 x 3) skew symmetric matrix containing components of the vector positioning point p from m.

$$[S_{mp}] = \begin{bmatrix} 0 & z_p & -y_p \\ -z_p & 0 & x_p \\ y_p & -x_p & 0 \end{bmatrix} \qquad \text{(III-9)}$$

Finally, it is pointed out that certain rows from (III-8) constitute rows of [b] and other rows of (III-8) are rows of matrix [B] .

C. INTERCONNECTION CONSTRAINT FORCES

The interconnection constraint forces/torques can be readily obtained by manipulations of the first and last portions of (III-2). Taking the first time deviative of part C of (III-2) gives

$$[b]\{\dot{u}\} = \{\ddot{\alpha}\} - [\dot{b}]\{u\} \qquad \text{(III-10)}$$

using (III-3) in a of (III-2) and together with (III-10) provides an expression for the constraint force/torque vector, $\{\lambda\}$,

$$\{\lambda\} = \left([b][m][b]\right)^{-1}\left[\{\ddot{\alpha}\} - \left([b]\{u\} + [b][m]^{-1}\{G\}\right)\right] \qquad \text{(III-11)}$$

Where we further note certain functional dependences.

$$\begin{aligned}
b &= b(\beta) \\
B &= B(\beta) \\
\dot{\beta} &= \dot{\beta}(\beta, u) \\
\dot{\delta} &= \dot{\delta}(\beta, \dot{\beta}, \delta, t) \\
G &= G(u, \dot{\delta}, t) \\
\dot{b} &= \dot{b}(\dot{\beta}, \beta) \\
\lambda &= \lambda(\beta, u, \dot{\beta}, \dot{\delta}, t) \\
\dot{u} &= \dot{u}(\beta, u, \dot{\beta}, \dot{\delta}, t)
\end{aligned} \qquad \text{(III-12)}$$

The variables denoted by δ and their time deviative, $\dot{\delta}$, represent control system type variables or other miscellaneous variables required to complete the simulation.

D. ARRANGEMENT OF THE STATE VECTOR

The variables for the configuration space, y^i, are arranged in vector form and appear as,

$$\begin{bmatrix} \{u\}_1 \\ \{u\}_2 \\ \vdots \\ \{u\}_{NB} \\ \beta_1 \\ \beta_2 \\ \vdots \\ \beta_{N\beta} \\ \delta_1 \\ \delta_2 \\ \vdots \\ \delta_{N\delta} \end{bmatrix} \qquad \text{IIII-13)}$$

Where NB represents the number of total "bodies" in the system, $N\beta$ is the total number of position coordinates necessary to the system, and $N\delta$ is the total number of auxilliary (control) differential equations required.

Now, given that the $\{y\}$ vector is known (numerically) from prescribed initial conditions or from numerical integration of $\{\dot{y}\}$, the primary task of the solution process is to numerically establish the $\{\dot{y}\}$ vector. The $\{\dot{y}\}$ vector is numerically (step by step) integrated so as to produce an incremented $\{y\}$ vector, thus a sequence of time point solutions.

In way of summary, a narrative description of the steps (numerical evaluations) necessary to produce $\{\dot{y}\}$ given $\{y\}$, follows.

The matrices $[B]_j$ and $[b]_j$ are kinematic coefficients that depend on position and modal displacement variables and are evaluated as the first step.

Now, if available numerical techniques (also computer software and hardware) were absolutely accurate, we would be assured that the $\{U\}_j$ vectors, resulting from numerical integration of the $\{\dot{U}\}_j$ vectors, would satisfy the constraint Equation, c of III-2. This is not the case; therefore, the second step of the solution process is to calculate the dependent elements of the $\{U\}_j$ vectors by using Equation c of III-2. In fact, due to anticipating numerical inaccuracies, only the independent element of the $\{U\}_j$ vectors are obtained by numerical integration. There are only n-m "integrators" involved in the solution process even though all of the elements of the $\{\dot{U}\}_j$ vectors are numerically evaluated (by use of Equation III-1); we have good numerical resolution in the independent $\{\dot{U}\}_j$ elements due to using the Lagrange multipliers $\{\lambda\}$.

A kinematically consistent system results from satisfying Equation c of III-2. The $\{U\}_j$ vectors may now be used with the selection and kinematic transformations as indicated and Equation b of III-2 to produce (numerically) position coordinate rates $\{\dot{\beta}\}$ completing the third step of the process.

Sufficient calculation has been completed to this point to then evaluate the control variable rates as per Equation III-12, producing $\{\dot{\delta}\}$. During the process of calculating the $\{\dot{\delta}\}$ vector, all of the required control actuator torques (or forces) are calculated, because sufficient numerical information is available. All of the constituents of the torques/force vectors, $\{G\}_j$, are now available and therefore $\{G\}_j$, $[m]_j$ and $[b]_j$ are numerically evaluated, (refer to the functional expressions of Equation III-12), which completes the fourth step of the process. With reference to Equation III-11, we note that there is now sufficient numerical information to evaluate $\{\lambda\}$, which is then used in Equation III-2 to calculate the $\{\dot{U}\}_j$, completing the fifth and final step of the process.

It is noted in the above discussions that the solution process may be carried out through completion, providing the state vector is numerically known. At any step of a simulation, the $\{y\}$ vector is known, of course, as the result of numerical integration. The initial state vector is another matter. It is difficult, if not impossible, for a user to prescribe $\{U\}_j$ vectors that are kinematically consistent with the conditions of Equation c of III-2; also, the nonholonomic velocities of $\{U\}_j$, when considered as a complete set, are of a somewhat abstract nature. The user is in a much better posture to prescribe initial values of $\{\dot{\beta}\}$ (the initial velocities that are

physically meaningful to him). Thus, to initiate the simulation (that is, to create an initial state vector from information, the user is in a position to prescribe) some preliminary steps must be taken as follows.

The user must prescribe initial values of the $\{\beta\}$, $\{\dot{\beta}\}$ and $\{\delta\}$ vectors. Now, in that $\{\dot{\alpha}\}$ (the prescribed position rates), are explicitly dependent on time and are always available, the kinematic equations, b of III-2 and c of III-2, may be used together to establish initial values of all $\{U\}_j$.

E. SINGLE TANK/LIQUID MASS COMBINATION

The specifics that relate to a single tank/liquid mass system will be identified in this section. The relevant geometry and separate coordinate systems are noted as:

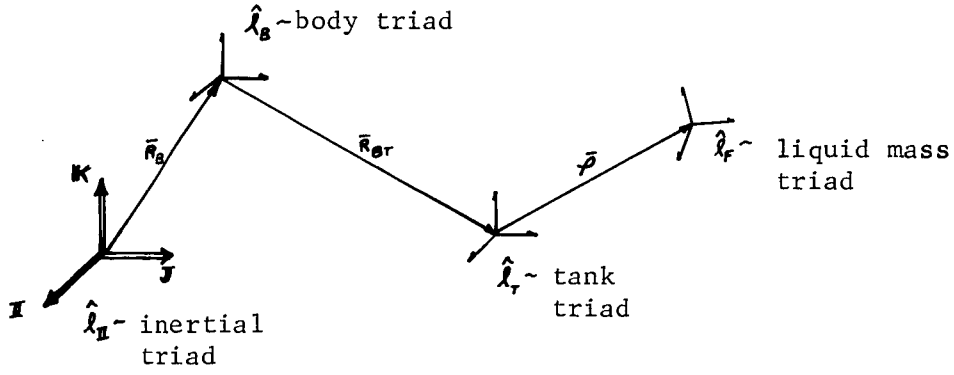

The above sketch depicts the general problem and we will make further simplifications which are helpful to our problem.

For our particular discussions, we will let the body and tank axis systems be coincident with each other. Furthermore, it will be convenient to introduce a polar spherical coordinate system to position the tank mass with respect to the tank axis system. Consider the following typical tank axis system.

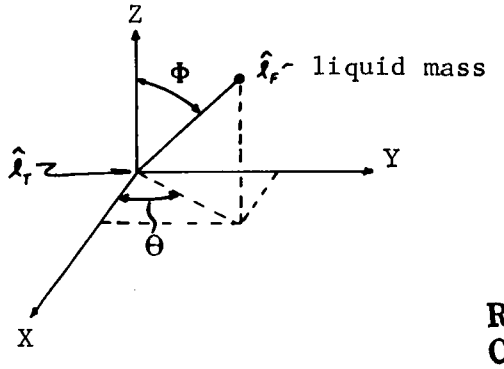

The spherical coordinate transformation is:

$$x = r \sin \Phi \cos \Theta$$
$$y = r \sin \Phi \sin \Theta \qquad \text{(III-14)}$$
$$z = r \cos \Phi$$

The equation for the assumed ellipsoidal surface is,

$$\left(\frac{x}{a}\right)^2 + \left(\frac{y}{b}\right)^2 + \left(\frac{z}{c}\right)^2 = 1 \qquad \text{(III-15)}$$

and for the axi-symmetric case, let b = a; thus the surface constraint equation becomes (in spherical coordinates),

$$r = \frac{a}{\left[\sin^2\Phi + \left(\frac{a}{c}\right)^2 \cos^2\Phi\right]^{\frac{1}{2}}} \qquad \text{(III-16)}$$

and upon taking the first time deviative

$$\dot{r} = \frac{dr}{dt} = \frac{-a \sin\Phi \cos\Phi \left(1 - \frac{a^2}{c^2}\right)}{\left[\sin^2\Phi + \left(\frac{a}{c}\right)^2 \cos^2\Phi\right]^{\frac{3}{2}}} \dot{\Phi} \qquad \text{(III-17)}$$

or more concisely, $\dot{r} = \sigma(\Phi)\dot{\Phi}$ (III-18)

where it is noted that the condition of axi-symmetry is responsible for the dependency of $\dot{r}$ on Φ and $\dot{\Phi}$ alone. The expression given as (III-18) in essence becomes the $\dot{\alpha}$ expression (III-2c). The following sketch portrays the actual mechanization of our problem.

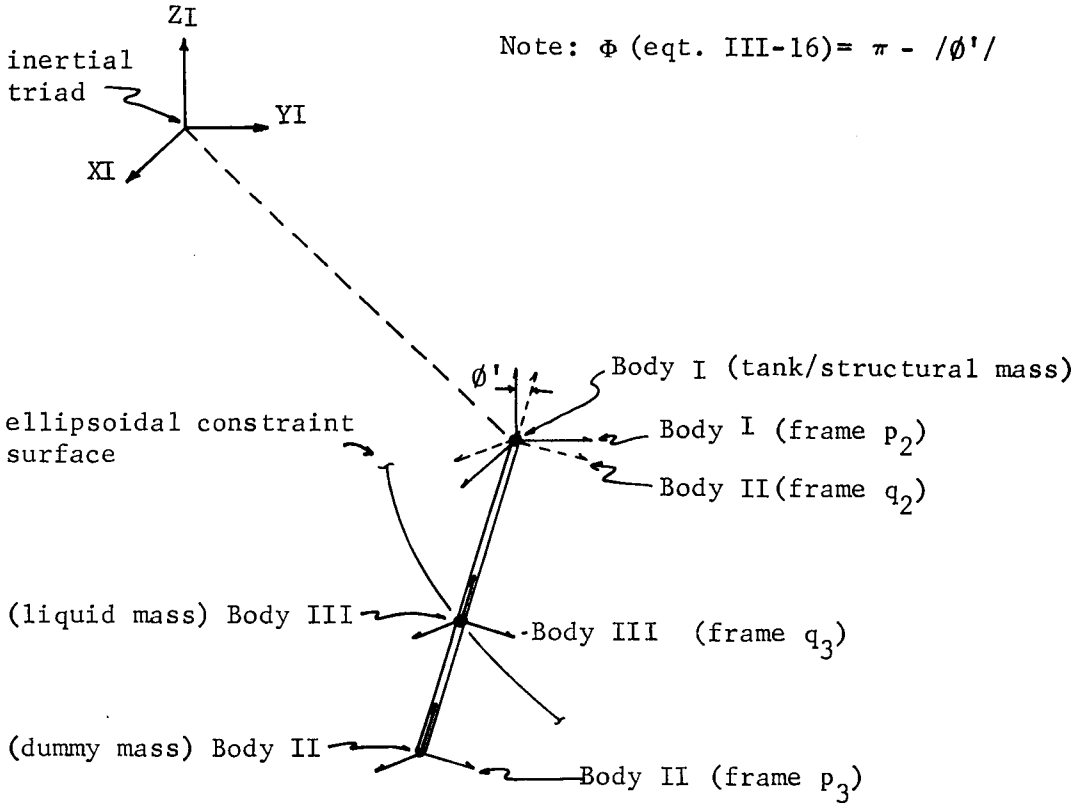

The frame for the fluid mass (q_3) is only permitted to move along the radius connecting body I to body III. Body III is a ficticious or dummy body that aids in the mechanization process. The radius between body I (the tank axis centroid) and body III remains constant in length; hence as the "pendulum" rotates the fluid mass moves inward and outward in such a manner as to maintain the necessary constraint (ellipsoidal constraint surface). It is further noted that a proper choice of Euler permutation for positioning frame q_2 with respect to frame p_2 will lead to an explicit expression for both polar spherical angle (and rate) as a function of β and $\dot{\beta}$ within the general dynamical equations of motion (III-2).

Next, with regard to the expression required for evaluating λ, given as III-11, it is noted that we need the derivative of $\dot{\alpha}$ (given as $\dot{r}$ in III-18). To accomplish this, we will use the analytical expression for an analog differentiation circuit.

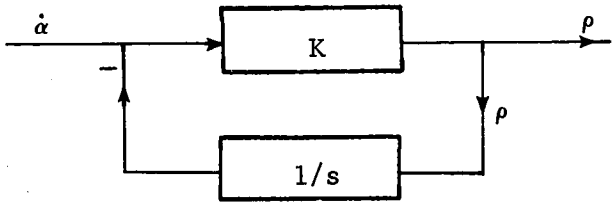

FIGURE III-2 DIFFERENTIATION CIRCUIT

With reference to Figure III-2, we observe that,

$$\rho = K\left(\dot{\alpha} - \frac{1}{s} \rho \right)$$

or

$$\frac{s\,\rho}{K} = s\,\dot{\alpha} - \rho$$

hence, $\ddot{\alpha} = s\,\dot{\alpha} = \rho\left(1 + \frac{s}{K}\right)$

Where, for K large, (with respect to $s = j\omega$), the desired expression for $\ddot{\alpha}$ is identified as the output variable, ρ, from the differentiation circuit.

Finally, it is pointed out that the tank fluid force is obtained from the λ vector as that constraint force necessary to enforce zero relative translation between the frames p_2 and q_2. Actually the output from the digital program gives this constraint force in the p_2 frame.

The mechanical analog discussed in this chapter has been implemented into a digital computer program (LAMPS3). A users guide for the program, with sample input and output, is presented in Appendix A.

IV. TEST/ANALYTICAL CORRELATION

This chapter presents a discussion of the Phase I and II test results, concentrating on Phase II results. The Interim Report (Reference 1) presented Phase I test results. In addition, this chapter presents a comparison of test and analytical results and comparisons of baffeled and smooth tank data. Appendix B presents all Phase II measured force time histories including a test log delineating applied accelerations for each test case.

A. OBSERVATIONS ON LIQUID MOTION

In addition to providing the force and center of mass motion needed for the analytical correlation, the experimental program provided some insight into the fluid dynamics of propellant reorientation. A brief survey of the current state-of-the-art in propellant reorientation will show how these tests extend the technology of this form of liquid motion.

Propellant reorientation has been studied for many years, primarily through the use of drop towers to simulate the low-g environment. Various parameters that influence the reorientation have been evaluated. Masica and Petrash (Reference 4) and Bowman (Reference 5) investigated reorientation in a flat-ended cylindrical tank while Salzman and Masica (References 6 and 7) considered a cylindrical tank with hemispherical domes, one of which was inverted. Reorientation in a spherical tank was investigated by Labus and Masica (Reference 8). All of this experimental work was performed using purely axial accelerations. Masica (Reference 9) also investigated the liquid motion produced by a purely lateral acceleration. By inclining the tank with respect to the acceleration vector, Bowman (Reference 10) considered the effect of an off-axis acceleration. However, the applied acceleration was still perpendicular to the initial gas/liquid interface. The initial condition for all of Bowman's tests was a flat gas/liquid interface, while in the other tests mentioned here a highly curved, near zero-g interface was established before applying the acceleration.

In all of these investigations the Bond number was used to categorize the liquid reorientation. It is the ratio of the gravity force to the surface tension force.

$$B_o = \frac{\rho a r^2}{\sigma}$$

where: ρ = liquid density

a = acceleration

r = tank radius

σ = liquid surface tension

When the interface is initially flat and the Bond number for the reorientation is less than 10, the motion of the liquid is along the tank wall. At larger values of Bond number, a central instability forms, whose size is a function of the Bond number. With this condition, a large portion of the liquid reorients through the center of the tank. However, with the initial low-g, highly-curved interface, the liquid motion was always totally along the tank wall for the range of Bond numbers evaluated (3 to 450).

When the tank was inclined at angles as small as one degree, the geometry of the tank relative to the interface influenced the liquid motion. The instability still formed in the center of the interface, but was laterally displaced so most of the flow was eventually along one side of the tank. Apparently the difference in interface curvature on opposite sides of the instability caused the force that produced its lateral displacement.

Another noteworthy experimental program was performed by arresting a free-falling tank (Reference 11). This allowed a larger tank and larger accelerations, yielding Bond numbers as large as 5800. When the acceleration was axial, the liquid motion was in the form of rain, traveling through the center of the tank. By laterally oscillating the liquid immediately before the test, off-axis effects were considered to some extent. At times, the liquid motion was along one side of the tank, depending upon when the tank was arrested in the slosh cycle.

The effect of ring baffles on the axisymmetric reorientation of the liquid in a cylindrical tank has also been evaluated (Reference 4).

1. Test with Baseline Tank - All of the Phase I tests, in this study, were conducted with the large tank which has smooth internal walls. In all cases, a lateral acceleration, acting parallel to the initial liquid interface, was applied. The test provided an evaluation of the influence of a true off-axis acceleration on the manner of reorientation.

In every case the liquid reoriented in an unsymmetrical manner, along one side of the tank. This was true for a wide range of lateral accelerations. In some of the tests, the lateral component was estimated to be 0.005g and lasted for a period of only 0.3 second at the beginning of the test. Compared to the axial component, the lateral component ranged from 5 % to 50%. Regardless, the manner of liquid motion remained essentially the same for all Phase I tests.

In those tests with the larger axial acceleration, the initial formation of an instability in the center of the interface was observed. It appeared as a hump in the surface that gradually joined the wall flow and disappeared. The size achieved by the instability was dependent on how long it had to grow before joining the wall flow.

As the liquid began to move, the liquid interface remained relatively flat so the motion appeared as a rotation of the interface about its center. This was most pronounced at the 25% and 50% liquid volumes. Once the leading edge of the flow reached the tank dome, the liquid interface began to acquire some curvature. In general, the liquid overshot its final equilibrium position, continuing on around the tank and recirculating a small percentage of the liquid. The liquid center of mass traveled beyond the equilibrium position and was coming to a stop as the test ended. If the test could have been continued, damped oscillation of the liquid about its equilibrium position would have been observed.

Very little splashing of the liquid was observed during the reorientation. The leading edge of the liquid strongly adhered to the tank wall and any turbulance was confined to the surface.

A typical test is shown in Figure IV-1. A small instability hump can be observed forming in the third photo, but by photo 4 it has joined the wall flow. In photo 5, the liquid has spread out and some of it is recirculating back to the initial position. At the end of the test (photo 6), the liquid is beyond the equilibrium position and some liquid is still being recirculated.

In all of the photos in this section, the axial acceleration is acting downward and the lateral acceleration acts to the left.

When the liquid volume was 75%, the reorientation was similar to that described above, except that the ullage assumed the form of a bubble and moved to the opposite end of the tank. The bubble followed the tank wall as it moved. Its surface was highly irregular due to the flow of liquid around it. At the end of the test, the bubble had become somewhat flattened and the center of gravity of the liquid had overshot the equilibrium position.

During the Phase II test program, two tests were performed in which only an axial acceleration was applied to see if the reorientation would be symmetrical. In one of the tests, the acceleration was in alignment with the tank axis. A sequence of photos from this test are shown in Figure IV-2. As expected, an instability formed in the center of the interface that had the shape of a hollow cylinder. By photo 3, the instability had become unsymmetrical and by photo 5, the bubble within the instability had grown so that most of the liquid was on the walls of the tank. At the end of the test (photo 6), the liquid was collected but was turbulent and numerous gas bubbles had been entrained. Some of the liquid was returning to the tank bottom.

In the second test, the tank was inclined at 45^{o}. The motion was similar to the above test but there was more distortion of the instability and more liquid recirculation due to the geometric configuration.

Based on these tests, it can be concluded that symmetric reorientation with its attendent instabilities and geysers as have been observed in past test programs, is a special case that is not very likely to occur in practice. Any lack of symmetry, caused by geometry or acceleration, will cause unsymmetrical reorientation of the liquid.

2. Tests with Baseline Tank Containing Baffles - Adding ring baffles to the large tank produces liquid motion much different than that observed in the tank with smooth internal walls. Three examples of the influence of the baffles are shown in Figures IV-3, IV-4 and IV-5.

As the leading edge of the liquid comes into contact with a baffle, the liquid is strongly deflected. Photos 2 and 3 of Figure IV-3 are the best example. The liquid was deflected by the lower baffle and it passed over the other baffles without

touching them. Photo 5 of the same test shows another deflection of the liquid after it had crossed the top of the tank. Some liquid was deflected back toward the tank bottom, but most of it was confined at the top of the tank by the upper baffle.

For the test shown in Figure IV-4 the leading edge of the liquid starts at the upper baffle but the liquid was still deflected away from the tank wall (Photo 2). At the end of the test there was more recirculation due to the relative orientation of the tank and the acceleration. Some liquid passed over the baffles and returned to the bottom of the tank (Photos 4 and 5).

In Figure IV-5 there was little deflection of the liquid as it first began to move. There was some deflection of the liquid (Photo 5) as it hit the baffles on the other side of the tank. However, this deflected liquid quickly recirculated so that most of the liquid was collected by the end of the test (Photo 6). The baffles were the most effective in this case and a minimum of turbulence was induced.

The motion presented in these photos is typical of the motion observed in all the baffled tank tests. As the leading edge of the liquid impacts a baffle, a significant deflection occurs. The baffles act to reduce the recirculation of the liquid that was observed in the tests with the smooth walled tank. It appears that the collection of the liquid at the equilibrium position is speeded, but added turbulence is induced.

3. Tests With Half-Sized Tank

The effective test time was increased by using the small tank which is one-half the size of the large tank. Two of the small tank tests are shown in Figures IV-6 and IV-7.

With the large tank, the liquid was observed to reorient, overshoot its equilibrium position and begin to come to rest. With the small tank the liquid reoriented, overshot the equilibrium position and came to a stop, and then moved back towards equilibrium again. It was nearly at rest at the equilibrium location at the end of the test. It appears that if additional test time were available there would be a small amount of liquid motion as it stabilized in its final position.

The portions of the reorientation that are common between the large and small tank appear the same. For example, compare the photos of Figure IV-1 with the first five photos of Figure IV-7. In both Figures IV-6 and IV-7, Photo 5 shows the liquid as it came to rest after overshooting the equilibrium position. Photo 6 shows the liquid as it nears the equilibrium position at the end of the test.

In all the tests the liquid became well collected as it was returning to the equilibrium position following the overshoot. Any liquid that broke away from the leading edge and recirculated, continued on around the tank and rejoined to form a single liquid mass.

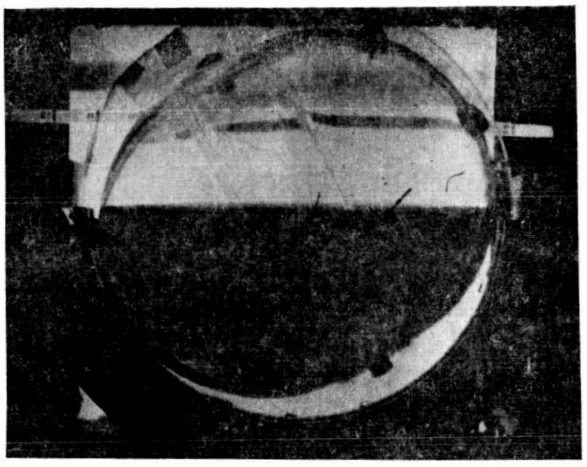

1

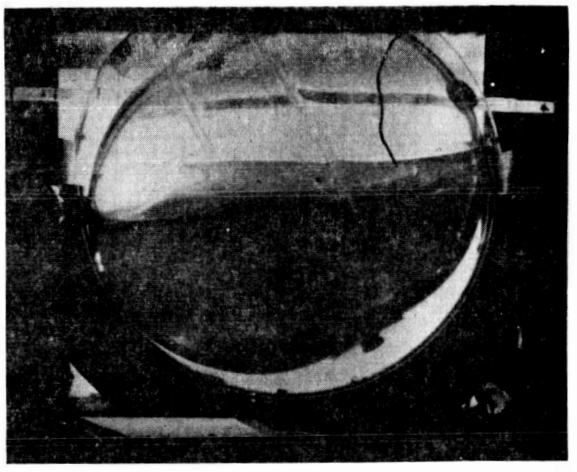

2

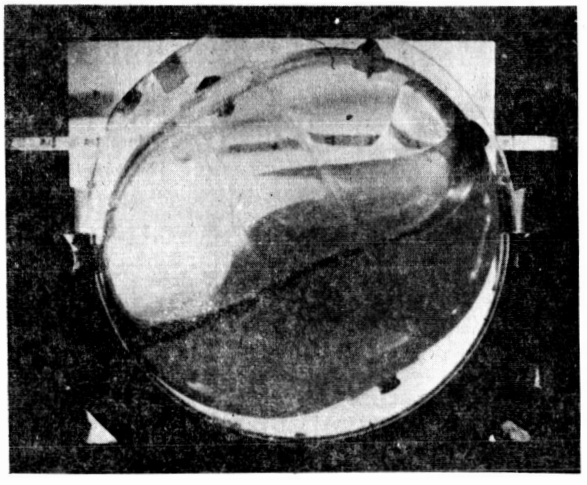

3

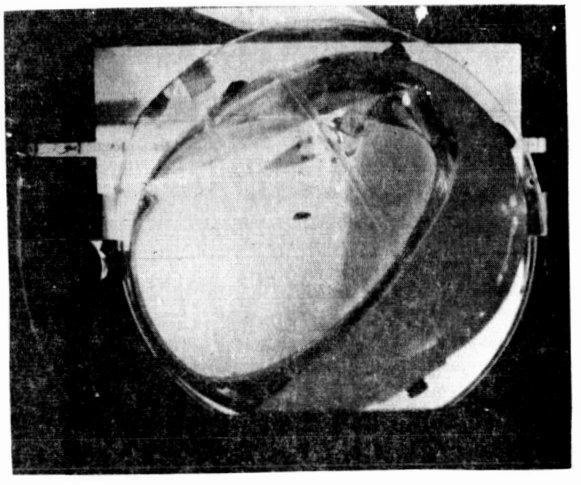

4

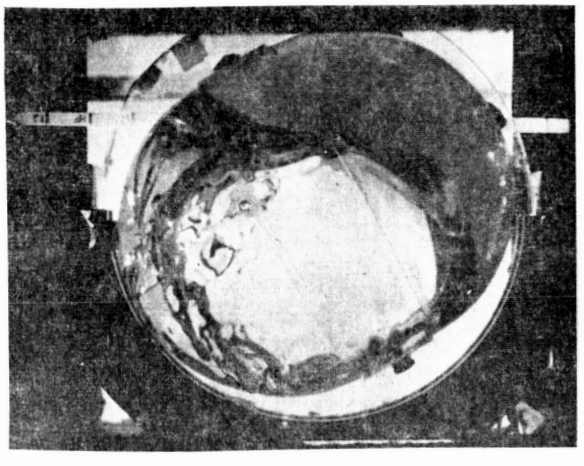

5

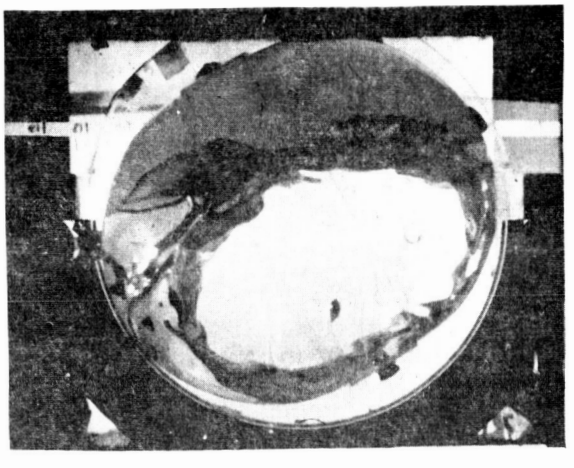

6

Figure IV-1. Test 8 , Phase I ; 50 % fill ; $\theta x = 60^\circ$; Aa= .045

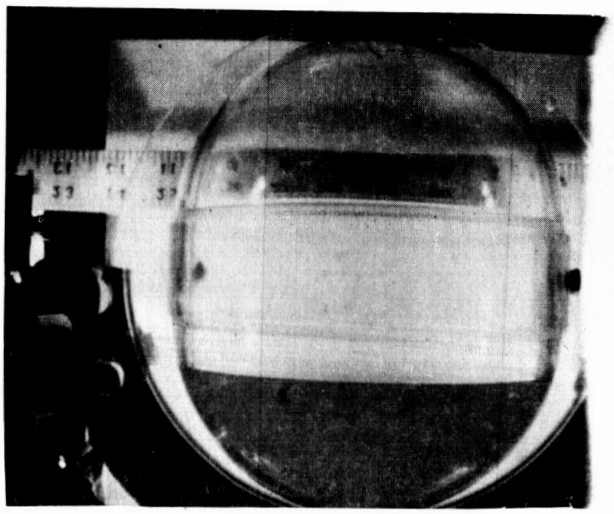

1. 0.0 sec

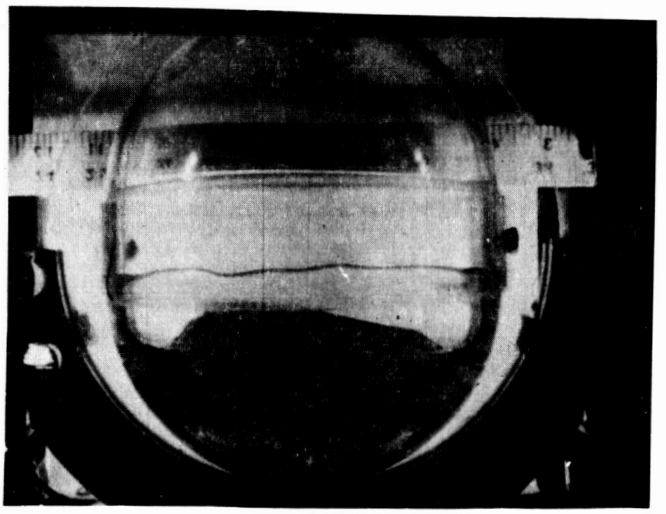

2. 0.4 sec

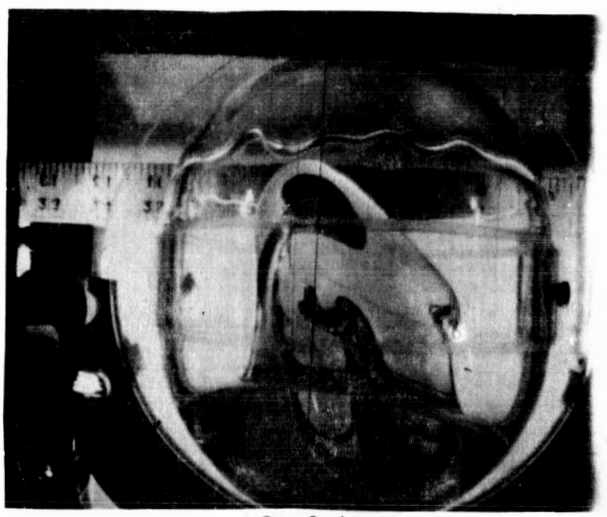

3. 0.6 sec

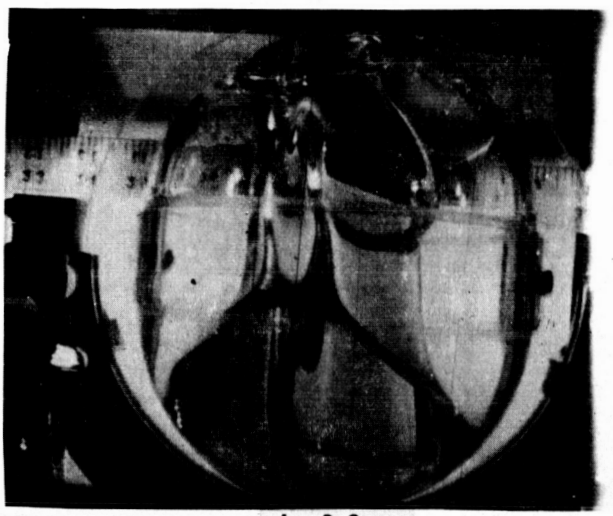

4. 0.8 sec

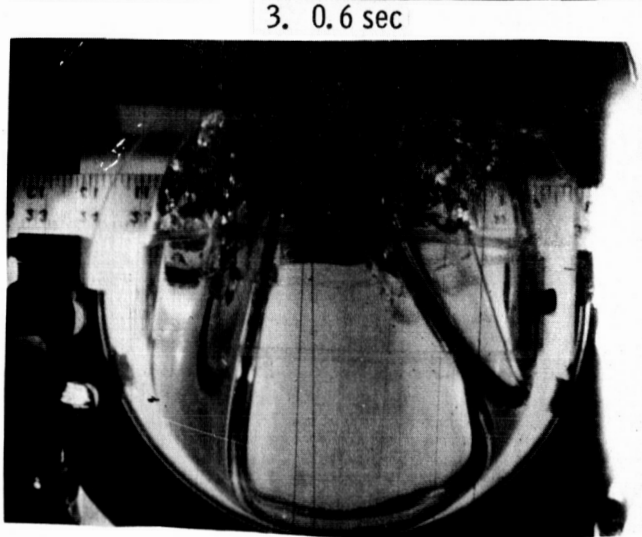

5. 1.1 sec

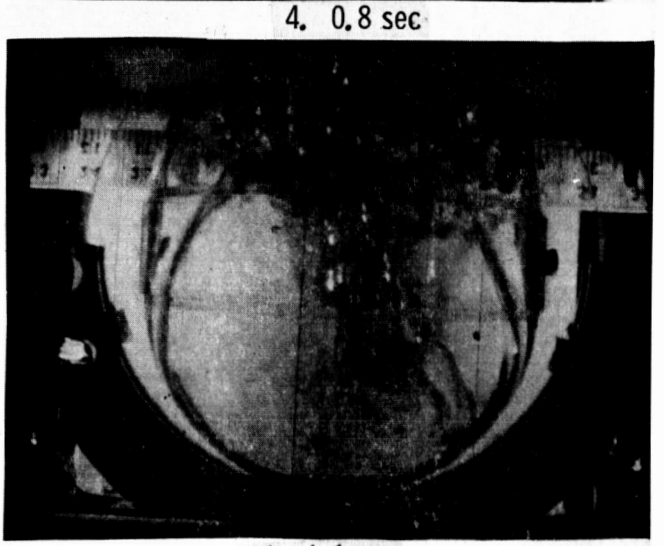

6. 1.6 sec

Figure IV-2. Test I, Phase II; 25 % fill; $\theta x = 0^\circ$; Aa= 0.084; no lateral acceleration

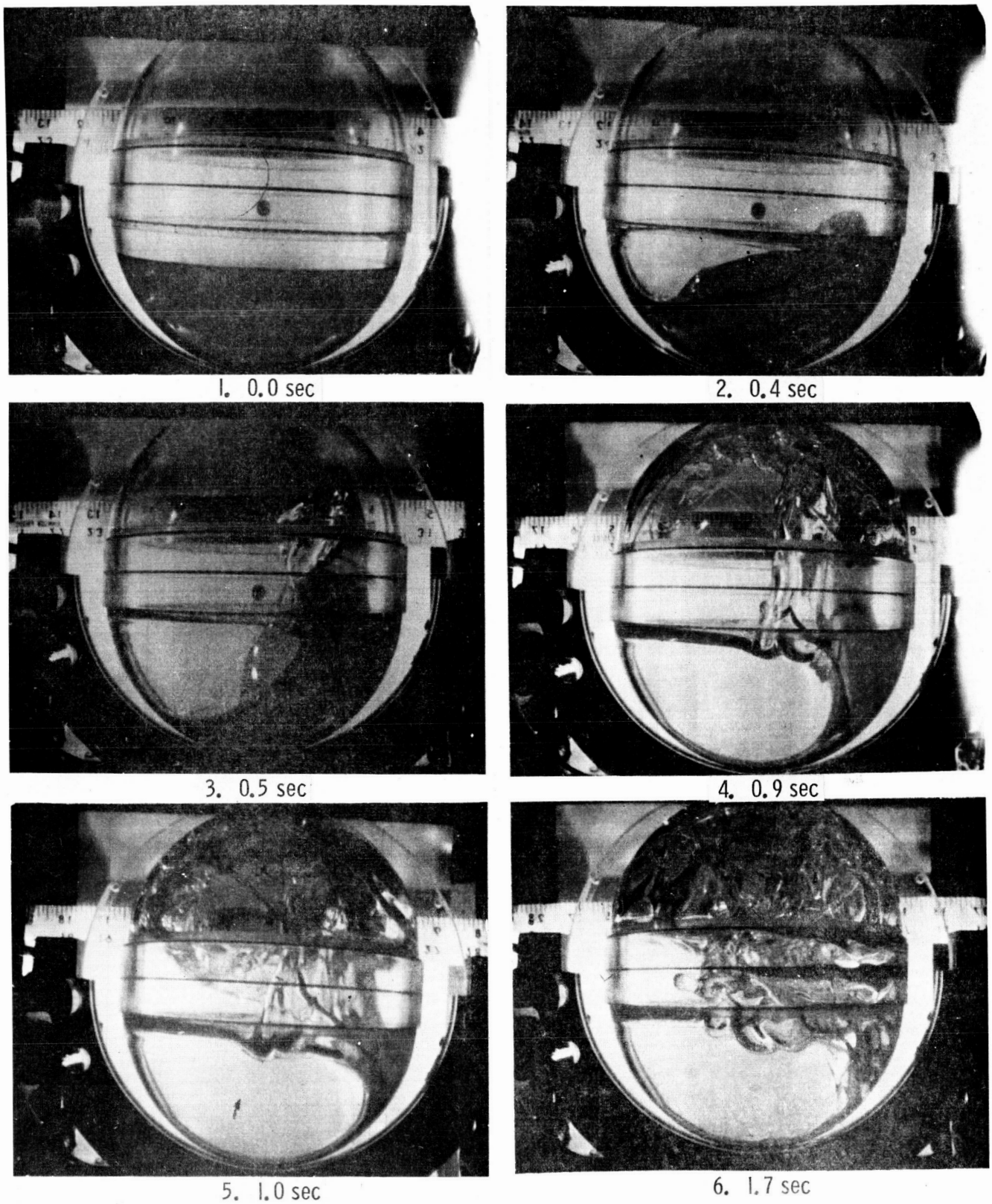

Figure IV-3. Test 6 , Phase II ; 25 % fill ; $\theta x = 0^{\circ}$; Aa= 0.074

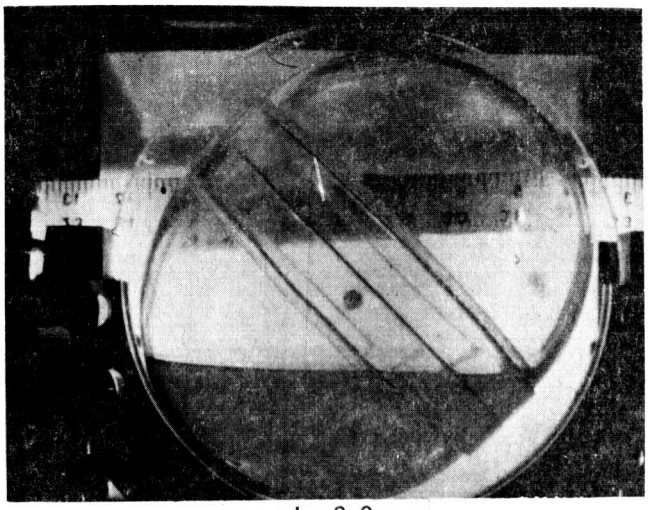

1. 0.0 sec

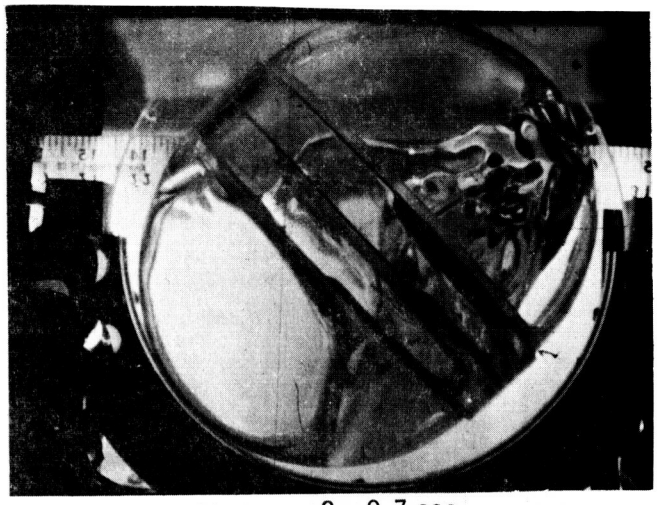

2. 0.7 sec

3. 0.9 sec

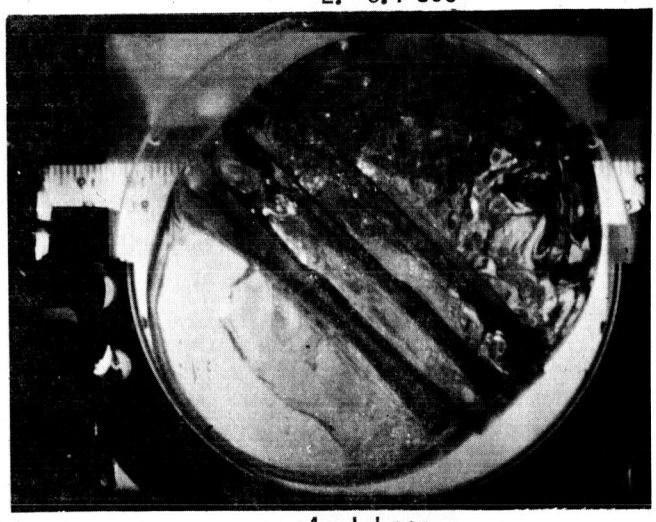

4. 1.1 sec

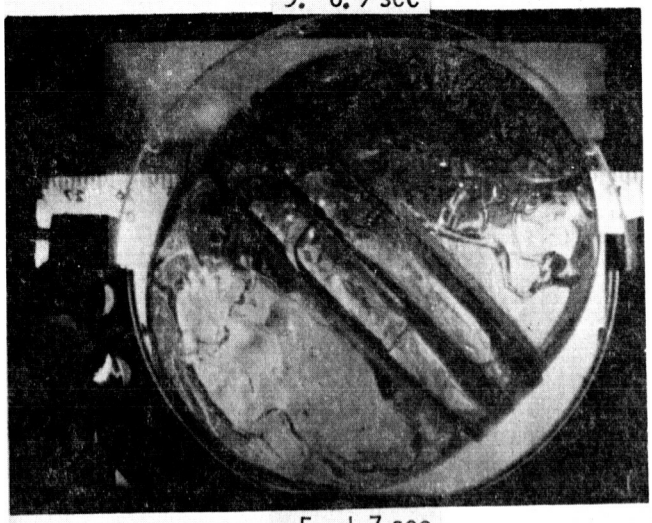

5. 1.7 sec

Figure IV-4. Test 7, Phase II; 25 % fill; $\theta x = 45°$; Aa= 0.074

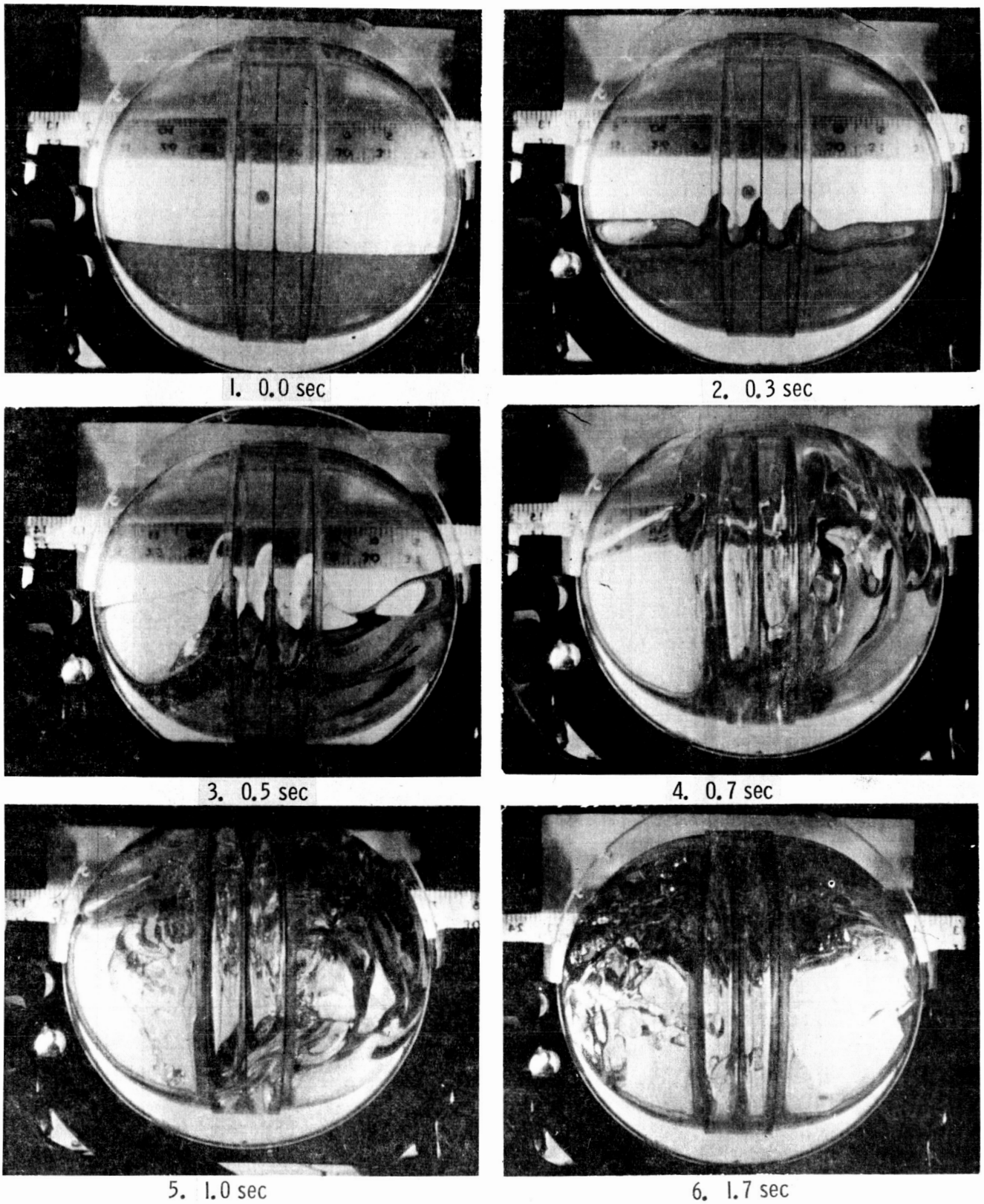

1. 0.0 sec

2. 0.3 sec

3. 0.5 sec

4. 0.7 sec

5. 1.0 sec

6. 1.7 sec

Figure IV-5. Test 8 , Phase II ; 25 % fill ; $\theta x = 90^\circ$; Aa=0.075

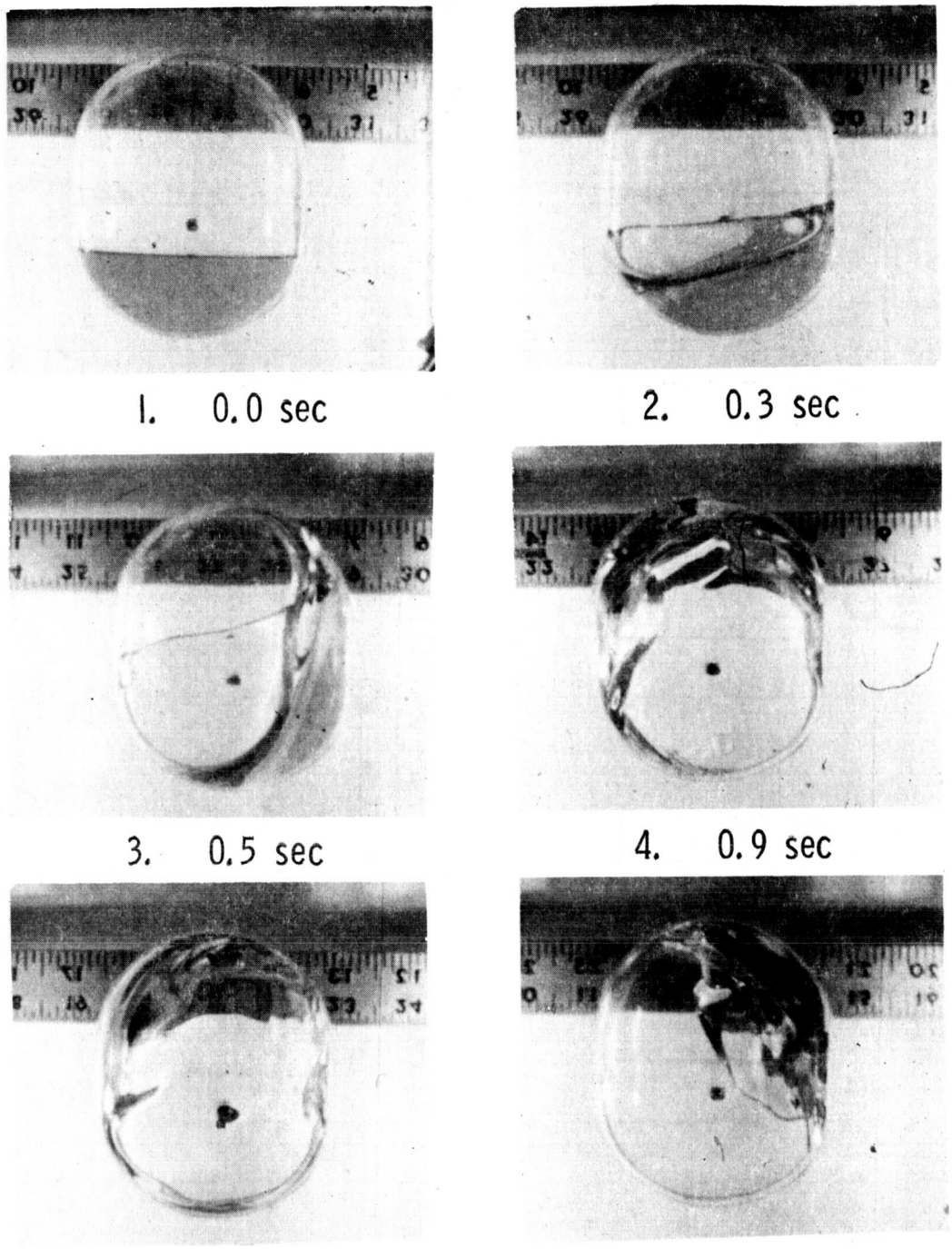

1. 0.0 sec
2. 0.3 sec
3. 0.5 sec
4. 0.9 sec
5. 1.2 sec
6. 1.7 sec

Figure IV-6. Test 15 - Phase II , 25 % fill , $\theta x = 0^\circ$, Aa= .074

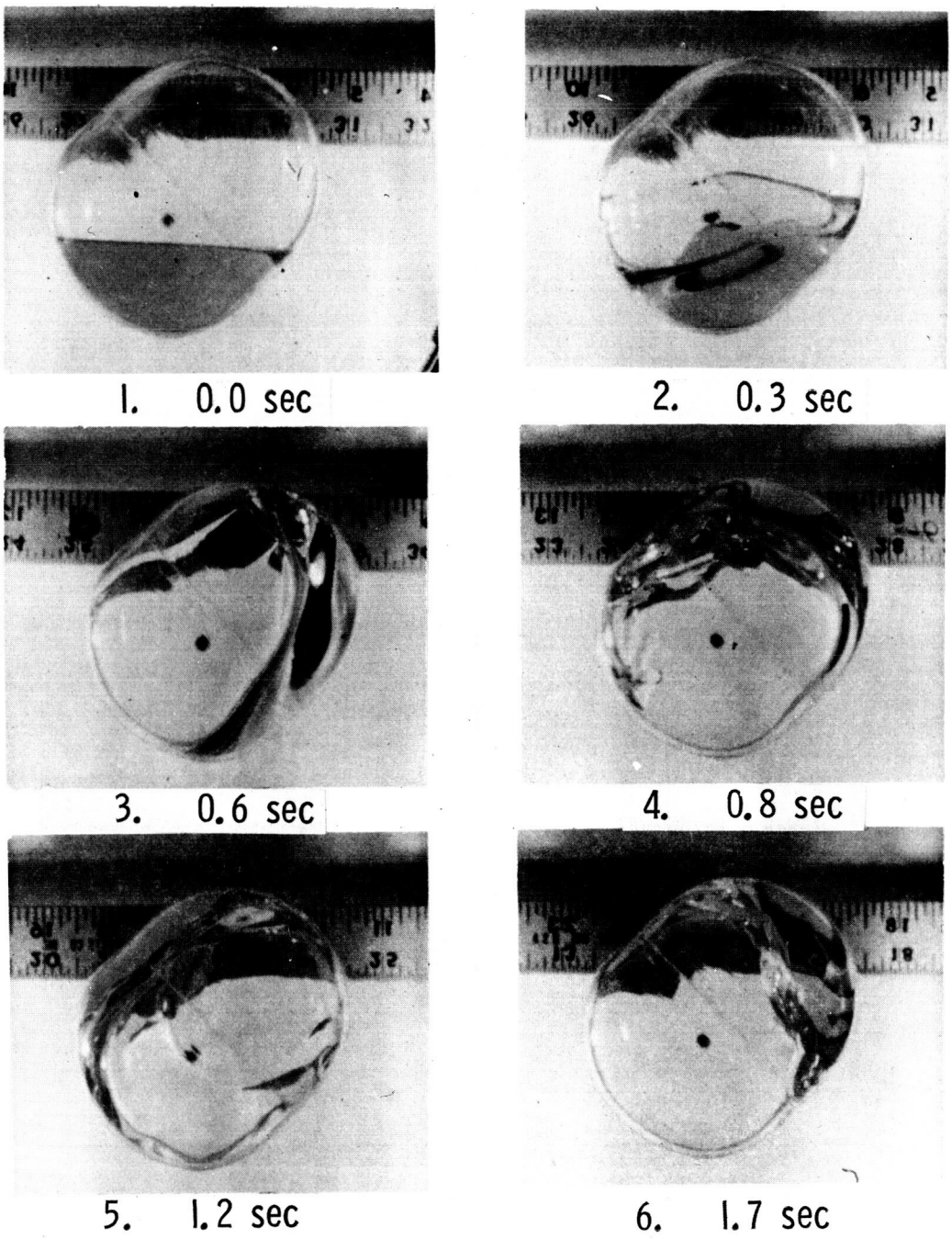

1. 0.0 sec
2. 0.3 sec
3. 0.6 sec
4. 0.8 sec
5. 1.2 sec
6. 1.7 sec

Figure IV-7. Test 16 - Phase II , 25 % fill , $\theta x = 45^\circ$, Aa= 0.074

B. DISCUSSION OF TEST/ANALYTICAL CORRELATION

This section presents a qualitative discussion of several aspects of the analytical model based on analysis of the test force data and photographic records. In particular, the concepts of effective liquid mass and fluid damping will be discussed in detail. Subsequent sections will present comparisons between analysis, test, Phase I and Phase II results.

1. Liquid Effective Mass - Phase I test/analytical correlation, as presented in Reference 1, always showed analytical force predictions to be of a larger magnitude than measured forces. The force exerted on the tank by the moving liquid is composed of two components: 1) a centripetal acceleration force due to liquid velocity, and 2) the D'Alembert force due to the applied acceleration field. In addition to this inertial reactive type force, there may also be a viscous dissipative force due to friction between the moving liquid and the tank wall.

During Phase I investigations, it was thought that the overall magnitude of liquid forces could be reduced by increasing this viscous dissipative force, thereby reducing the liquid velocity and decreasing the centripetal acceleration component of force. Subsequent analyses indicated that, indeed, the liquid forces were reduced, however, the decrease in liquid velocity degraded the time correlation of peak forces when comparing analytical and measured data. Increasing the viscous dissipative force enough to reduce the analytical force peaks to match measured data resulted in unacceptable time delays in the peak analytical force. Initial Phase II studies attempted to define this viscous dissipative force in a manner which would improve correlation in force magnitudes while maintaining time correlation. These efforts proved unsuccessful.

Damping investigations eventually lead to the development of the concept of liquid effective mass. Indepth studies of photographic records of the drop tests revealed that during liquid reorientation, the liquid begins to assume a somewhat curved interface as it accelerates, resulting from expansion of the liquids surface area. This characteristic can be observed in Figures IV-1, IV-6 and IV-7. Analytically breaking the liquid into finite sections, as shown in Figure IV-8, reveals that each segment exerts a centripetal acceleration force on the tank, perpendicular to its velocity vector. From Figure

IV-8, it is obvious that the net centripetal acceleration force exerted on the tank is less than that obtained by lumping the total liquid mass at the liquid center of mass (cm).

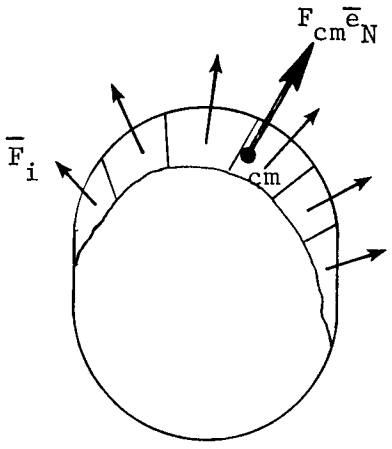

$$\sum \bar{F}_i \Big|_{\bar{e}_N \text{ direction}} < F_{cm}\,\bar{e}_N$$

where:

$\bar{e}_N$ = unit normal vector to the constraint surface at the liquid cm

$\bar{F}_i$ = segment centripetal acceleration forces

F_{cm} = centripetal acceleration force resulting from lumping total mass at liquid cm

Figure IV-8. Liquid Effective Mass Justification

Based on test results, the effective mass appears to be a function of tank percent fill volume. It may also be a function of tank L/d, however, all tests were run with similar aspect ratio tanks so this functionality cannot be assessed here.

Figure IV-9 delineates the liquid effective mass factor which when applied to the centripetal acceleration component of liquid force, best reproduces the test results. The effective mass factor (expressed as a percentage of the total liquid mass) is presented as a function of tank fill volume.

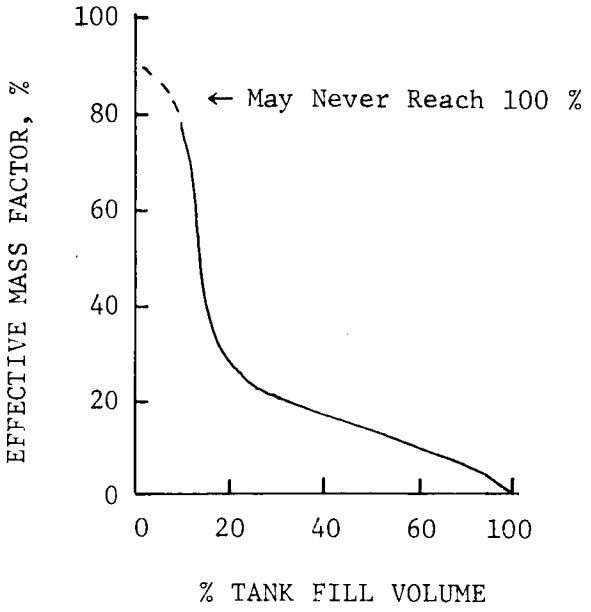

Figure IV-9. Liquid Effective Mass Factor

The moving liquid force can be expressed as:

$$F = MASFAC * F_{CENT} + F_{D'ALEMBERT} \qquad (IV-1)$$

where: MASFAC = effective mass factor (Figure IV-9)

F_{CENT} = centripetal acceleration force component

$F_{D'ALEMBERT}$ = D'Alembert force component

Note that the effective mass factor is only applied to the centripetal acceleration component of liquid force; the velocity dependent part. When the liquid totally reorients and comes to rest, velocity equals zero, the force exerted by the liquid is equal to:

$$F = -M_{LIQUID} A_{APPLIED}, \qquad (IV-2)$$

the D'Alembert force, where M_{LIQUID} is the total liquid mass.

Application of the effective mass factor in the analytic model resulted in good correlation between analytical and

measured force magnitudes, while maintaining good time correlation of peak forces. The curve of effective mass factor in Figure IV-9 is based on tests ranging from 10% to 75% tank fill volumes. As the fill volume increases, the centripetal acceleration force component decreases drastically due to the nature of the reorientation. At 75% fill volumes, the liquid was observed to flow around a bubble formed by the ullage gas which tended to traverse the tank wall. This behavior results in smaller liquid velocities and, therefore, decreased centripetal forces. On the other hand, in the 10% fill case, the centripetal force tended to approach the value based on the total liquid mass. Intuitively, based on test results, it is doubtful that an effective mass factor of 100% is ever reached.

2. Liquid Damping - Two criteria exist for evaluating the worth of the analytical model; one is the force time history comparison and the second is how well the analytic liquid cm position compares with the liquid motion photographically recorded during the tests. As discussed above, the effective mass factor provides good force magnitude correlation, and peak force timing appears to correlate well without any viscous dissipative forces applied. However, a study of the drop test films indicates that, through some mechanism, the energy of the moving liquid is dissipated. It appears that the liquid is slowed by a continuity phenomena. That is to say, as the liquid velocity builds, the liquid crossectional area decreases, increasing the liquids surface area. This expansion of the liquids' surface area appears to convert flow energy into strain energy (surface area tends to maximize), thus slowing the liquid. This expansion is especially evident as the liquid traverses the tank dome. The expansion appears to include some out of plane flow since the liquid in the tests was not physically constrained to two dimensions. As the liquid slows, a contraction process occurs, resulting in minimum surface area as the liquid comes to rest. This expansion and contraction is best delineated by the small tank reorientations shown in Figures IV-6 and IV-7.

Phase II comparisons of liquid cm position compared to film records of various tests, indicated that some dissipative force was required to maintain a reasonable liquid cm time history correlation. Obviously, a point mass model cannot hope to actually represent the expansion and contraction phenomena discussed above. However, a compromise has been found which appears to maintain a realistic center of mass location, during reorientation, without degrading force magnitude or force/time

correlation. The photographic records indicate that the liquid expands and slows the most as it traverses the tank dome. To represent this phenomena, a dissipative force of the form, $f = \mu / \dot{\beta} /$, has been incorporated in the analytical model. In this formulation $\dot{\beta}$ is the angular rate (RADIANS/SEC) of the liquid cm as it orbits the center of the tank on the elliptical constraint surface (see Figure IV-10). The parameter, μ, is the "damping" coefficient. It has been found that a value of $\mu = .00002$, provides satisfactory center of mass location correlation for both the baseline tank (Phase I) and the half size tank (Phase II). This correlation is presented in Figures IV-11 through IV-16. In these tests the analytic liquid cm position maintains fairly good correlation with the intuitive cm location. Since the dissipative force, f, is not intended to represent a wall friction effect, it is not included in liquid force calculations. It is only used as a force on the liquid cm to dissipate flow velocity. It is felt that liquid/wall friction forces are extremely small compared to inertial reactive forces between the tank and liquid.

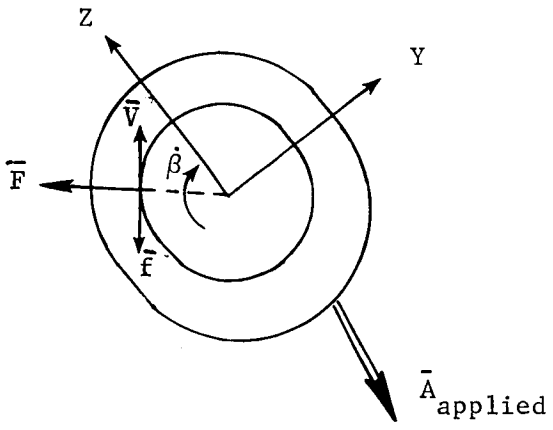

where: $\bar{f}$ = liquid dissipative force, $f = \mu / \dot{\beta} /$

$\bar{F}$ = inertial reactive force between the tank and liquid

$\bar{V}$ = liquid velocity vector

Figure IV-10. Liquid Damping Visualization

It is not known whether the value of μ used in analysis of the test cases is applicable for a large class of tanks. It would appear that the value would have to be a function of tank size and perhaps other variables. However, based on the limited parametric variations in the Phase I and Phase II tests and the small size of the tanks, a definitive evaluation of the functional characteristics of μ could not be conducted. Further

data utilizing much larger tanks is required. However, it should be noted that neglecting the dissipative force, all together, results in conservative force magnitudes which may be sufficient for some analyses.

3. Constraint Surface Definition - The mechanical analog developed during Phase I investigations portrayed the liquid as a point mass moving on a constraint surface which was determined by rotating the tank (analytically) in a one-g field; the constraint surface was defined as the locus of center of mass locations prescribed during the rotation, assuming the free surface was planar. This constraint surface was approximated by piecewise continuous elliptical segments. When the liquid cm deviated some tolerance from the constraint surface, the elliptical coefficients were updated to return the liquid cm to the desired surface. During Phase II it was decided to alter the constraint surface definition slightly. It was found that updating the elliptical coefficients resulted in slight analytical force discontinuities. To correct this problem, the constraint surface is now defined as the ellipsoid which best fits the constraint surface discussed above. Hence, for any given tank geometry and fill volume, the constraint surface is approximated by a single set of elliptical surface coefficients; no updating is performed. Comparisons have shown that this does not substantially alter the analytical liquid forces, but does clean up the analytical results.

4. Test/Analytical Comparisons - Bare Tank - Utilizing the concepts of effective liquid mass and liquid damping discussed above, the analytical model (computer program LAMPS, Reference 1) was used to simulate several Phase I (large tank) and Phase II (small tank) tests to assess the degree of correlation. Figures IV-11 through IV-13 present the correlation for three Phase I (1974) tests: 13, 16 and 17. Tests 13 and 16 (Figures IV-11 and IV-12) were conducted using the baseline tank (2.5 inch radius) and a 25% fill volume. Test 17 (Figure IV-13) was conducted with the same tank and a 50% fill volume. The figures present an overlay of analytical and test force time histories in the Y and Z directions (tank axis system). In addition, sketches are presented which depict the liquids' cross sectional shape, traced from film recordings, overlayed with the analytical liquid cm position. For these tests the correlation of both force and liquid cm position is very good.

In the Phase II test program, a half sized tank (1.25 inch radius) was used to repeat several of the 1974, Phase I

tests. Use of the half sized tank results in a greater equivalent test time. Figures IV-14 through IV-16 present analytical correlations for three of these small tank tests. Tests 15 and 16 (Figures IV-14 and IV-15) were run using a 25% fill volume and correspond to tests 13 and 16 (respectively) in the Phase I test program using the large tank. Test 21 (Figure IV-16) was run with a 25% fill volume and approximately twice the lateral acceleration of Test 16 (Phase II).

The forces due to the moving liquid in the small tank tests are much smaller than those in the Phase I tests. Consequently, the sensitivity settings of the charge amplifiers for the load cells were greatly increased to insure adequate force resolution. The load cells are susceptible to thermal drift from the drop capsule lighting system and the increased sensitivity, required for the small tank appears to have resulted in some drift, even though the load cells were insulated. Figures IV-14 through IV-16 show fair force correlation for the small tank tests.

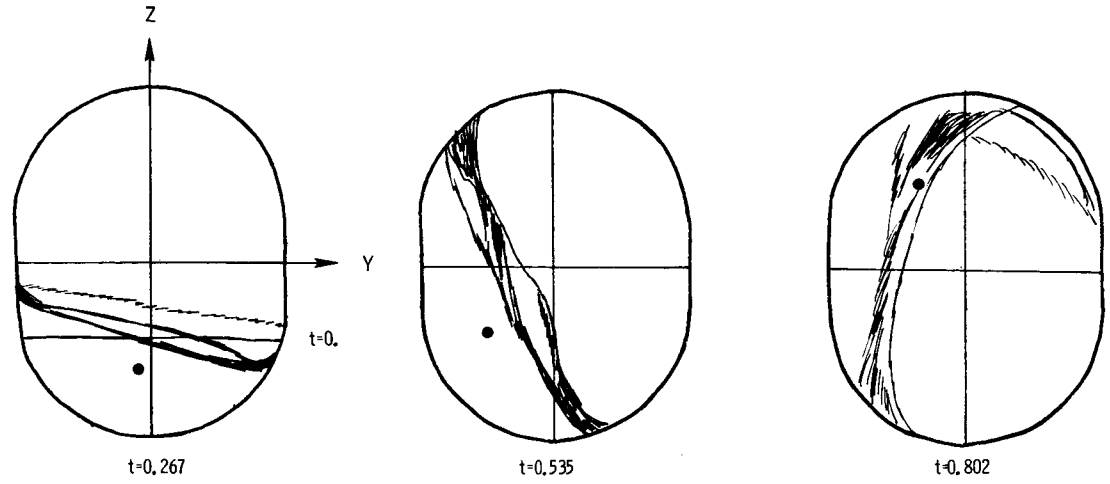

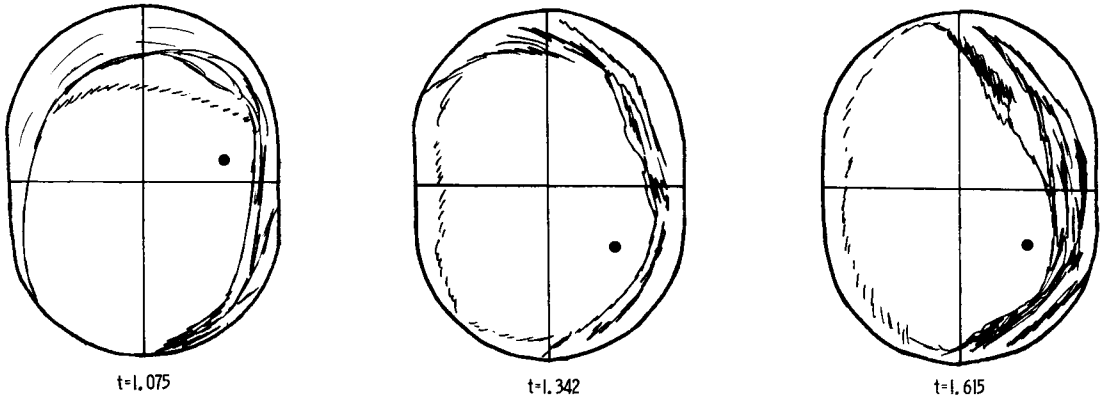

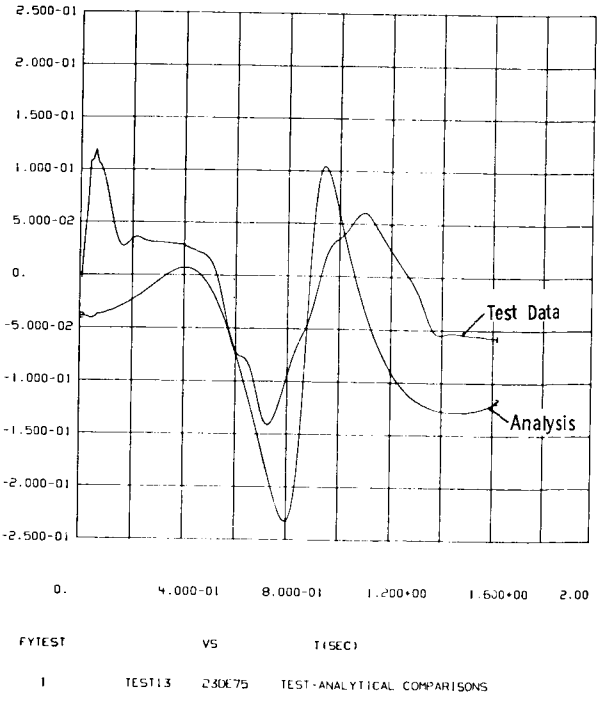

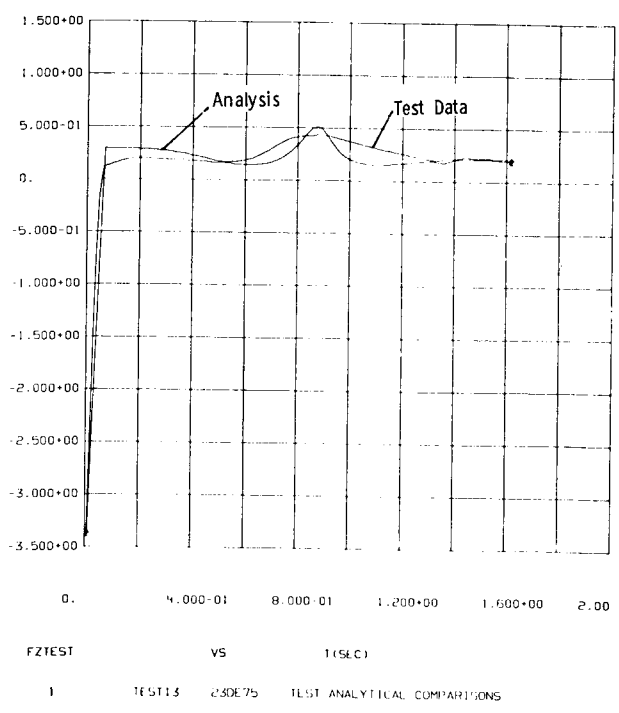

Figure IV-11. Test/Analytical correlation- Phase I Test 13
tank radius= 2.5 in.; 25 % fill volume; $\theta x = 0°$

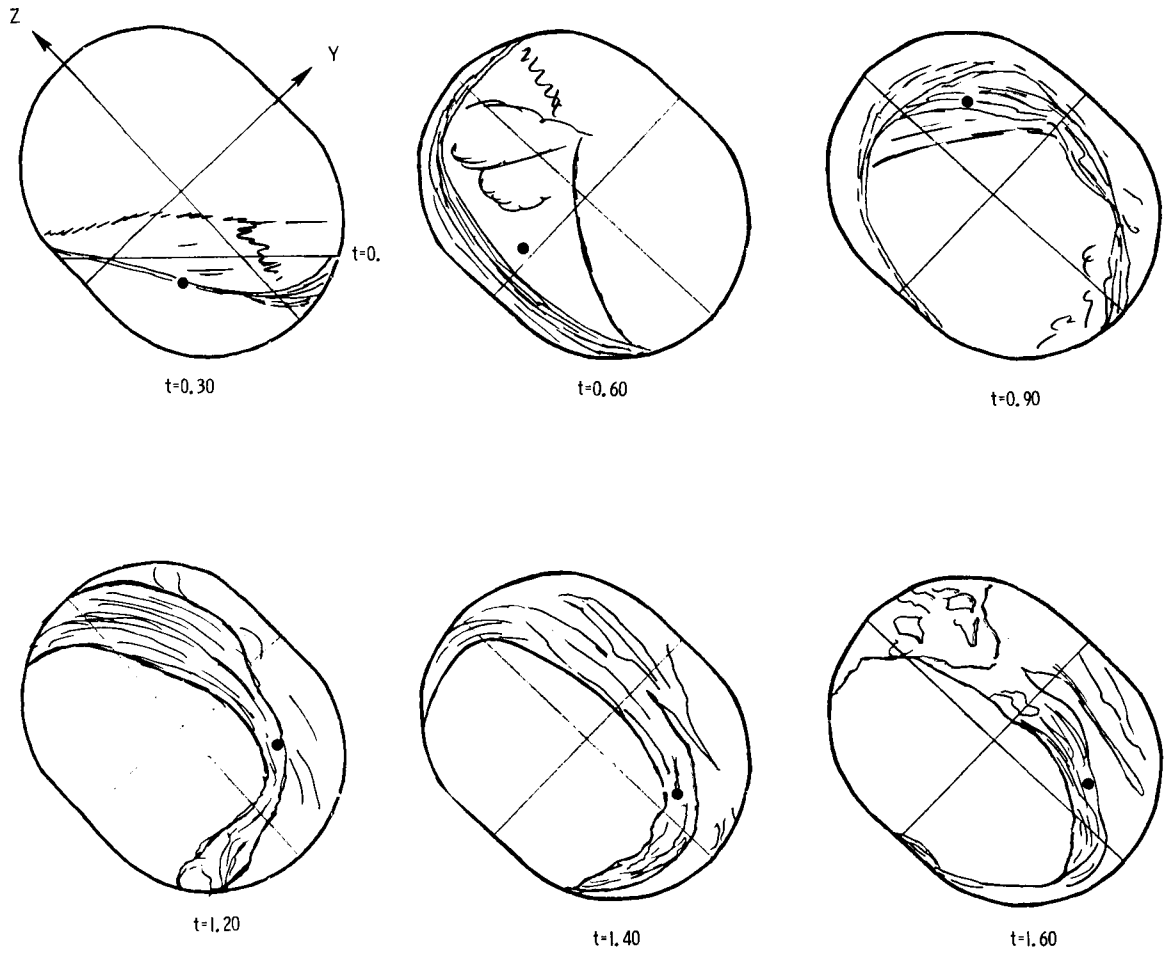

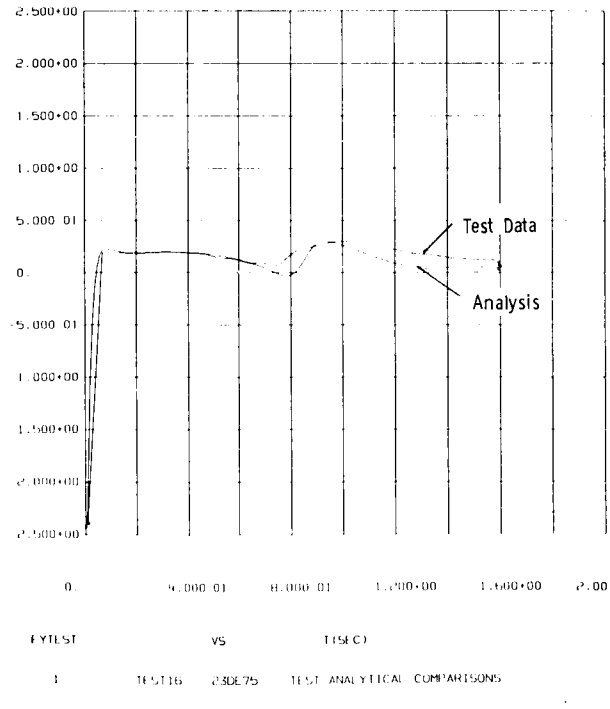

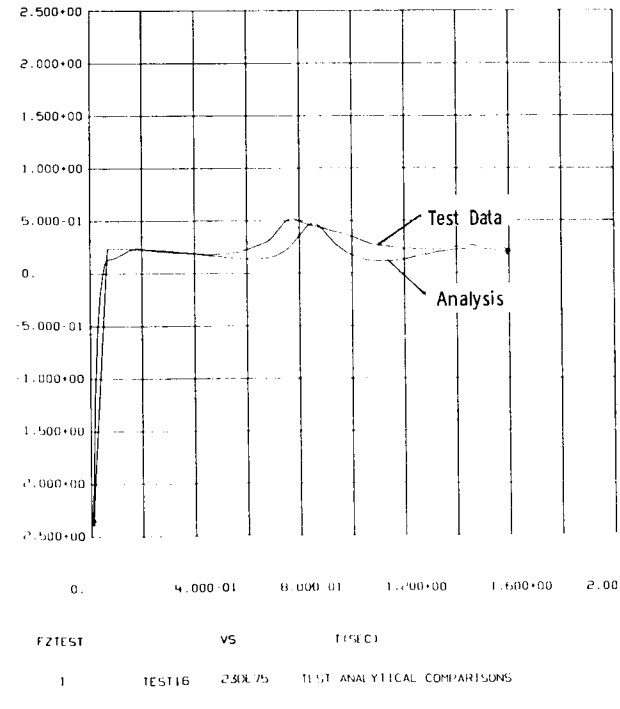

Figure IV-12. Test/Analytical correlation- Phase I Test 16
tank radius= 2.5 in.; 25 % fill volume; $\theta x = 45^{\circ}$

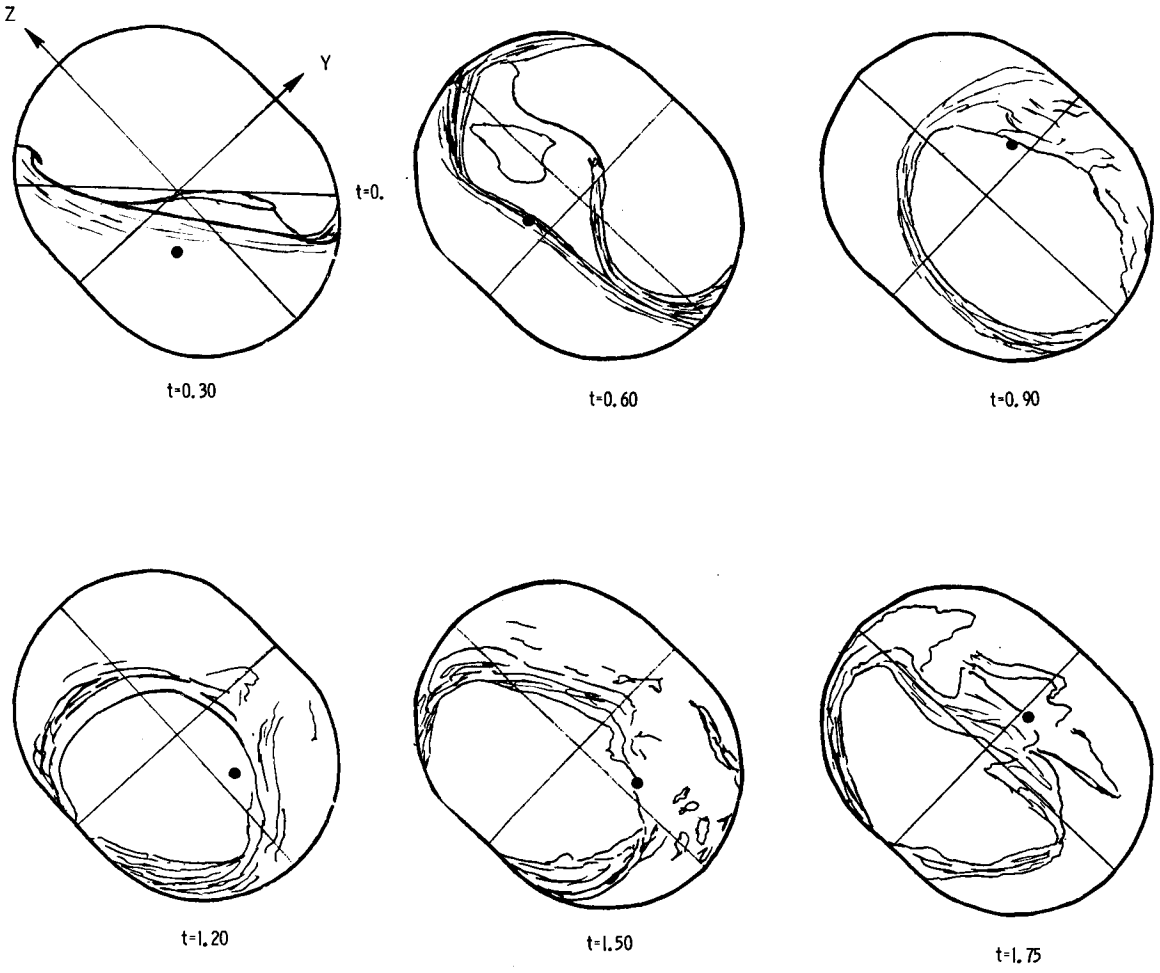

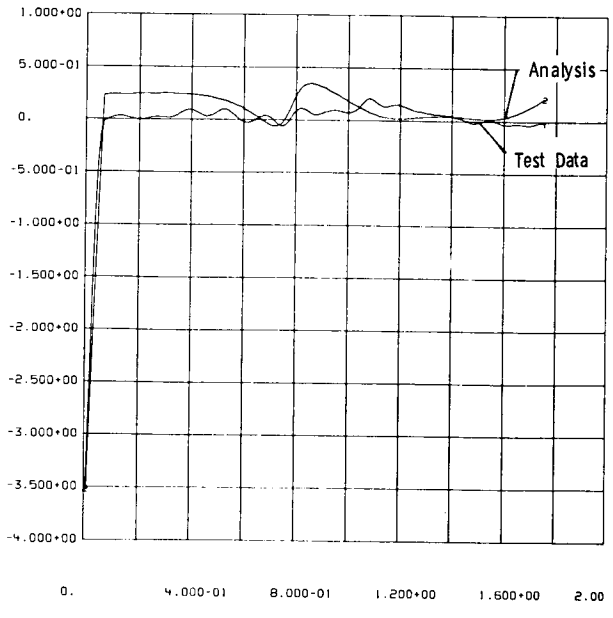

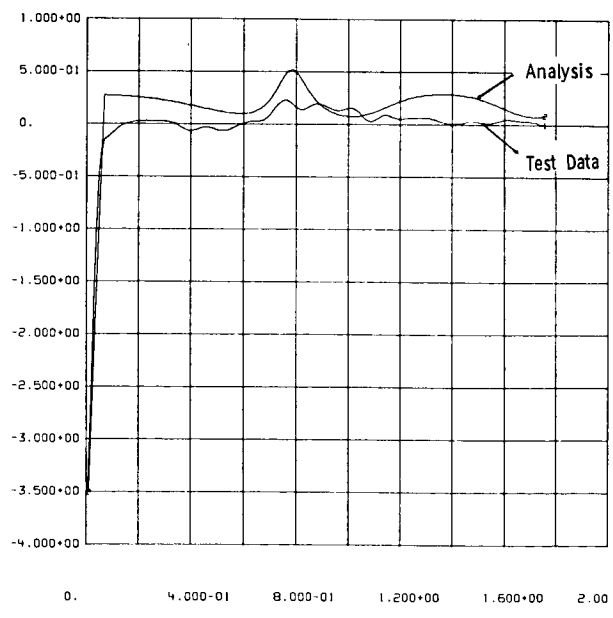

Figure IV-13. Test/Analytical correlation- Phase I Test 17
tank radius= 2.5 in.; 50 % fill volume; $\theta x = 45^\circ$

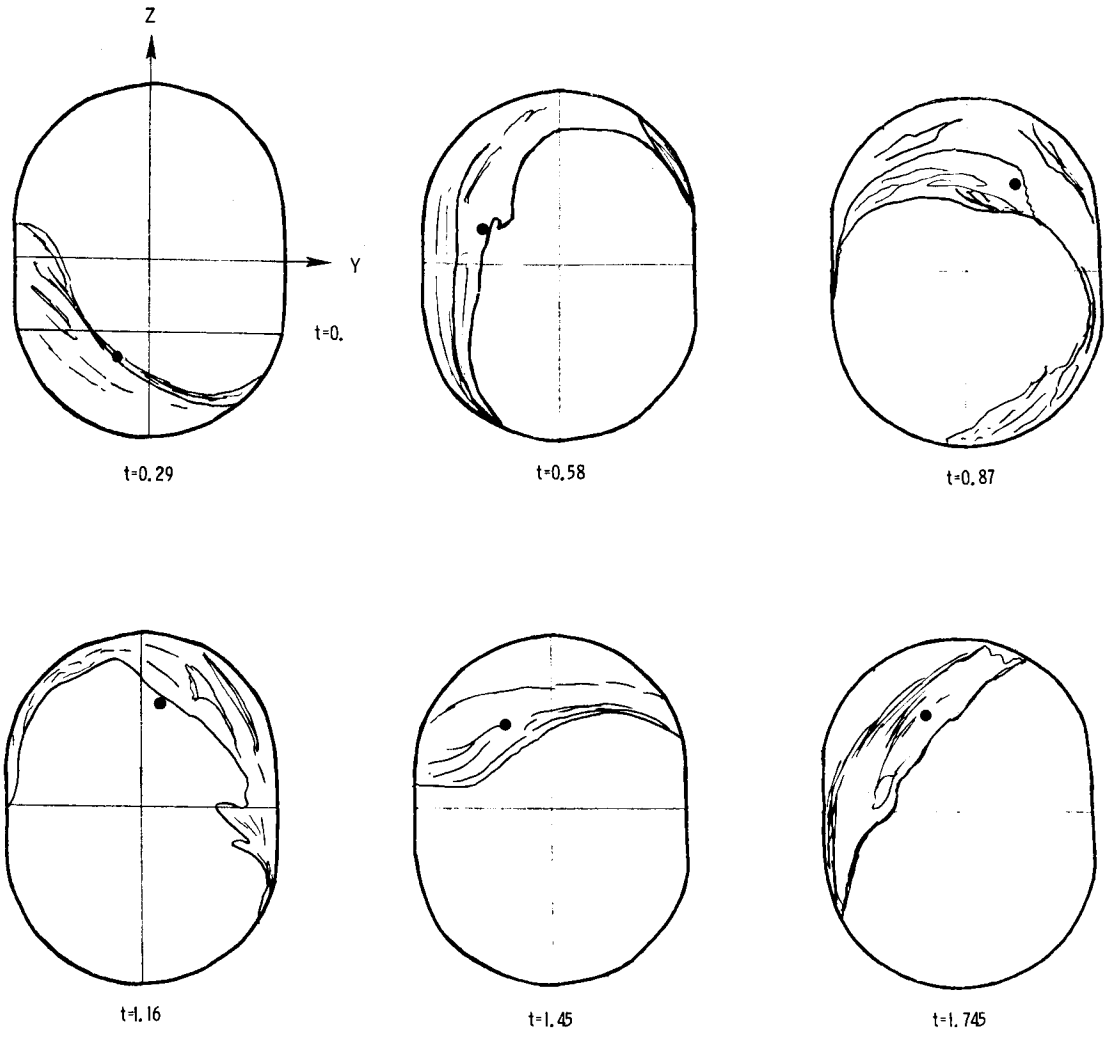

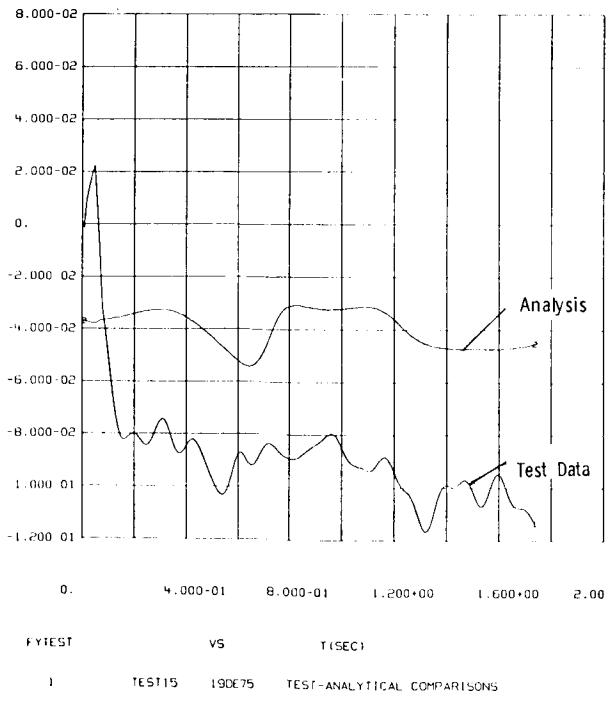

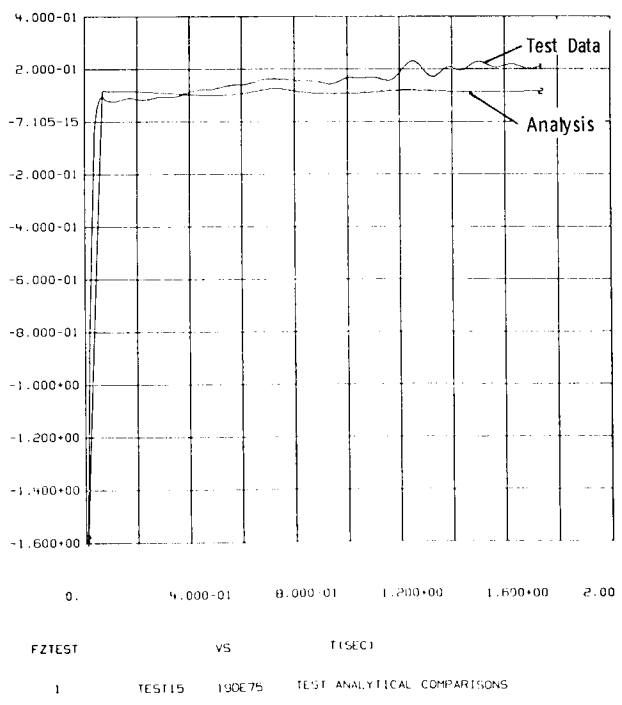

Figure IV-14. Test/Analytical correlation- Small Tank , Test 15
tank radius= 1.25 in.; 25 % fill volume; ex= 0°

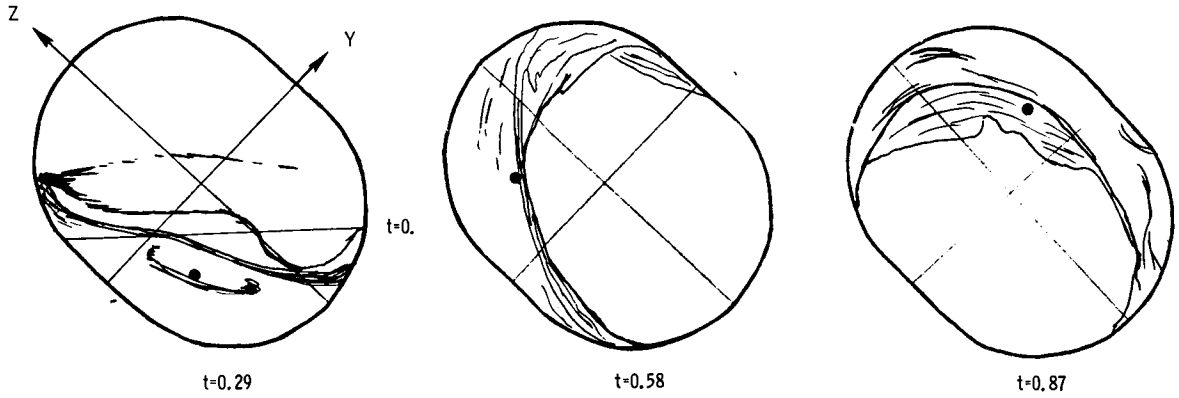

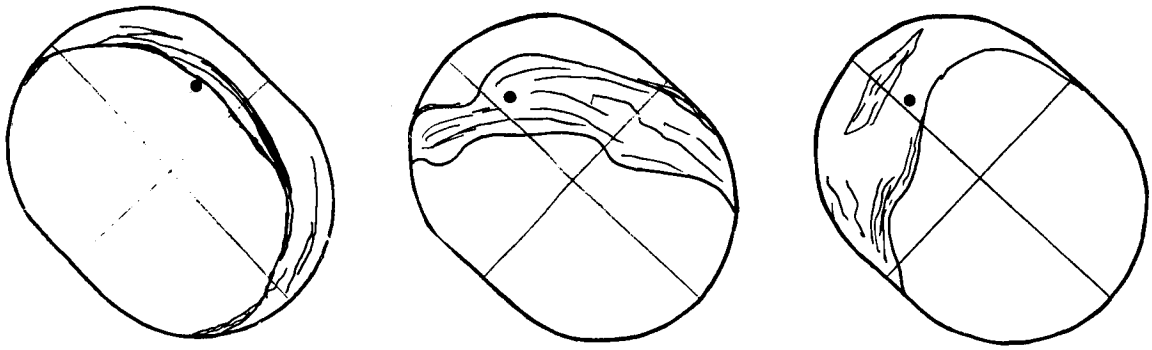

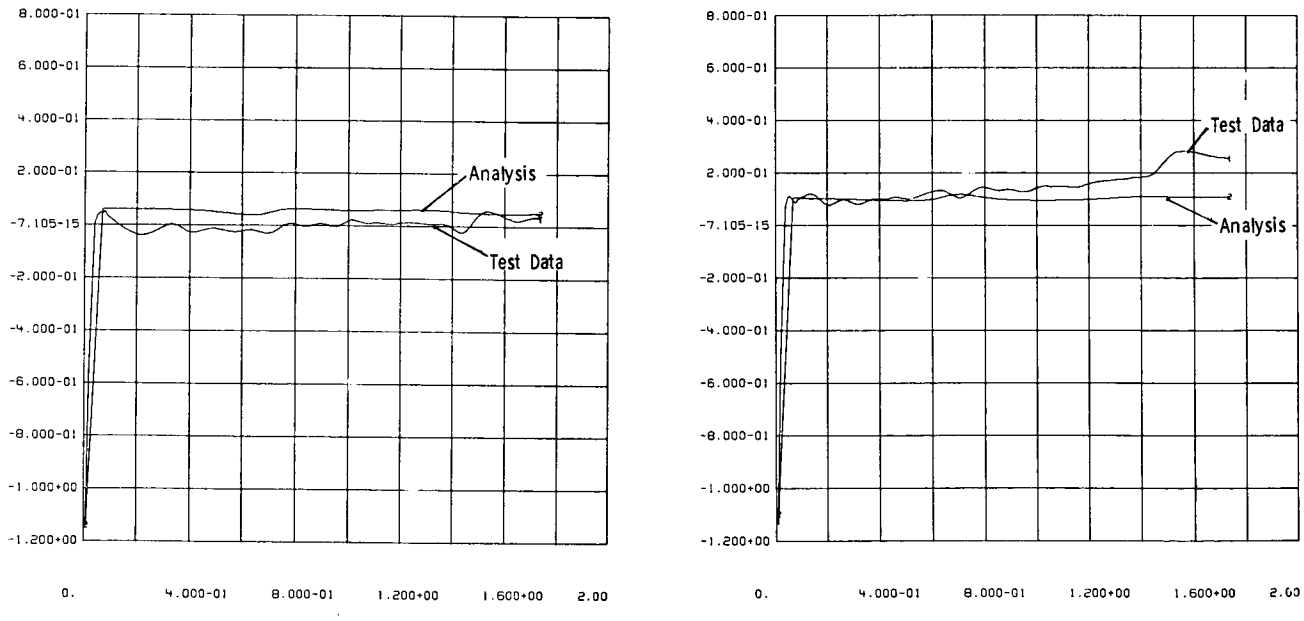

Figure IV-15. Test/Analytical correlation- Small Tank , Test 16
tank radius= 1.25 in.; 25 % fill volume; $\theta x = 45^{\circ}$

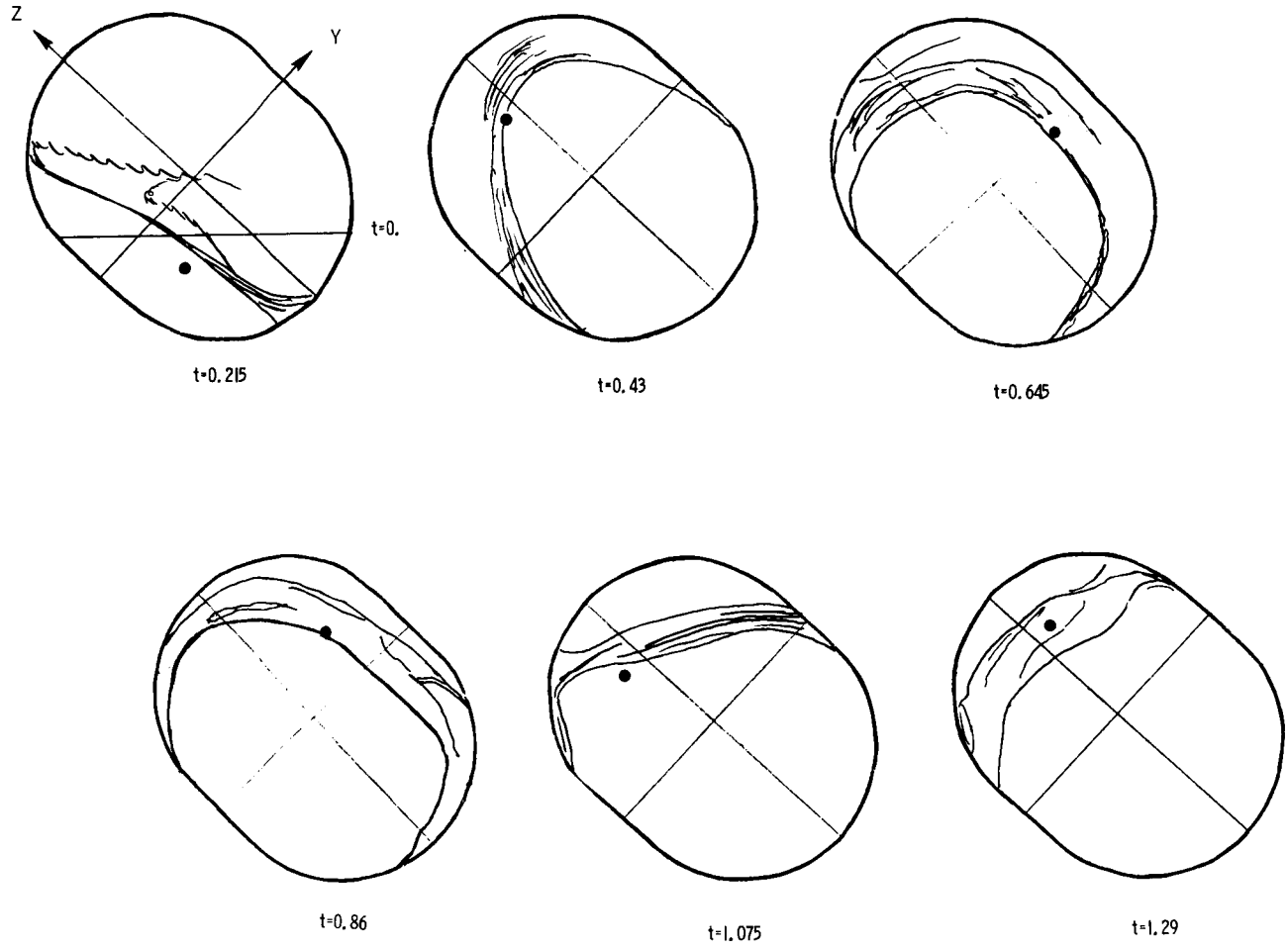

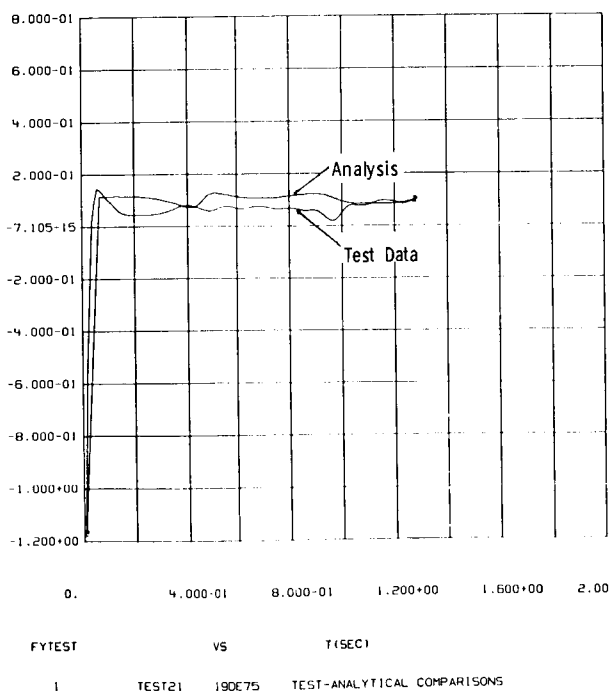

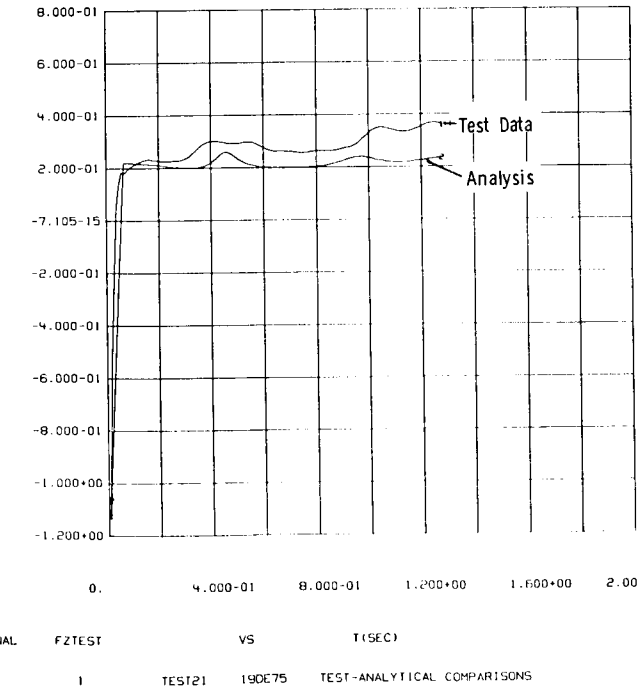

Figure IV-16. Test/Analytical correlation- Small Tank , Test 21
tank radius= 1.25 in.; 25 % fill volume; α= 45°

However, the cm location timing appears to be excellent. It is felt that the small force magnitude in these tests coupled with thermal drift tend to make the measured data suspect. However, based on the large tank tests and the center of mass correlation on the small tank tests, it appears that the analytical model provides reasonable results even for the small tank. Study of Test 21 results (Figure IV-16) indicates similar force trends between measured and predicted forces. This test of course employed larger lateral acceleration's and, hence, larger liquid forces.

Overall applicability of the analytical model concept of a point mass moving on an ellipsoidal constraint surface is considered to be excellent. The test correlations with the bare tanks (Phase I and Phase II) indicate that the analytical model provides a reasonable approach for predicting forces due to transient liquid motion.

5. Discussion of Baffled Tank Test Results - During Phase II testing twelve drops were performed using the Phase I tank (2.5 inch radius) with three ring baffles installed (see Chapter II). It was initially hoped that baffles could be analytically represented by some form of drag or friction force within the framework of the current point mass model. However, the observed liquid motion during the Phase II tests indicated that this approach was not feasible. During the low g reorientations simulated, the baffles, when encountered, essentially redirected the liquid flow to the tank interior. Figures IV-17 through IV-21 present the results of five of the baffled tank tests. From the sketches of liquid motion, it is noted that some liquid is trapped under the baffles and laterally traverses the tank. Eventually, at second contact with the baffles, the liquid becomes a spray. The simulation of these complex flow patterns is not feasible with a point mass model.

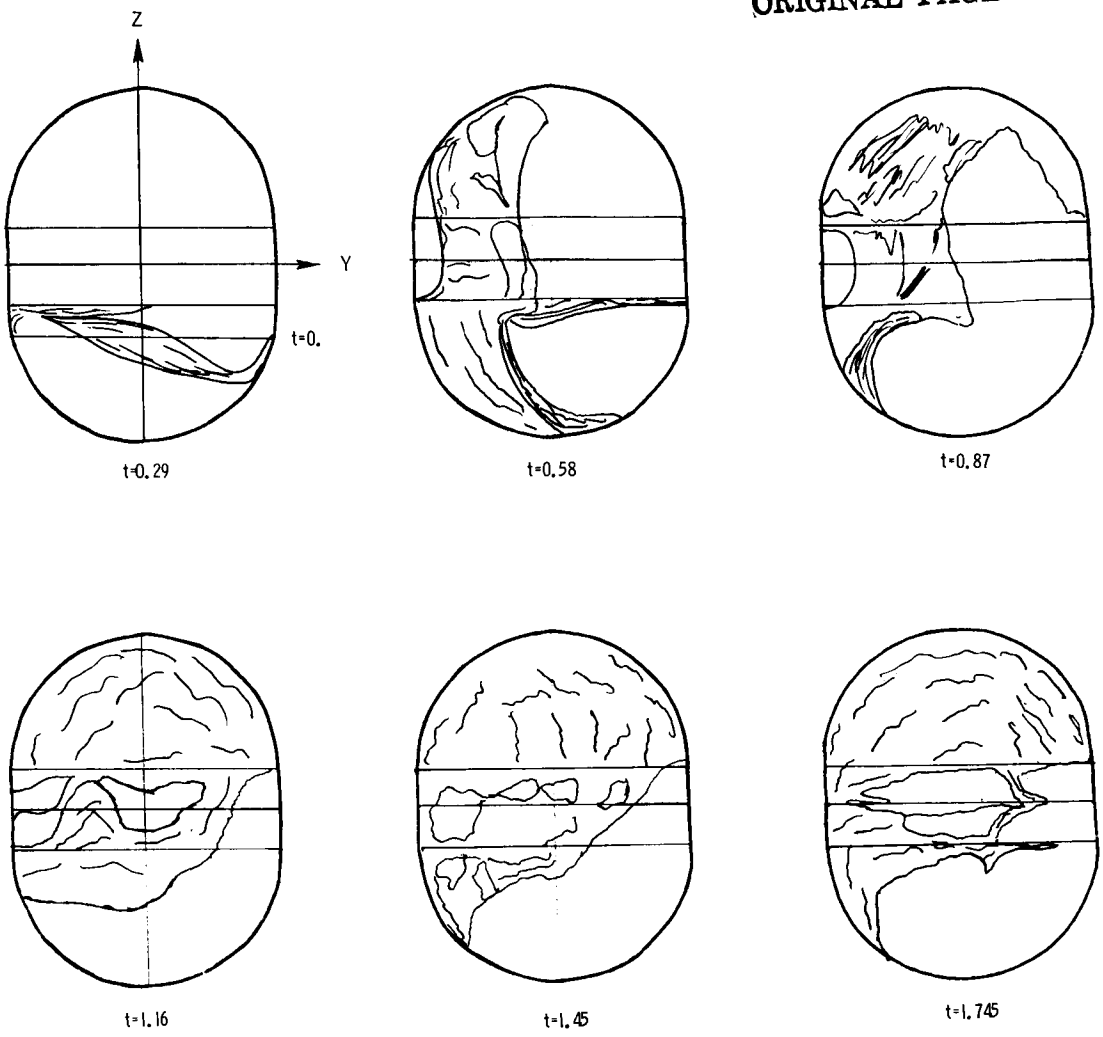

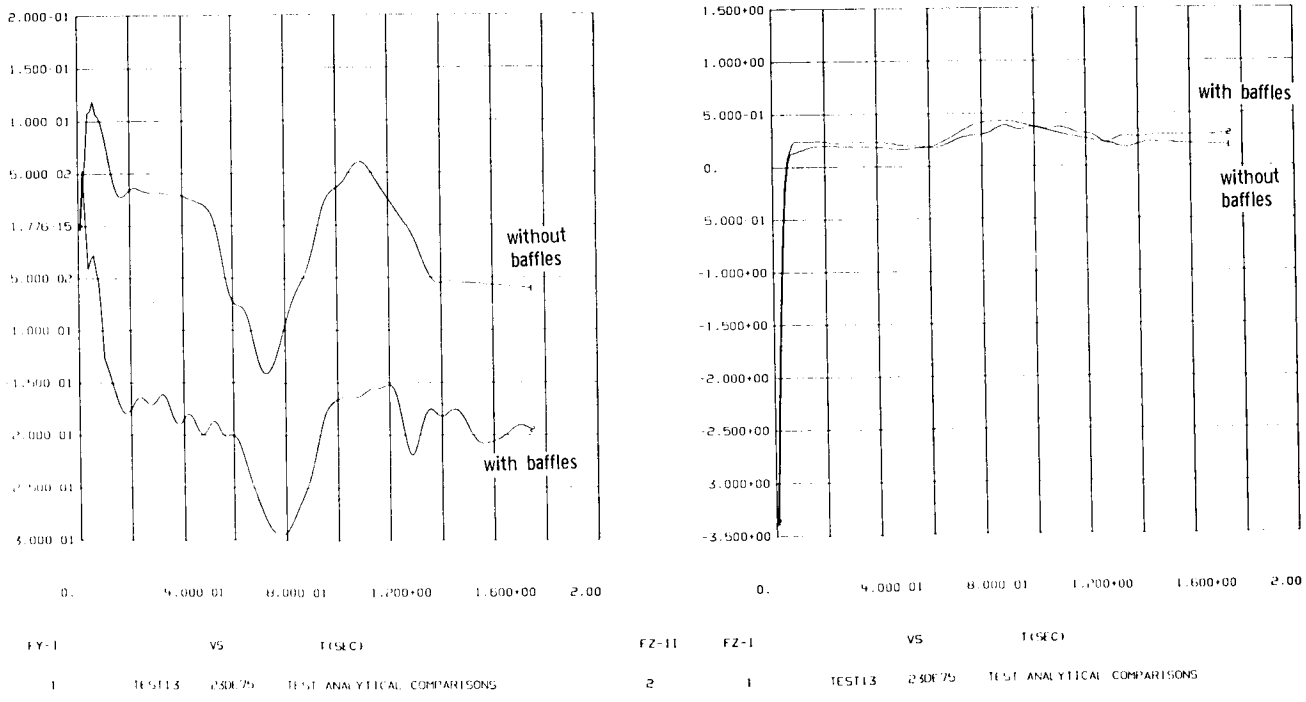

Figure IV-17. Baffled Tank Comparison-
Phase I Test 13 / Phase II Test 6

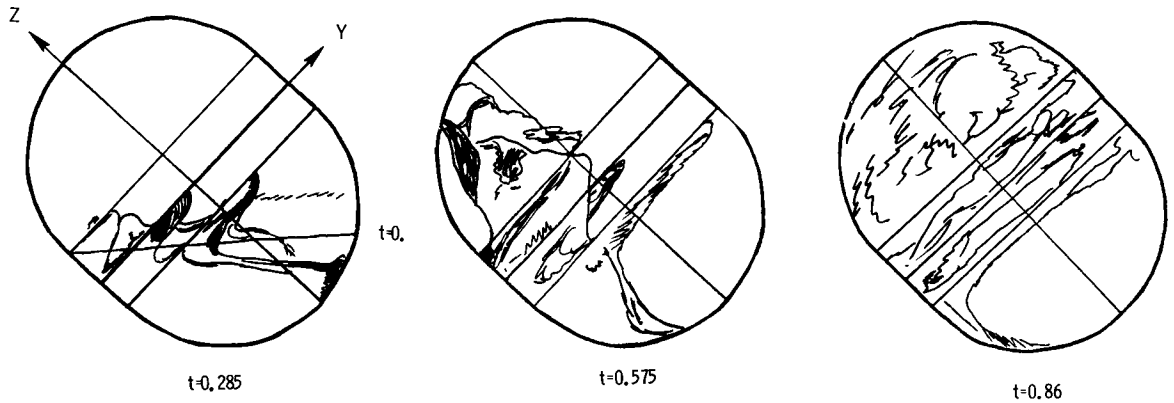

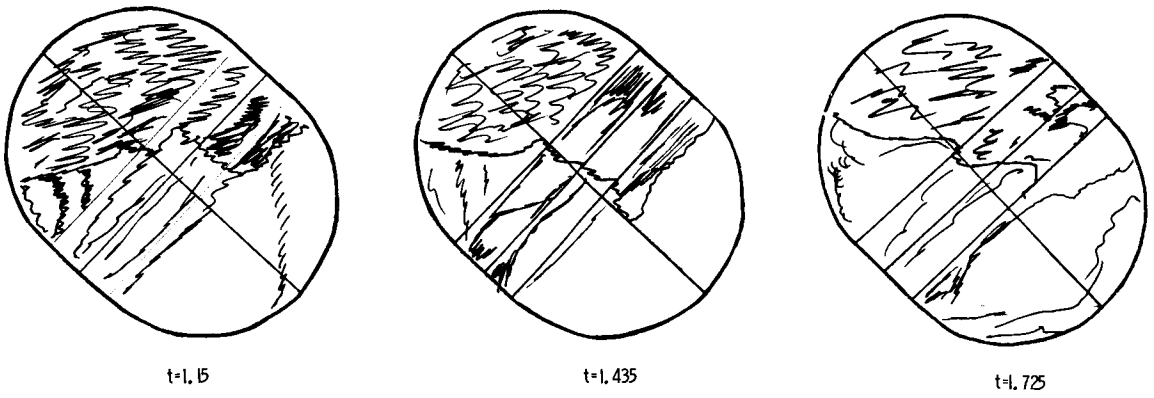

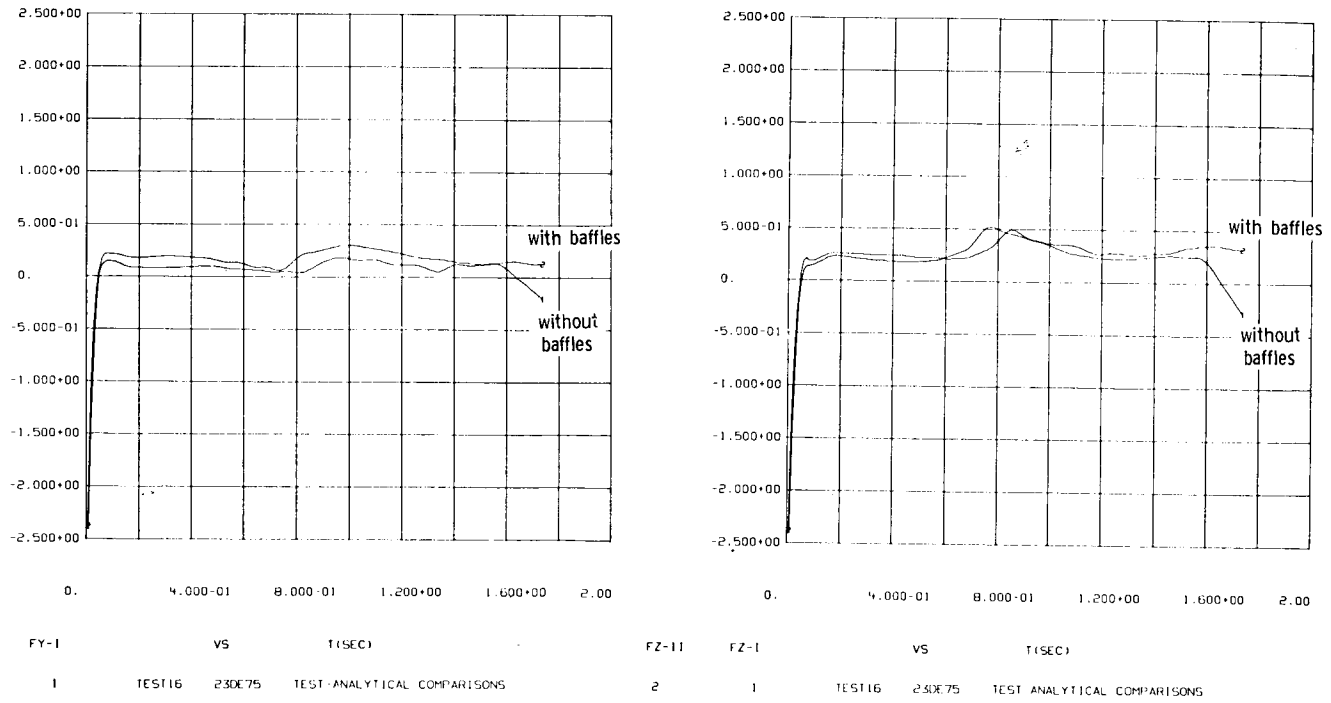

Figure IV-18. Baffled Tank Comparison-
Phase I Test 16 / Phase II Test 7

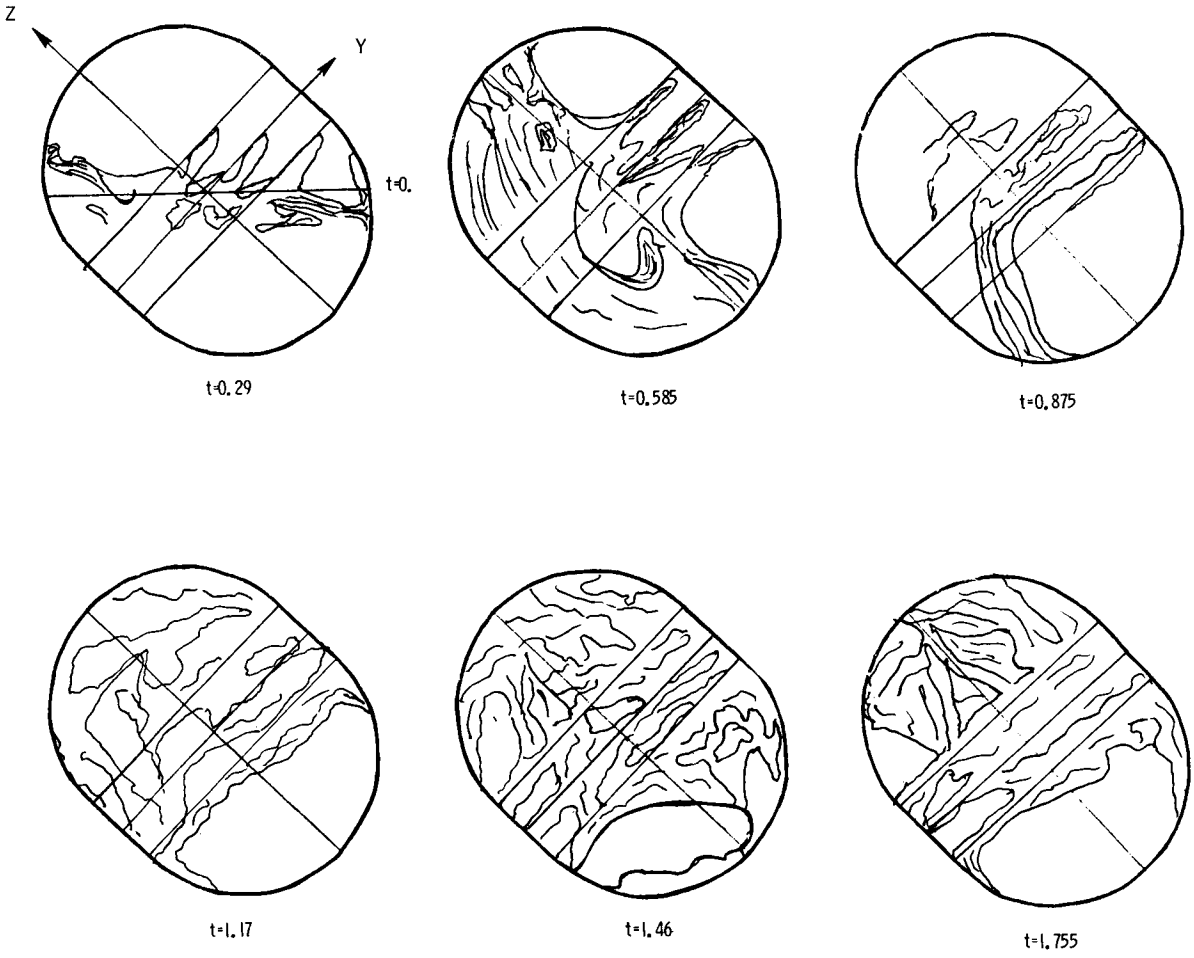

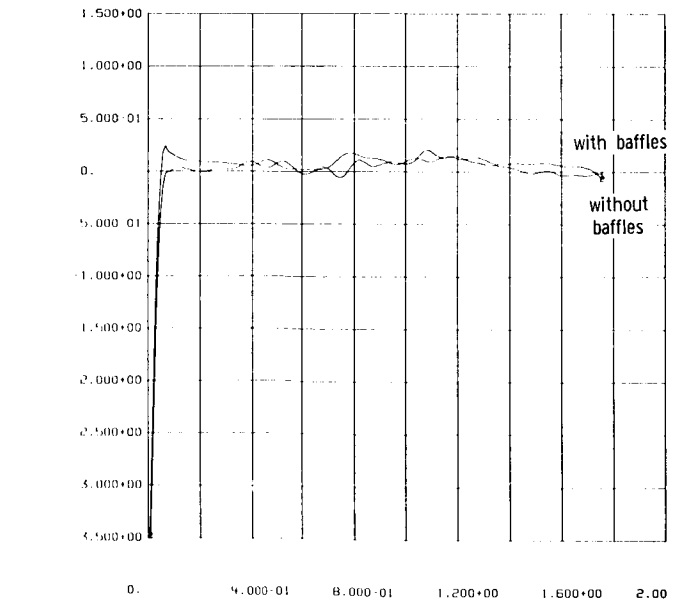

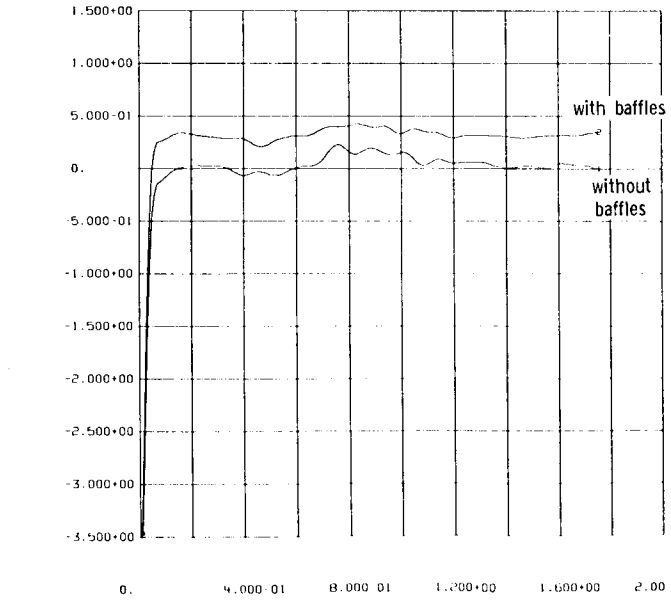

Figure IV-19. Baffled Tank Comparison-
Phase I Test 17 / Phase II Test 10

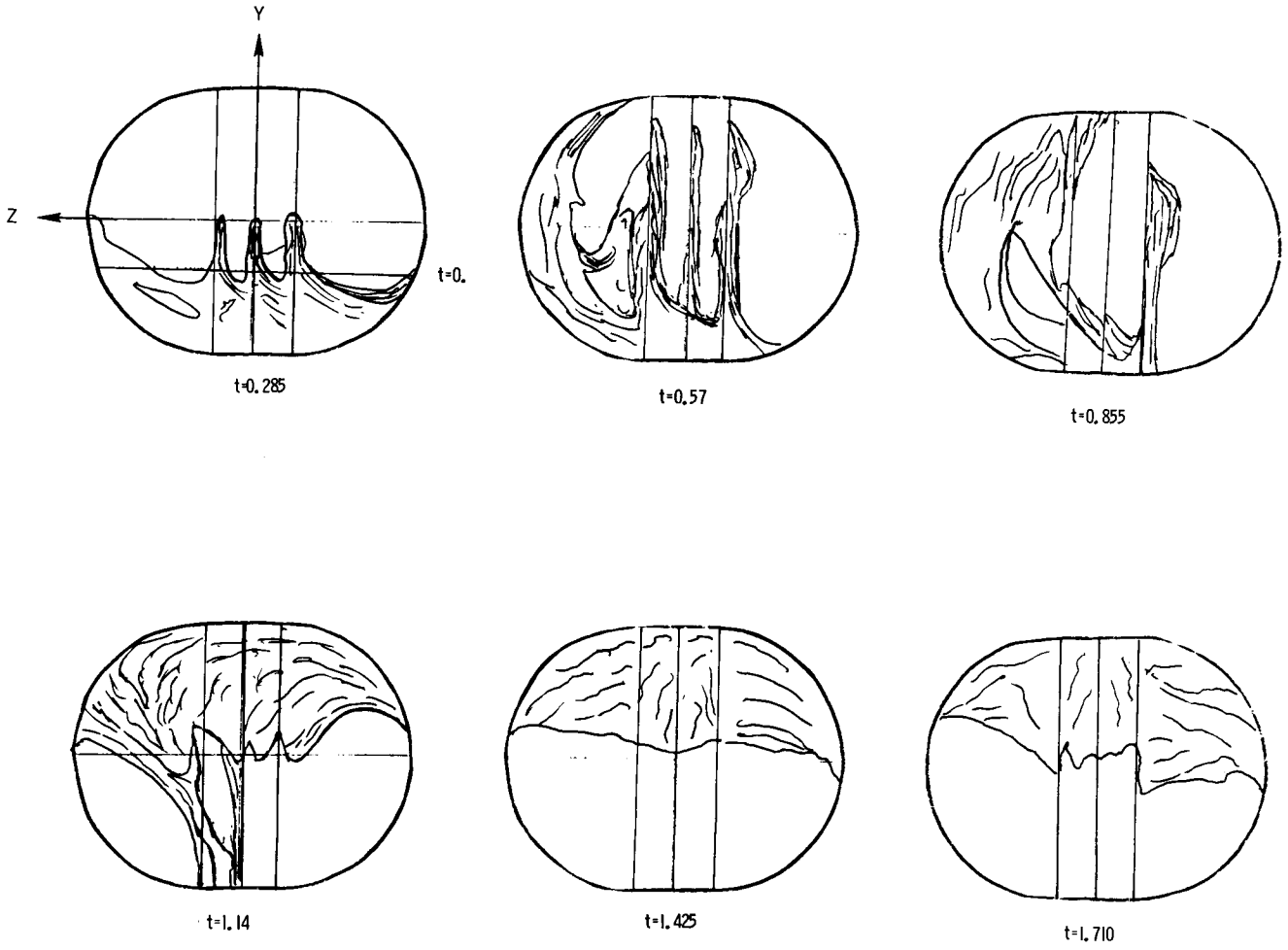

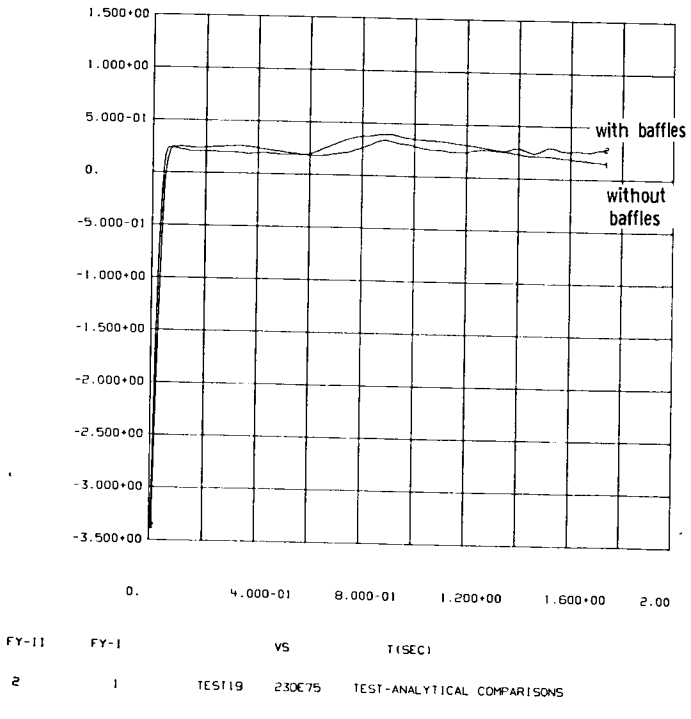

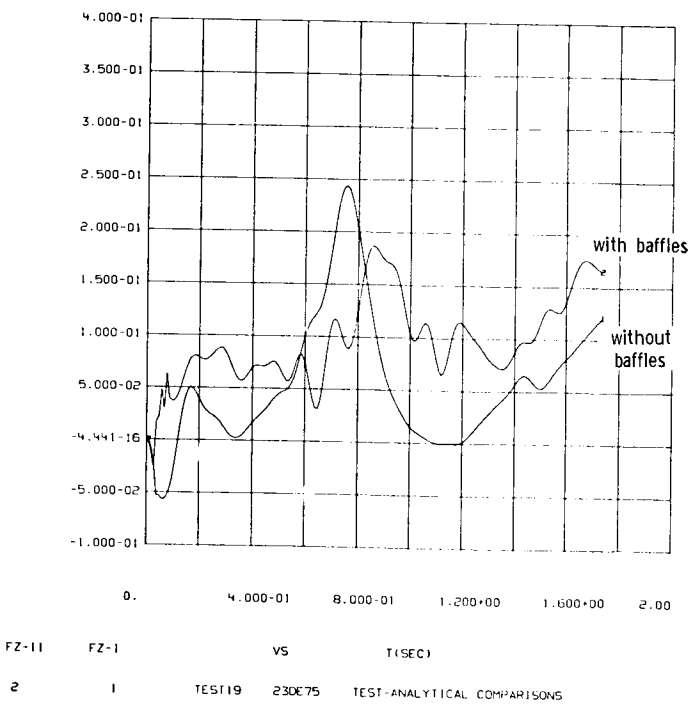

Figure IV-20. Baffled Tank Comparison-
Phase I Test 19 / Phase II Test 8

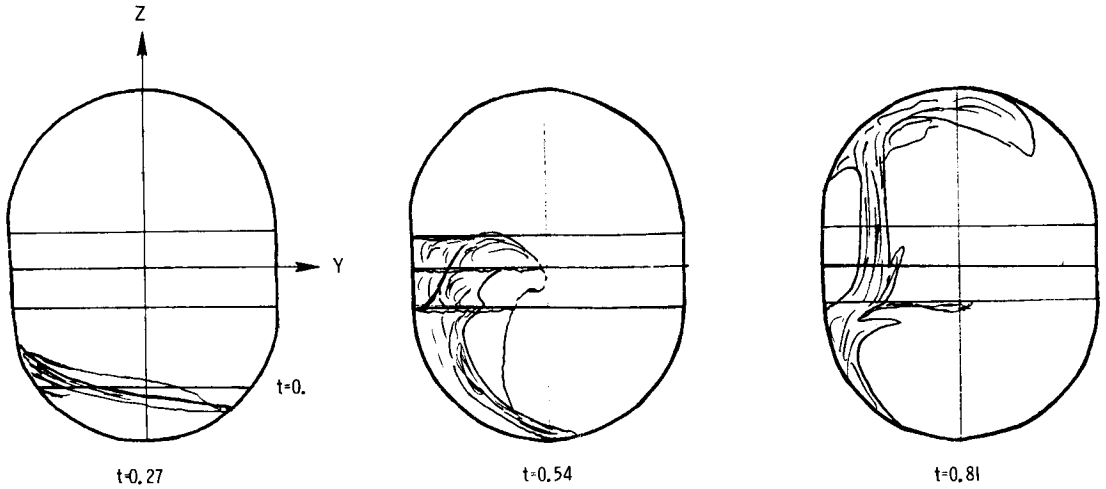

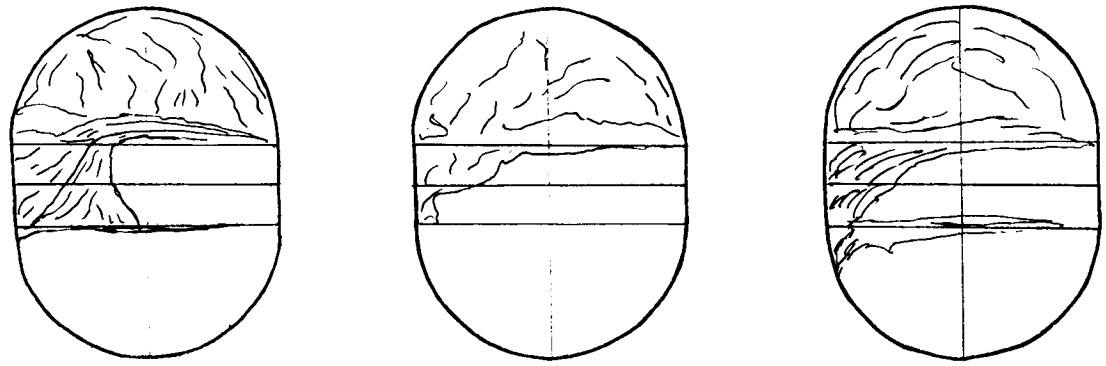

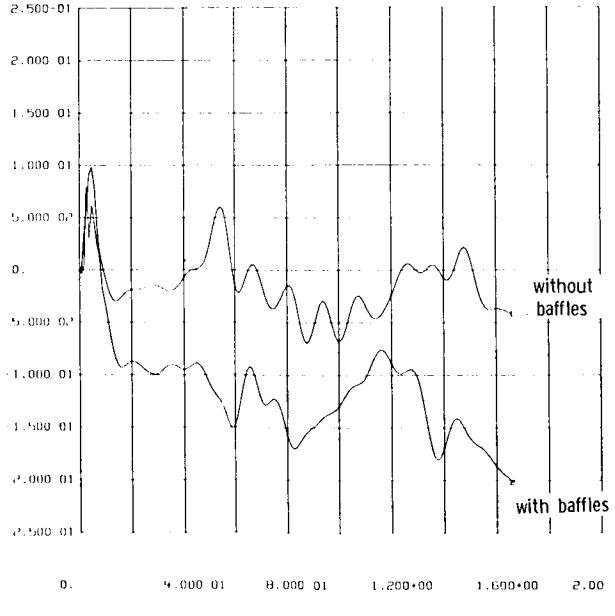

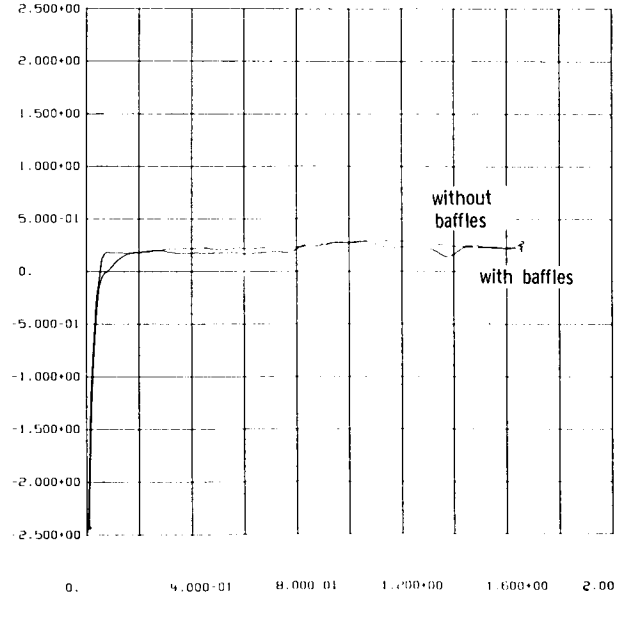

Figure IV-21. Baffled Tank Comparison-
Phase I Test 22 / Phase II Test 3

Although the analytical model cannot simulate the flow for the baffled test cases, much was learned about liquid reorientation from these tests. A study of the force data from these tests has also yielded some interesting observations. Many of the baffled test cases repeated the test conditions used in the unbaffled tests of Phase I. In Figures IV-17 through IV-21, in addition to liquid motion sketches, force time history comparisons are shown between the particular baffled test case and its corresponding Phase I, unbaffled test case. It is interesting to note the extreme similarity in measured data. In general, the baffles tend to somewhat reduce the force levels and delay the peak forces. However, this is only a general qualitative evaluation. It appears, however, that using the analytical model and neglecting the baffles, would result in fairly reasonable force predictions. The results would at least be conservative in most cases. Larger fill volume cases (i.e., 50%) exhibit flow which better approximates the flow in unbaffled cases. In these cases, the baffles might be represented as an increase in liquid damping force, at least during the initial part of the reorientation.

6. Symmetric Reorientation - The Phase II test program included two tests using the Phase I tank (2.5 inch radius, no baffles) in which only axial acceleration was applied. Section A of this chapter discussed the observed reorientation in these cases. It has been found, in this study and others, that symmetric reorientation, where the liquid does not follow the tank wall, but traverses the tank interior, is a special case which will not generally occur in practice. This type of reorientation requires that the liquid is completely at rest and the applied acceleration must be perpendicular to the liquid surface and along the tank axis of symmetry. Test 1 of the Phase II test program satisfied these requirements. The reorientation is shown by the photographs in Figure IV-2. Due to the limited occurance of this type of reorientation and the limited test data available for correlation, the analytical model was not structured to simulate these cases. However, the measured force data does provide some useful information.

Previous studies have been conducted on impact forces on model propellant tanks produced by symmetric reorientation (Stephens, Reference 11). These tests were conducted at higher acceleration levels than those used in this program. Stephens found that impact forces on the order of 2 to 3 times the hydrostatic force ($M_{LIQUID}\ A_{APPLIED}$) were measured for applied

acceleration on the order of 0.2 to 0.5 g. For Test 1 of this study, however, it was found that the measured force was approximately equal to the hydrostatic force. During reorientation the axial force on the tank slowly increased as the liquid traversed the tank or collected at the tank dome (Figure IV-2); no impact type force was observed. Figure IV-22 delineates these results for Test 1.

Based on the contradiction between the results of Reference 11, and Test 1 of Phase II, it appears that more tests would be helpful in understanding symmetric reorientation in low g environments. However, since this type of reorientation is considered a special case, resolution of the problem is mostly of academic interest.

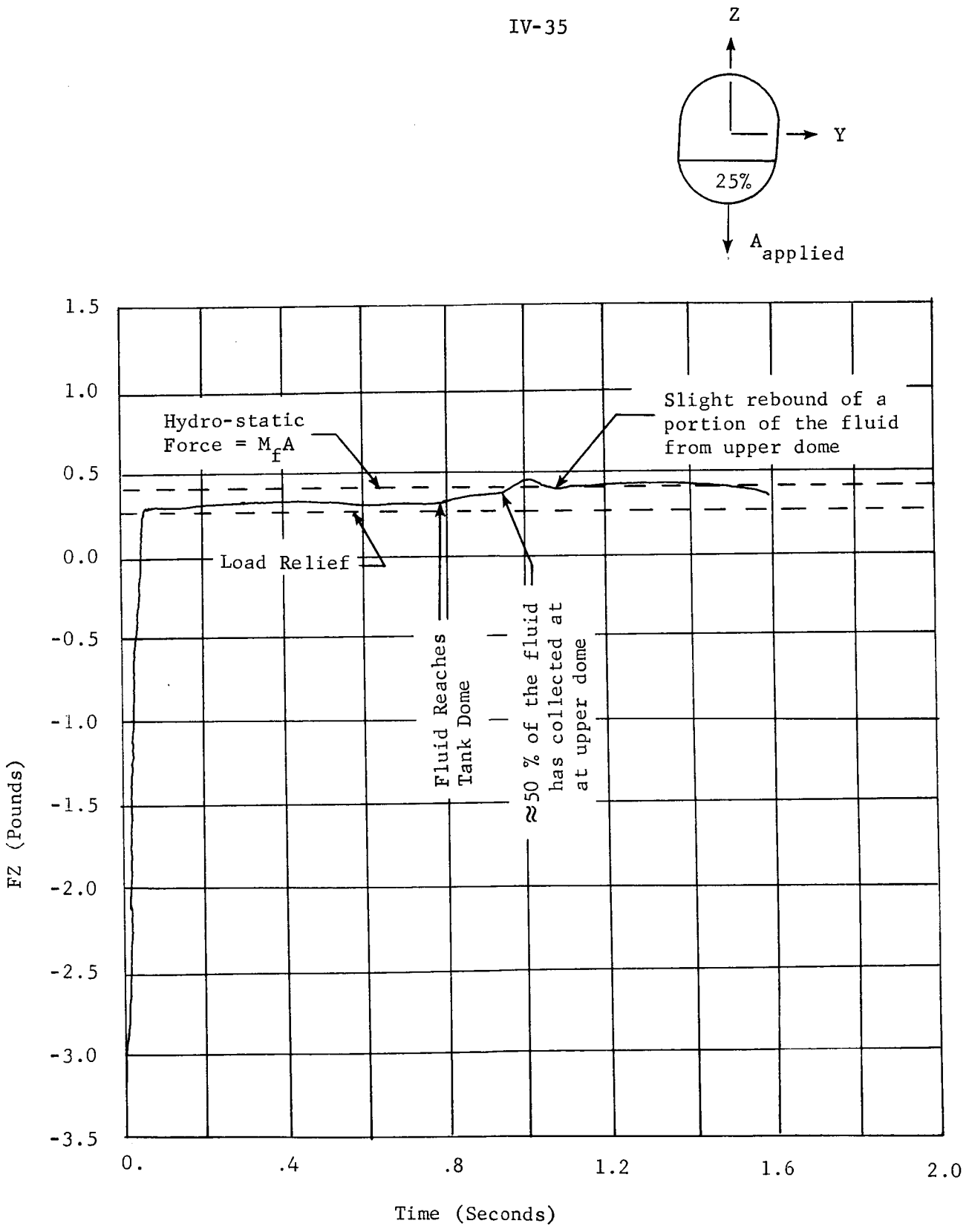

Figure IV-22. Symmetric Reorientation Forces

V. CONCLUSIONS AND RECOMMENDATIONS

Transient liquid motion, in low g environments can be accurately simulated by an analytical model which represents the liquid as a point mass moving on an ellipsoidal constraint surface. The concepts of liquid effective mass and liquid damping developed in the Phase II study have greatly improved the accuracy of the model's force predictions and center of mass location correlation.

The mechanical analog has been cast in a framework which allows the incorporation of tank/liquid systems into general spacecraft simulation problems. The three dimensional model has been structured to facilitate incorporation into general spacecraft equations for use in a variety of analyses: i.e., control interaction during orbital maneuvers, reentry analyses, loads analyses, etc.

1. The mechanical analog should be integrated into ongoing and future analytical efforts to improve the simulation of liquid/structure interactions: i.e., Shuttle ET reentry studies, Space Tug control system design and maneuver analyses, etc.

The test system developed during this program is capable of providing insight to the character of liquid reorientation and the forces exerted on Spacecraft by moving liquid. It provides the capability to apply arbitrary low g accelerations while recording transient liquid forces and providing photographic documentation of the test.

2. Further testing should be conducted to build the data bank necessary for further analytical model verification. Testing should include various tank geometries; ogive, conical, etc. Additional scale propellant management devices should be incorporated into the tests; various baffle arrangements, surface tension management devices, etc.

Reorientation in baffled tanks has been found to be a complicated phenomena. Simulation of the observed flow patterns with a point mass model is not feasible. However, comparison of similar tests with and without baffles revealed a striking similarity in measured force trends. Baffles, in general, tend

to reduce force levels and delay (time wise) force peaks. Based on these observations, it appears that the analytical model may be used, neglecting the baffles, for conservative force predictions in some applications.

VI. REFERENCES

1. R. L. Berry and J. R. Tegart: "Experimental Study of Transient Liquid Motion in Orbiting Spacecraft", Interim Report, MCR-75-4, Martin Marietta Corporation, Denver, Colorado, February 1975.

2. T. A. Coney: "Surface Tension, Viscosity and Density Measurements of Two Fluorocarbon Solvents, FC-43 and FC-78", NASA TMX-1862, Lewis Research Center, Cleveland, Ohio, August 1969.

3. C. S. Bodley, A. D. Devers and A. C. Park: "Dynamic Analysis of a Flexible Spacecraft with Rotating Components", MCR-75-18 (NAS8-30761), Martin Marietta Corporation, Denver, Colorado, August 1975.

4. W. J. Masica and D. A. Petrash: "Motion of Liquid-Vapor Interface in Response to Imposed Acceleration", NASA TN D-3005, NASA Lewis Research Center, Cleveland, Ohio, September 1965.

5. T. E. Bowman: "Cryogenic Liquid Experiments in Orbit; Vol. I, Liquid Settling and Interface Dynamics", Martin Marietta Corporation, Denver, Colorado, December 1966.

6. J. A. Salzman and W. J. Masica: "Experimental Investigation of Liquid Propellant Reorientation". NASA TN D-3789, NASA Lewis Research Center, Cleveland, Ohio, January 1967.

7. J. A. Salzman and W. J. Masica: "Low-Gravity Reorientation in a Scale-Model Centaur Liquid-Hydrogen Tank", NASA TN D-7168, NASA Lewis Research Center, Cleveland, Ohio, February 1973.

8. T. L. Labus and W. J. Masica: "Liquid Reorientation in Spheres by Means of Low-G Accelerations", NASA TM X-1659, NASA Lewis Research Center, Cleveland, Ohio, October 1968.

9. W. J. Masica: "Experimental Investigation of Liquid Surface Motion in Response to Lateral Acceleration during Weightlessness", NASA TN D-4066, NASA Lewis Research Center, Cleveland, Ohio, July 1967.

10. T. E. Bowman: "Response of the Free Surface of a Cylindrically Contained Liquid to Off-Axis Accelerations", Proceedings of the 1966 Heat Transfer and Fluid Mechanics Institute Stanford University Press, 1966.

11. D. G. Stephens: "Experimental Investigations of Liquid Impact in a Model Propellant Tank", NASA TN D-2913, NASA Langley Research Center, Hampton, Virginia, October 1965.

APPENDIX A - THREE DIMENSIONAL MECHANICAL ANALOG COMPUTER PROGRAM USERS GUIDE (LAMPS3)

This appendix discusses, in detail, the implementation of the tank/liquid system into the framework of the DYNAMO computer program (Reference 3). Chapter III discussed the general analytical techniques employed in DYNAMO: in this appendix we shall concentrate on the specifics of the mechanization, in particular the required input data.

Method of Mechanization

The implementation of the mechanical analog into DYNAMO required some significant alterations to the basic computer code. In particular, the specification of a state dependent constraint surface (ellipsoidal) required the addition of a capability to differentiate $\dot{\alpha}$ (see Chapter III, Section E). The modified DYNAMO program has been named LAMPS3 (Large AMPlitude Slosh 3 dimensional). This version only contains the nonlinear time response options in DYNAMO and is restricted to an interconnected system of rigid bodies.

The specific implementation of the tank/liquid mechanical analog is shown in Figure A-1.

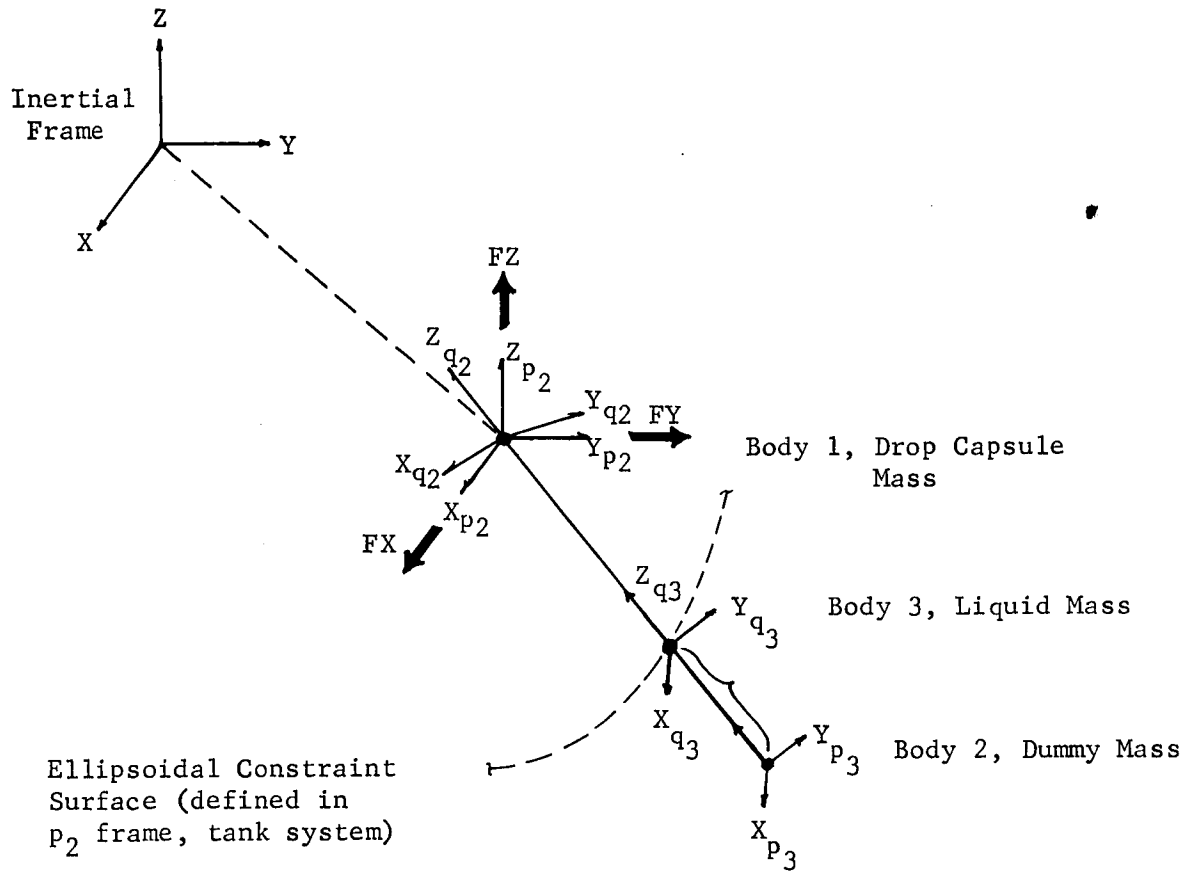

FIGURE A-1. TANK/LIQUID MECHANICAL ANALOG

In the simulation, Body 1 represents the drop capsule mass (ie, rigid spacecraft). Body 2 is a dummy mass required for mechanization of the mechanical analog in the framework of DYNAMO. Body 2 remains a fixed distance from Body 1 during the simulation. Body 3 represents the liquid mass and is constrained to move along the vector from Body 1 to Body 2. Body 3 slides along this vector in order to remain on the ellipsoidal constraint surface. The bodies are connected at "hinge points". Bodies 1 and 2 are connected at the hinge represented by the origin of coordinate systems p_2 and q_2 (Figure A-1). At this hinge, translation between the frames is prohibited but there is free rotation. Bodies 2 and 3 are joined by the hinge represented by coordinate systems p_3 and q_3. Frame q_3 is only allowed to translate in the Z_{p_3} direction, all other

relative motion between the frames is prohibited. Hence, it can be seen that the simulation represents a variable length pendulum, free to rotate at the hinge p_2/q_2. The length of the pendulum varies such that Body 3 (the fluid mass) always remains on the prescribed ellipsoidal constraint surface. External forces (Fx, Fy, Fz) are applied to Body 1. These forces represent the spring motor forces applied to the drop capsule during the test program (see Chapter II). In a more general sense, these forces could represent reaction control system forces acting on an orbiting spacecraft.

The position of the liquid mass at any time can be expressed in terms of spherical coordinates relative to the tank coordinate system (frame p_2, Figure A-1). Figure A-2 delineates the spherical coordinate set used in the simulation.

Where:

$X_{cm} = R \sin \phi \cos \theta$

$Y_{cm} = R \sin \phi \sin \theta$

$Z_{cm} = R \cos \phi$

$0^\circ \leq \phi \leq 180^\circ$

$0 \leq \theta \leq 360^\circ$

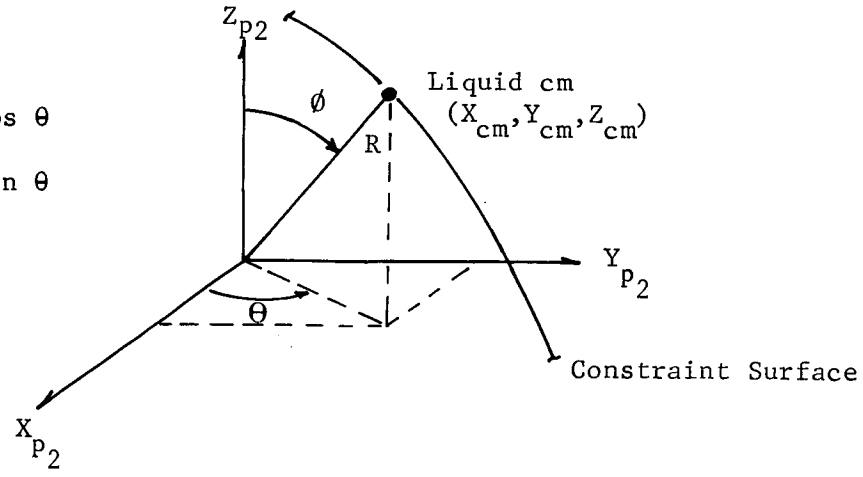

FIGURE A-2. SPHERICAL COORDINATE SET

The constraint surface is assumed to be an axisymmetric ellipsoid. The equation of this surface can be written:

$$a\,x^2 + a\,y^2 + c\,z^2 = 1 \qquad \text{(A-1)}$$

where a and c are the ellipsoid surface coefficients.

Transforming equation (A-1) to spherical coordinates and solving for R, yields:

$$R = \frac{\sqrt{1/a}}{\left[\sin^2\phi + \frac{c}{a}\cos^2\phi\right]^{\frac{1}{2}}} \qquad \text{(A-2)}$$

Differentiating equation (A-2) results in the required rate of change of length of the pendulum in our simulation.

$$\dot{R} = \frac{-\sqrt{\frac{1}{a}}\sin\phi\cos\phi\left[1-\frac{c}{a}\right]\dot{\phi}}{\left[\sin^2\phi + \frac{c}{a}\cos^2\phi\right]^{3/2}} \qquad \text{(A-3)}$$

Note that $\dot{R}$ is only a function of ϕ and $\dot{\phi}$ due to the Z axis symmetry of the constraint surface. $\dot{R}$ is the $\dot{\alpha}$ discussed in Chapter III (equation III-2c). As pointed out in Chapter III, it is necessary to compute $\ddot{\alpha}$, or $\ddot{R}$ in our case, in order to correctly calculate the λ's; forces exerted by the liquid on the tank. The analog differentiation circuit discussed in Section E of Chapter III was employed for this purpose. That is, $\ddot{R}$ was expressed as per equation III-19,

$$\ddot{R} = K\dot{R}\left(1 + \frac{S}{K}\right) \qquad \text{(A-4)}$$

For values of K large compared to $S = j\omega$, where ω is the system response frequency, $\ddot{R}$ simply becomes,

$$\ddot{R} \approx K\dot{R} \qquad \text{(A-5)}$$

This algorithm has been found to work exceedingly well for our application. LAMPS3 outputs plots of $\ddot{R}(t)$ and $\int\ddot{R}(t)$ for comparison with the explicitly defined $\dot{R}(t)$, equation (A-3) (see the sample output at the end of this appendix). A value of K=200 was found to be adequate for this simulation. Note that the plot of $\ddot{R}$ is not absolutely smooth. This slight roughness is reflected in the liquid forces. However, the effect of

this roughness on the overall simulation is negligible and greatly outweighed by the increased capability achieved by implementing the mechanical analog in the more general framework of DYNAMO. The value of K=200 can be overridden by the input data if required to achieve a better definition of $\ddot{R}$.

In the context of our simulation, by specifying $\dot{R}$ and $\ddot{R}$, we are really specifying the motion of the q_3 frame relative to the p_3 frame in the Z_{p3} direction (Figure A-1, $Z_{3/2}$). Note that the rate of change of R and $Z_{3/2}$ are just compliments of each other.

The radial motion of Body 3 ($\dot{R}$) requires the definition of ϕ and $\dot{\phi}$, the spherical coordinate angle. The values of ϕ and $\dot{\phi}$ are not readily available in the mechanization. However, the Euler angle rotations and rotational rates of frame q_2 relative to frame p_2 are available. These are the β's and $\dot{\beta}$'s expressed in equation III-2 (Chapter III). From these β's and $\dot{\beta}$'s, ϕ and $\dot{\phi}$ (also θ) can be determined as follows.

Figure A-3 depicts unit vector triads in the p_2 and q_2 frames.

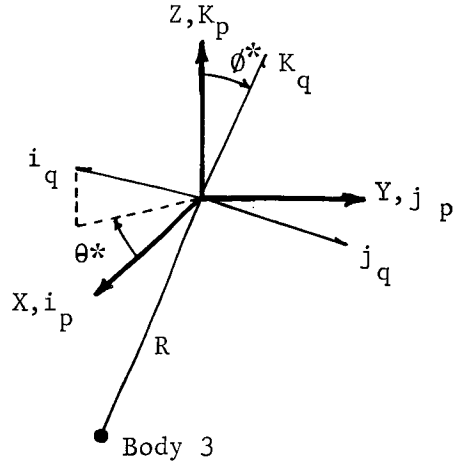

q_2 and p_2 triads

FIGURE A-3. RELATIVE ROTATIONS BETWEEN q_2 AND p_2 TRIADS

Program DYNAMO allows the user to select the Euler angle permutation order desired. We have chosen the order:

$$\theta\, Y_q\,(\beta_1), \theta\, Z_q\,(\beta_2), \theta\, X_q\,(\beta_3).$$

The rotation $\theta\, Z_q$ has also been constrained to zero since spinning about the radius, R, has no meaning. Based on this selected order, we can express the unit vectors of the p triad in terms of the q triad via the direction cosines.

$$\begin{Bmatrix} \hat{i}_p \\ \hat{j}_p \\ \hat{k}_p \end{Bmatrix} = \begin{bmatrix} \cos\beta_1 & 0 & \sin\beta_1 \\ 0 & 1 & 0 \\ -\sin\beta_1 & 0 & \cos\beta_1 \end{bmatrix} \begin{bmatrix} 1 & 0 & 0 \\ 0 & 1 & 0 \\ 0 & 0 & 1 \end{bmatrix} \begin{bmatrix} 1 & 0 & 0 \\ 0 & \cos\beta_3 & -\sin\beta_3 \\ 0 & \sin\beta_3 & \cos\beta_3 \end{bmatrix} \begin{Bmatrix} \hat{i}_q \\ \hat{j}_q \\ \hat{k}_q \end{Bmatrix}$$

$$= \begin{bmatrix} \cos\beta_1 & \sin\beta_1 \sin\beta_3 & \sin\beta_1 \cos\beta_3 \\ 0 & \cos\beta_3 & -\sin\beta_3 \\ -\sin\beta_1 & \cos\beta_1 \sin\beta_3 & \cos\beta_1 \cos\beta_3 \end{bmatrix} \begin{Bmatrix} \hat{i}_q \\ \hat{j}_q \\ \hat{k}_q \end{Bmatrix}$$

Based on the definition of the angles θ^* and ϕ^* in Figure A-3, we can now write the following equations.

$$\hat{K}_q \cdot \hat{k}_p = \cos\phi^* = \cos\beta_1 \cos\beta_3 \qquad \text{a}$$

$$\hat{K}_q \cdot \hat{i}_p = \sin\phi^* \cos\theta^* = \sin\beta_1 \cos\beta_3 \qquad \text{b} \qquad \text{(A-6)}$$

$$\hat{K}_q \cdot \hat{j}_p = \sin\phi^* \sin\theta^* = -\sin\beta_3 \qquad \text{c}$$

Hence, from equation (A-6)a:

$$\phi^* = \cos^{-1}(\cos\beta_1 \cos\beta_3) \quad , \qquad \text{(A-7)}$$

and ratioing parts b and c of equation (A-6),

$$\theta^* = \text{Tan}^{-1}\left(\frac{-\sin\beta_3}{\sin\beta_1\cos\beta_3}\right) \tag{A-8}$$

Differentiating equation (A-7) results in,

$$\dot{\phi}^* = \frac{\dot{\beta}_1 \sin\beta_1 \cos\beta_3 + \dot{\beta}_3 \cos\beta_1 \sin\beta_3}{\sin\phi^*} \tag{A-9}$$

All of the β's and $\dot{\beta}$'s required to calculate ϕ^*, θ^* and $\dot{\phi}^*$ are known and available within the LAMPS3 program.

Note that the magnitude of the spherical coordinate rate $\dot{\phi}$ (Figure A-2) is the same as $\dot{\phi}^*$ (equation (A-9)). The sign of $\dot{\phi}$ is based on whether Body 3 is going toward or away from the Z_{p_2} axis. By observation, we can also define the spherical coordinates ϕ and θ as:

$$\begin{aligned} &\phi = 180^\circ - |\phi^*| \quad , \quad 0^\circ \leq \phi^* \leq 180^\circ \\ \text{and} \quad &\theta = \theta^* - \Pi \quad , \quad 0^\circ \leq \theta^* \leq 360^\circ \end{aligned} \tag{A-10}$$

LAMPS3 also calculates these variables (ϕ, θ, $\dot{\phi}$) and plots their time history to facilitate locating the liquid cm at any time.

Liquid damping, as discussed in Chapter IV (Section B2), is easily implemented within LAMPS3. Within the code, an allowance is made to specify rotational dampers at the "hinges". Liquid damping is achieved by specifying damping proportional to $\dot{\beta}_1(\dot{\theta}y)$ and $\dot{\beta}_3(\dot{\theta}x)$ at hinge p_2/q_2. Damping (μ) is assumed proportional to $\dot{\phi}$, and based on equation A-9, the equivalent damping on $\dot{\beta}_1$, and $\dot{\beta}_2$ is calculated as follows.

$$\mu\beta_1 = \left| \frac{\mu \sin \beta_1 \cos \beta_3}{\sin \emptyset} \right|$$

$$\mu\beta_3 = \left| \frac{\mu \cos \beta_1 \sin \beta_3}{\sin \emptyset} \right| \qquad \text{(A-11)}$$

The concept of effective mass (discussed in Chapter IV-B1) is implemented as follows. As discussed in Chapter IV, the effective mass factor (equation IV-1) is only to be applied to the centripital acceleration component of force. Separation of the centripital acceleration component of force from the other components by altering the basic kinematic equations of the DYNAMO program is not feasible. A simpler method of incorporating the effective mass factor is to apply an external force to the liquid mass which cancels the desired proportion of the centripital force. Figure A-4 delineates the application of this force.

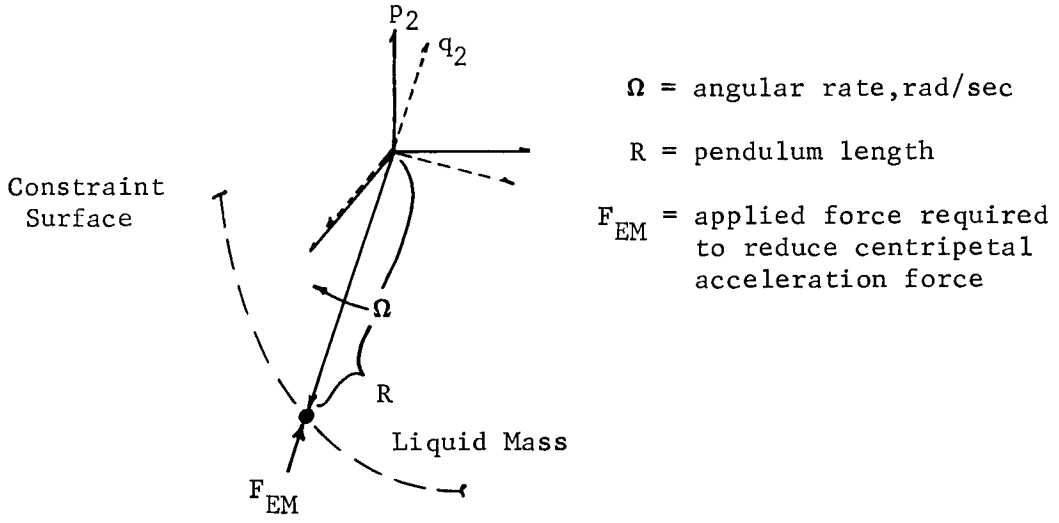

FIGURE A-4. LAMPS3 IMPLEMENTATION OF EFFECTIVE MASS FACTOR

The force F_{EM} in Figure A-4 is defined as:

$$F_{EM} = M_F \text{ (1-MASFAC) } R \ \Omega^2 \qquad \text{(A-12)}$$

where: M_F = liquid mass

MASFAC = effective mass factor

R = pendulum instantaneous length

Ω = angular rate of the pendulum

This applied force is opposite in direction to the centripital acceleration force exerted by the liquid on the tank, and hence, cancels the undesired portion of that force. The application of this force is automatically built into LAMPS3. Its magnitude is determined by the value of MASFAC supplied by the user in the input data.

Input Data for LAMPS3

The input data for LAMPS3 follows the basic format for DYNAMO (Reference 3, Volume II). Once the input data has been established, only a few of the values ever change; the rest of the input data always remains the same. Part of the input data requires knowledge of the initial position of the liquid cm. In order to preserve the input format used in DYNAMO, a separate program (TANK) has been coded which generates the initial liquid cm position, constraint surface coefficients, and liquid mass for input to LAMPS3. Table A-1 delineates the required input data for this program. A sample output from program TANK is

TABLE A-1. PROGRAM TANK INPUT DATA FORMAT

INPUT DATA

```
  999 READ(A6,4X,3A6)RUNNO,UNAME
      IF(RUNNO,EQ. 4H STOP)STOP
      READ(12A6)          TITLE1
      READ(12A6)          TITLE2
      CALL COMENT         COMMENT CARDS,LAST CARD=10 ZEROS COLS 1-10
      READ(5E10.3)        XL,TR,TD,PCVOL,FDEN
      READ(3E10.3,2I5)    G(1),G(2),G(3),ITRIAD,ITYPE
      IF(ITRIAD.EQ.1)GO TO 10
      READ(5E10.3)        ANG(1),ANG(2),ANG(3)
   10 GO TO 999
```

DEFINITION OF INPUT VARIABLES

RUNNO = Run number printed in page headings
UNAME = User name
TITLE1 = Title card printed in page heading
TITLE2 = Title card printed in page heading
XL = Length of propellant tank cylindrical section
TR = Tank radius
TD = Height of tank domes from end of cylindrical section
PCVOL = Percentage tank fill. LE. 100.
FDEN = Liquid mass density
G(1-3) = Initial acceleration field acting on tank to cause initial liquid positioning.
- G(1) = X axis acceleration
- G(2) = Y axis acceleration
- G(3) = Z axis acceleration

ITRIAD = 1,G(i) supplied in tank triad
- 0,G(i) supplied in inertial triad; Euler angles must be supplied to relate tank triad to this inertial triad.

ITYPE = Euler angle permutation type if ITRIAD=0

ITYPE =	1	2	3	4	5	6	7	8	9	10	11	12
axis of 1st rotation	X	X	X	X	Y	Y	Y	Y	Z	Z	Z	Z
axis of 2nd rotation	Y	Y	Z	Z	Z	Z	X	X	X	X	Y	Y
axis of 3rd rotation	Z	X	X	Y	X	Y	Y	Z	Y	Z	Z	X

ANG(1-3) = X,Y and Z Euler rotation angles as specified by ITYPE above (in degrees)

presented near the end of this appendix. The primary data from program TANK used in program LAMPS3 consists of:

1. elliptical surface coefficients (a,c): page 6 of the sample output;

2. liquid mass: page 8 of the sample output;

3. spherical coordinate location (R, $\emptyset$, θ) of the initial liquid cm position: corrected values page 10 of the sample output. "Corrected" refers to the fact that the liquid cm has been adjusted to the"best fit" ellipsoidal constraint surface.

Having run program TANK the input for LAMPS3 is simple to implement. Table A-2 delineates the coded input for the LAMPS3 sample case. The user is referred to Reference 3, Volume II for a detailed definition of the input for DYNAMO. The input presented for LAMPS3 is identical in format to the DYNAMO input for nonlinear time response of interconnected rigid bodies. In Table A-2 the names of the input variables that change to reflect a specific tank/liquid system are shown in parenthesis; ie, (R_o)*. Table A-3 details the nature of these variables for the user. All other input is unchanging and reflects the mechanization of the three dimensional model.

Sample output for LAMPS3 is presented at the end of this appendix. The user is directed to Reference 3 for a full definition of the output variables. At each integration time interval (as selected by the PR input parameter) the values of the state vector and its derivative, Y and YDT, are printed. There are 34 variables in each vector (as defined in equation

TABLE A-2. LAMPS3 SAMPLE INPUT DATA

FORMA

NAME R. L. BERRY   PAGE 1 OF 4

```
         1         2         3         4         5         6         7         8
12345678901234567890123456789012345678901234567890123456789012345678901234567890
TLM113    DYNAMØ                                (RUNNØ ; UNAME)*
SIMULATIØN ØF TLM TEST CASE 13 (PHASE I)         (TITLE1)*
TRANSIENT LIQUID MØTIØN...PHI=0 DEG, 25 % FILL   (TITLE2)*
  3 DIMENSIØNAL LARGE AMPLITUDE SLØSH MØDEL     } (CØMMENT)*
  SAMPLE CASE                                   }
0000000000
    3    3    2    0    7
ITØPØL   2    3     HINGE TØPØLØGY
    1    1    1    2    3
    2    1    0    1    2
0000000000
IRGFLX   1    3     RIGID BØDY SPECIFICATIØN
0000000000
IFTSMW   1    2     SENSØR PØINT LØCATIØNS
    1    1    1    3
0000000000
INDATA   7    3     HINGE CØNSTRAINT DATA
    1    1    5    5    5
    2    1    0    0    1
    3    1    0    1    1
    4    1    0    0    1
    5    1    0    1    1
    6    1    0    1    1
    7    1    0    1    2
0000000000
BETIAW   6    3     INITIAL HINGE BETAS
    1    2    0.  (ØY)*
    2    2    0.  (ØZ)*
    3    2    0.  (ØX)*
    4    2    0.
```

41074 (5-74)

TABLE A-2. (CONTINUED)

FORMA

NAME: R. L. BERRY
PAGE 2 OF 4

1–5	6–10	11–27	28–44	45–61
5	2	0.		
6	2	0.		
0000000	00000			
BETA0	6	3 INITIAL	HINGE BETA DOTS	
0000000	00000			
TIMES	1	3 START,	DELTA, END	
1	1	0.0 (T0)*	0.01 (ΔT)*	1.6 (TF)*
0000000	00000			
IPDATA	1	3 OUTPUT	CONTROL INFO.	
1	1	1(PR)* 1(PL)* 0		
0000000	00000			
CWTDTA	1	100 USER SU	PPLIED PARAMETERS	
1	20	0.4451 (R)*	0.271 (C)*	(K)* K=200 IS ASSUMED IF NOT INPUT
1	31	0.0 (FX)*	7.28125 (FY)*	-130.095126 (FZ)*
1	34	1.0 (MASFAC)*		
1	35	1.92031 (R0)*		
1	71	0.0 (M)*		
0000000	00000			
MXYZ	1	4 BODY 1	(DROP CAPSULE MASS)	
1	1	0.87 (M1)*		
0000000	00000			
INERT	1	6		
1	1	0.0 (IXX)*	0.0 (IYY)*	0.0 (IZZ)*
0000000	00000			
2	1	HINGE 2,	BODY 1	
0.0		0.0 0.0		
0.0		0.0 0.0		
1	1	SENSOR 1,	BODY 1	
0.0		0.0 0.0		
0.0		0.0 0.0		

TABLE A-2. (CONTINUED)

FORMA

NAME: R.L. BERRY
PAGE 3 OF 4

Col. 1–5	Col. 6–10	Col. 11–20	Col. 21–27	Col. 28–44	Col. 45–61	Col. 62–72
MXYZ	1	4	BØDY 2	(DUMMY MASS)		
1	1	0.0000010001				
00000	00000					
INERT	1	6				
1	1		1.E-04	1.E-04	1.E-04	
00000	00000					
2	1		HINGE 2,	BØDY 2		
0.0		0.0	0.0			
0.0		0.0	1.9203	(R0)*		
3	1		HINGE 3,	BØDY 2		
0.0		0.0	0.0			
0.0		0.0	0.0			
MXYZ	1	4	BØDY 3	(FLUID)		
1	1	0.00409	(M3)*			
00000	00000					
INERT	1	6				
1	1		1.E-04	1.E-04	1.E-04	
00000	00000					
3	1		HINGE 3,	BØDY 3		
0.0		0.0	0.0			
0.0		0.0	0.0			
2	1		SENSØR 2,	BØDY 3		
0.0		0.0	0.0			
0.0		0.0	0.0			
TRANS	IENT	LIQUID	MØTION	PLØTS		
2						
13						
1	26	27 28	60	61 62 71	72 73 77 78	79
1	2	3				
TIME		RADIAN		TEST	31-1974 BETA 2/1	

(TEST 31-1974 = PTITLE)*

DEN 410740 (6-74)

TABLE A-2. (CONCLUDED)

FORMA

NAME R.L. BERRY
PAGE 4 OF 4

```
         1         2         3         4         5         6         7         8
12345678901234567890123456789012345678901234567890123456789012345678901234567890
    1    4
TIME      INCHES                        TEST 13-1974 BETA 3/2
    1    5    6
TIME      RAD/SC                        TEST 13-1974 BETADT 2/1
    1    7
TIME      IN/SEC                        TEST 13-1974 BETADT 3/2
    1    8    9   10
TIME      PØUNDS                        TEST 13-1974 FØRCES 2/1
    1   11   12   13
TIME      PØUNDS                        TEST 13-1974 FØRCES 3/2
0000000000
   10
    1   29   62   63   64   65   66   67   68   69
    1    2    3
TIME      IN/SEC                        TEST 13-1974 ALPHAD
    1    4
TIME      IN/SC2                        TEST 13-1974 ALPHADD
    1    5    6
TIME      DEG                           TEST 13-1974 THETA, PHI
    1    7
TIME      DEG/SK                        TEST 13-1974 PHIDT
    1    8    9   10
TIME      PØUNDS                        TEST 13-1974 LIG. FØRCES FX, FY, FZ
0000000010
STØP
```

TABLE A-3. INPUT VARIABLE DEFINITIONS FOR LAMPS3

VARIABLE		DESCRIPTION (FORMAT)≠
RUNNO UNAME	= =	Run number printed in page heading User name printed in page heading } (A6,4X,3A6)
TITLE1	=	Title card printed in page heading (12A6)
TITLE2	=	Title card printed in page heading (12A6)
COMMENT	=	Comment cards, last card = zeros in columns 1 through 10
θY,θZ,θX	=	Initial β's for hinge q_2/p_2 (Figure A-1) θY = 0 radians θZ = -(π/2) + THETA radians θY = π - PHI radians where: THETA = output of program TANK (if PHI=0° or PHI=180° use THETA= π/2 radians) PHI = output of program TANK
T_o	=	Start time, seconds
ΔT	=	Time interval for integration, seconds
T_E	=	End time for the program, seconds
PR	=	Print every PRth time interval
PL	=	Plot every PLth time interval
a,c	=	Ellipsoidal surface coefficients from program TANK
K	=	Differentiation algorithm gain
FX,FY,FZ	=	Forces applied to Body 1, see Figure A-1
MASFAC	=	Effective mass factor
R_o	=	Spherical coordinate distance to liquid cm at T_o
μ	=	Liquid damping, based on $\dot{\emptyset}$ (used in equation (A-11))
M1	=	Mass of the drop capsule (or rigid spacecraft) Body 1
I_{xx}, I_{yy}, I_{zz}	=	Principle moments of inertia of Body 1
M3	=	Liquid mass (Body 3) from program TANK
PTITLE	=	This portion of the plot titles may be changed to reflect problem being simulated

≠ Most of the input changes are to matrix inputs. These matrices are input via subroutine READ which is a FORMA subroutine. For details on subroutine READ see: R.L.Wohlen, "Synthesis of Dynamic Systems Using FORMA - Fortran Matrix Analysis". Martin Marietta Corp., MCR-71-75, Vol. IV, NAS8-25922, May 1971. Note: on the coding sheets (Table A-2) the allowable field for the numerical inputs is delineated by underlining, ie, 0. (θZ)* .

III-13). The specific variables in the state vector (Y) for our mechanization are as follows, (the variables in YDT are just the derivatives of the Y variables):

STATE VECTOR LOCATION	VARIABLE	
1	ω_x	Body 1 - Tank (Rigid Spacecraft)
2	ω_y	
3	ω_z	
4	u	
5	v	
6	w	
7	ω_x	Body 2 - Dummy
8	ω_y	
9	ω_z	
10	u	
11	v	
12	w	
13	ω_x	Body 3 - Liquid
14	ω_y	
15	ω_z	
16	u	
17	v	
18	w	
19	θ_y	β's: Body 1 to Inertial Triad
20	θ_z	
21	θ_x	
22	X	
23	Y	
24	Z	
25	θ_y	β's: Body 2 to Body 1
26	θ_x	
27	$Z_{3/2}$	β: Body 3 to Body 2
28	$\dot{\alpha}(R)$	Rehonomic $\dot{Z}_{3/2}$
29	$\int\theta$	$\int$ Spherical Coordinates of Liquid cm
30	$\int\phi$	
31	$\int\dot{\phi}$	
32	$\int FX_{L/T}$	$\int$ Liquid Forces Exerted on the Tank (Body 1)
33	$\int FY_{L/T}$	
34	$\int FZ_{L/T}$	

The liquid forces exerted on the tank, Body 1, are printed in the YDT vector; locations 32, 33 and 34.

The spherical coordinates of the liquid cm position are also found in the YDT vector; locations 29 and 30 $(\theta,\emptyset)$. The spherical coordinate, R, is found by:

$$R = R_o - Y(27) = R_o - Z_{3/2}$$

As mentioned earlier, the success of this implementation was dependent on differentiating $\dot{\alpha}$. The error in this differentiation can be assessed by comparing $Y(28), \int \ddot{\alpha}$, and $YDT(27)$, $\dot{Z}_{3/2}$. Both of these values are equivalent to $\dot{R}$. LAMPS3 plots these two variables for comparison. Along with the sample output presented at the end of this appendix are the plots generated by LAMPS3. Plots of FY and FZ from the two dimensional model LAMPS are also presented for comparison with the liquid forces generated by LAMPS3.

It will be noted that the two dimensional model, LAMPS, predicts slightly higher forces than LAMPS3. This is a result of the differences in implementation of the kinematics between the two programs. LAMPS3 includes the force feedback onto Body 1 due to the moving fluid, which results in altered gross accelerations during the course of the simulation. Program LAMPS does not include this feedback. In LAMPS, accelerations are applied directly to the liquid mass as opposed to forces applied to Body 1 in LAMPS3. The kinematics of LAMPS3 are correct for simulating actual spacecraft/liquid interactions.

SAMPLE OUTPUT ---- PROGRAM TANK

RUN NO. TANK13

DATE 10FE76
RUN BY RL BEPPY

11.46.51 CLOCK TIME
5.249 SEC. CPTIME
10 SEC. PPTIME

TEST 13 PHASE 1
3D MODEL

TEST 13
TANK INCLINATION =0.0
25 PERCENT FILL

11.47.19 CLOCK TIME
18.720 SEC. CPTIME
10 SEC. PPTIME

TEST 13 PHASE 1
3D MODEL

FLUIDCS CONSTRAINT SURFACE

/PHI(DEG)/	R
.00000	1.49893
90.00000	1.92103

RUN NO. TANK13

DATE 10FE76
RUN BY RL BERRY

PAGE NO.

11.47.19 CLOCK TIME
18.742 SEC. CPTIME
10 SEC. PPTIME

TEST 13 PHASE 1
30 MODEL

OUTPUT MATRIX Y7 (2 X 2)

		(1)	(2)	(3)	(4)	(5)	(6)	(7)	(8)	(9)	(10)
1	1	2.247E+00	2.788E-26								
2	1	9.665E-24	3.690E+00								

END OF WRITE.

11.47.19 CLOCK TIME
18.773 SEC. CPTIME
10 SEC. PPTIME

TEST 13 PHASE 1
3D MODEL

(1) (2) (3) (4) (5) (6) (7) (8) (9) (10)

SUBROUTINE INV5 HAS CALCULATED THE DATA BELOW

THE (A**-1)*(A) INVERSION CHECK GIVES

THE DIAGONAL ELEMENTS ARE

1.00000000 1.00000000

THE MAXIMUM OFF-DIAGONAL ELEMENT IS 1.175E-38 AT (2, 1)

11.47.19 CLOCK TIME
19.804 SEC. CPTIME
10 SEC. PPTIME

TEST 13 PHASE 1
3D MODEL

OUTPUT MATRIX VZI (2 X 2)

		(1)	(2)	(3)	(4)	(5)	(6)	(7)	(8)	(9)	(10)
1	1	4.451E-01	-3.363E-27								
2	1	-1.166E-24	2.710E-01								

END OF WRITE.

11.47.19 CLOCK TIME
18.841 SEC. CPTIME
11 SEC. PPTIME

TEST 13 PHASE 1
3D MODEL

ELLIPTICAL SURFACE COEFS
AC= 4.451E-01
CC= 2.719E-01

AC*X**2+AC*Y**2+CC*Z**2=1

11.47.20 CLOCK TIME
18.861 SEC. CPTIME
11 SEC. PPTIME

TEST 13 PHASE 1
3D MODEL

SUBROUTINE FLUIDCG

INPUT DATA

TANK ORIENTATION GX= 0.
GY= 0.
GZ= 1.00000
TANK GEOMETRY XL= 1.40000
A= 2.50000
B= 2.50000
% FLUID FILL PCVOL= 25.00000
INTEGRATION PARAMS NR= 50
NTHET= 50
ITERATION CUTOFF ABS(V-VN).LT.(VXX*VFLUID/100.)= .46469

Z AXIS INTERCEPT	FLUID VOLUME	% FILL	V(N)	V(N-1)	ITERATION
1.37500	57.29395	61.647	0.	57.29395	1
1.37500	59.74832	64.288	59.74832	57.29395	2
-.48467	23.33728	25.110	23.33728	59.74832	3
-.48987	23.23846	25.004			4

FLUID CG IS LOCATED AT
XBAR= -.00000
YBAR= .00000
ZBAR= -1.92103

*****VOLUMES - VTANK= 92.93870
VFLUID= 23.23468

11.47.35 CLOCK TIME
25.412 SEC. CPTIME
11 SEC. PPTIME

TEST 13 PHASE 1
3D MODEL

TANK PROPERTIES

XL	=	1.40
TP	=	2.50
TD	=	2.50
PCVOL	=	25.01
FDEN	=	1.78E-04

TANK AND FLUID VOLUMES

TANK VOLUME=	92.9387	CU UNITS
FLUID VOLUME=	23.2347	CU UNITS
FLUID MASS=	.0041	F-SEC**2/L

11.47.35 CLOCK TIME
25.448 SEC. CPTIME
11 SEC. PPTIME

TEST 13 PHASE 1
3D MODEL

INITIAL ACCELERATION FIELD
TANK TRIAD GX= 0. GY= 0. GZ= 1.0000

TEST 13 PHASE 1
3D MODEL

11.47.35 CLOCK TIME
25.490 SEC. CPTIME
11 SEC. PPTIME

** FLUID CM-TANK TRIAD **

	CARTESIAN X	Y	Z	SPHERICAL R	PHI	THETA
	-.0000	.0000	-1.9210	1.9210	180.0000	179.9998
CORRECTED	-.0000	.0000	-1.9210	1.9210	180.0000	179.9998

SAMPLE OUTPUT ---- PROGRAM LAMPS3

12.08.50 CLOCK TIME
36.740 SEC. CPTIME
29 SEC. PPTIME

SIMULATION OF TLM TEST CASE 13 (PHASE I)
TRANSIENT LIQUID MOTION...PHI=0 DEG, 25 % FILL

3 DIMENSIONAL LARGE AMPLITUDE SLOSH MODEL
SAMPLE CASE

12.08.50 CLOCK TIME
36.791 SEC. CPTIME
29 SEC. PPTIME

SIMULATION OF TLM TEST CASE 13 (PHASE I)
TRANSIENT LIQUID MOTION...PHI=0 DEG, 25 % FILL

CARD INPUT INTEGER MATRIX ITOPOL (2 X 3) HINGE TOPOLOGY -0

1	1	1	2	3
2	1	0	1	2

END OF READIM.

12.08.50 CLOCK TIME
36.801 SEC. CPTIME
29 SEC. PPTIME

SIMULATION OF TLM TEST CASE 13 (PHASE I)
TRANSIENT LIQUID MOTION...PHI=0 DEG, 25 % FILL

CARD INPUT INTEGER MATRIX IRGFLX (1 X 3) RIGID BODY SPECIFICATION -0

END OF READIM.

12.09.50 CLOCK TIME
36.856 SEC. CPTIME
29 SEC. PPTIME

SIMULATION OF TLM TEST CASE 13 (PHASE I)
TRANSIENT LIQUID MOTION...PHI=0 DEG, 25 % FILL

CARD INPUT INTEGER MATRIX IFTSMW (1 X 2) SENSOR POINT LOCATIONS -0

1 1 1 3

END OF READTM.

SIMULATION OF TLM TEST CASE 13 (PHASE I)
TRANSIENT LIQUID MOTION...PHI=0 DEG, 25 % FILL

12.08.50 CLOCK TIME
36.892 SEC. CPTIME
29 SEC. PPTIME

CARD INPUT INTEGER MATRIX IHDATA (7 X 3) HINGE CONSTRAINT DATA

-0

1	1	5	5	5
2	1	0	0	1
3	1	0	1	1
4	1	0	0	1
5	1	0	1	1
6	1	0	1	1
7	1	0	1	2

END OF READIM.

12.08.50 CLOCK TIME
36.946 SEC. CPTIME
29 SEC. PPTIME

SIMULATION OF TLM TEST CASE 13 (PHASE T)
TRANSIENT LIQUID MOTION...PHI=0 DEG, 25 % FILL

CARD INPUT MATRIX BETAH (6 X 3) INITIAL HINGE BETAS

-0

END OF READ,

12.08.51 CLOCK TIME
36.983 SEC. CPTIME
29 SEC. PPTIME

SIMULATION OF TLM TEST CASE 13 (PHASE I)
TRANSIENT LIQUID MOTION...PHI=0 DEG, 25 % FILL

CARD INPUT MATRIX BETAHD (6 X 3) INITIAL HINGE BETA DOTS -0

END OF READ.

12.08.51 CLOCK TIME
37.016 SEC. CPTIME
29 SEC. PPTIME

SIMULATION OF TLM TEST CASE 13 (PHASE I)
TRANSIENT LIQUID MOTION...PHI=0 DEG, 25 % FILL

CARD INPUT MATRIX TIMES (1 X 3) STARTT,DELTAT,ENDT -0

1 1 0. 1.00000000E-02 1.60000000E+00

END OF READ.

SIMULATION OF TLM TEST CASE 13 (PHASE I)
TRANSIENT LIQUID MOTION...PHI=0 DEG, 25 % FILL

12.08.51 CLOCK TIME
37.061 SEC. CPTIME
29 SEC. PPTIME

CARD INPUT INTEGER MATRIX IPDATA (1 X 3) OUTPUT CONTROL INFO. -0

1 1 1 1 0

END OF READIM.

12.08.51 CLOCK TIME
37.061 SEC. CPTIME
29 SEC. PPTIME

SIMULATION OF TLM TEST CASE 13 (PHASE I)
TRANSIENT LIQUID MOTION...PHI=0 DEG, 25 % FILL

CARD INPUT MATRIX CNTDTA (1 X 100): USER SUPPLIED PARAMETERS -0

1	20	4.45100000E-01	2.71000000E-01	-0.	-0.
1	32	7.28125000E+00	-0.	-0.	-0.
1	33	-3.00352600E+01	-0.	-0.	-0.
1	34	1.00000300E+00	-0.	-0.	-0.
1	35	1.92030000E+00	-0.	-0.	-0.
1	71	0.	-0.	-0.	-0.

END OF READ.

12.08.51 CLOCK TIME
37.134 SEC. CPTIME
29 SEC. PPTIME

SIMULATION OF TLM TEST CASE 13 (PHASE I)
TRANSIENT LIQUID MOTION...PHI=0 DEG, 25 % FILL

SUMMARY OF TRANSIENT LIQUID MOTION INPUT DATA * * * * * * * * * *

ACTUAL SIZES			MAXIMUM SIZES			INTEGRATION DATA		MISC. DATA	
NP	=	3	NPMAX	=	6	START	= 0.	NOPRNT	= 1
NH	=	3	NHMAX	=	6	DELTAT	= 1.000E-02	NOPLOT	= 1
NSET	=	2	NSPMAX	=	10	END	= 1.600E+00		
NOEMO	=	0	NMWMAX	=	5				
NDELTA	=	7	NMWPOD	=	3				
NU	=	18	NMOPOD	=	1				
NETA	=	9	KMU	=	10				
NLAM	=	10	KY	=	250				
NEQ	=	34	KU	=	55				

THE TOPOLOGY ARRAY (ITOPOL) FOR THIS CASE FOLLOWS

		(1)	(2)	(3)
1	1	1	2	3
2	1	0	1	2

THE CONSTRAINT SPECIFICATIONS FOR THIS CASE FOLLOW

		(1)	(2)	(3)
1	1	5	5	5
2	1	0	0	1
3	1	0	1	1
4	1	0	0	1
5	1	0	1	1
6	1	0	1	1
7	1	0	1	2

THE SPECIFIED INITIAL HINGE ANGLES AND DISPLACEMENTS (BETAH) FOLLOW

		(1)	(2)	(3)
1	1	0.	0.	0.
2	1	0.	0.	0.
3	1	0.	0.	0.
4	1	0.	0.	0.
5	1	0.	0.	0.
6	1	0.	0.	0.

THE SPECIFIED INITIAL HINGE RATES (BETAHD) FOLLOW

		(1)	(2)	(3)
1	1	0.	0.	0.
2	1	0.	0.	0.
3	1	0.	0.	0.
4	1	0.	0.	0.
5	1	0.	0.	0.
6	1	0.	0.	0.

12.08.51 CLOCK TIME
37.265 SEC. CPTIME
29 SEC. PPTIME

STMULATION OF TLM TEST CASE 13 (PHASE I)
TRANSIENT LIQUID MOTION...PHI=0 DEG, 25 % FILL

THE NO. OF ELASTIC MODES/BODY ARRAY (IRGFLX) FOLLOWS

		(1)	(2)	(3)
1	1	0	0	0

THE NO. OF P/O HINGE POINTS/BODY ARRAY (NHPOT) FOLLOWS

		(1)	(2)	(3)
1	1	1	2	1

THE NO. OF SENSOR POINTS/BODY ARRAY (NSPOT) FOLLOWS

		(1)	(2)	(3)
1	1	1	0	1

THE MOM. WHEEL/BODY TABLE (NMOW) FOLLOWS

		(1)	(2)	(3)
1	1	0	0	0
2	1	0	0	0
3	1	0	0	0
4	1	0	0	0
5	1	0	0	0

THE STATE VECTOR LENGTH ARRAY (LENU) FOLLOWS

		(1)	(2)	(3)	(4)	(5)	(6)	(7)	(8)
1	1	6	6	6	0	0	0	3	7

THE STATE VECTOR LOCATION ARRAY (LOCU) FOLLOWS

		(1)	(2)	(3)	(4)	(5)	(6)	(7)	(8)
1	1	1	7	13	19	19	19	19	28

THE SPECIFIED SENSOR POINT/BODY CORRELATION ARRAY (IFTSMW) FOLLOWS

		(1)	(2)
1	1	1	3

12.08.51 CLOCK TIME
37.328 SEC. CPTIME
29 SEC. PPTIME

SIMULATION OF TLM TEST CASE 13 (PHASE I)
TRANSIENT LIQUID MOTION...PHI=0 DEG, 25 % FILL

THE FOLLOWING DATA IS SPECIFIED MOM. WHEEL INFORMATION (IF ANY) AND CONTROLLER INFORMATION

THE SPECIFIED CONTROLLER INITIAL CONDITIONS AND CHARACTERISTICS FOLLOW
(THE FIRST NDELTA ARE INITIAL CONTROLLER STATE VARIABLES, THERE ARE 93 ADDITIONAL CONTROL PARAMETERS)

		(1)	(2)	(3)	(4)	(5)	(6)	(7)	(8)	(9)	(10)
1	1	0.	0.	0.	0.	0.	0.	0.	0.	0.	0.
1	11	0.	0.	0.	0.	0.	0.	0.	0.	0.	4.451E-01
1	21	2.710E-01	-0.	-0.	0.	0.	0.	0.	0.	0.	0.
1	31	0.	7.291E+00	-3.010E+01	1.000E+00	1.920E+00	-0.	-0.	-0.	0.	0.
1	41	0.	0.	0.	0.	0.	0.	0.	0.	0.	0.
1	51	0.	0.	0.	0.	0.	0.	0.	0.	0.	0.
1	61	0.	0.	0.	0.	0.	0.	0.	0.	0.	0.
1	71	0.	-0.	-0.	-0.	0.	0.	0.	0.	0.	0.
1	81	0.	0.	0.	0.	0.	0.	0.	0.	0.	0.
1	91	0.	0.	0.	0.	0.	0.	0.	0.	0.	0.

SIMULATION OF TLM TEST CASE 13 (PHASE I)
TRANSIENT LTOUTD MOTION...PHT=0 DEG, 25 % FILL

12.08.51 CLOCK TIME
37.426 SEC. CPTIME
29 SEC. PPTIME

CARD INPUT MATRIX MXYZ (1 X 4) BODY 1 (DROP CAPSULE MASS)

-0

1 1 8.70000000E-01 -0. -0. -0.

END OF READ.

SIMULATION OF TLM TEST CASE 13 (PHASE I)
TRANSIENT LIQUID MOTION...PHI=0 DEG, 25 % FILL

12.08.51 CLOCK TIME
37.456 SEC. CPTIME
29 SEC. PPTIME

CARD INPUT MATRIX INERT (1 X 6)

-0

1 1 1.00000000E+01 1.00000000E+01 1.00000000E+01 -0.

END OF READ.

12.08.51 CLOCK TIME
37.509 SEC. CPTIME
29 SEC. PPTIME

SIMULATION OF TLM TEST CASE 13 (PHASE I)
TRANSIENT LIQUID MOTION...PHI=0 DEG, 25 % FILL

SUMMARY OF INPUT DATA FOR BODY 1 WHICH IS PIGID.

THE 6X6 INERTIA MATRIX IS ---

		(1)	(2)	(3)	(4)	(5)	(6)
1	1	1.000E+01	0.	-0.	0.	-0.	0.
2	1	0.	1.000E+01	-0.	0.	0.	-0.
3	1	-0.	-0.	1.000E+01	-0.	0.	0.
4	1	0.	0.	-0.	8.700E-01	0.	0.
5	1	-0.	0.	0.	0.	8.700E-01	0.
6	1	0.	-0.	0.	0.	0.	8.700E-01

FOR BODY 1 THE P-O HINGE NO. AND THE EULER ROTATION TYPE APPEAR IN THE FOLLOWING INTEGER ARRAY WHICH IS FOLLOWED BY AN ARRAY CONTAINING EULER ANGLES (1,2,3), AND POSITION VECTOR COMPONENTS (4,5,6) THAT POSITION THE HINGE TRIAD WRT THE BODY TRIAD

		(1)	(2)
1	1	2	1

		(1)	(2)	(3)	(4)	(5)	(6)
1	1	0.	0.	0.	0.	0.	0.

FOR BODY 1 THE SENSOR POINT NO. AND THE EULER ROTATION TYPE APPEAR IN THE FOLLOWING INTEGER ARRAY WHICH IS FOLLOWED BY AN ARRAY CONTAINING EULER ANGLES(1,2,3), AND POSITION VECTOR COMPONENTS (4,5,6) THAT POSITION THE SENSOR TRIAD WRT THE BODY TRIAD

		(1)	(2)
1	1	1	1

		(1)	(2)	(3)	(4)	(5)	(6)
1	1	0.	0.	0.	0.	0.	0.

SIMULATION OF TLM TEST CASE 13 (PHASE I)
TRANSIENT LIQUID MOTION...PHI=0 DEG, 25 % FILL

12.08.52 CLOCK TIME
37.589 SEC. CPTIME
30 SEC. PPTIME

CARD INPUT MATRIX MXYZ (1 X 4) BODY 2 (DUMMY MASS) -0

1	1	1.00010000E-05	-0.	-0.	-0.

END OF READ.

12.08.52 CLOCK TIME
37.634 SEC. CPTIME
30 SEC. PPTIME

SIMULATION OF TLM TEST CASE 13 (PHASE I)
TRANSIENT LIQUID MOTION...PHI=0 DEG, 25 % FILL

CARD INPUT MATRIX INERT (1 X 6) -0

1 1 1.00000000E-04 1.00000000E-04 1.00000000E-04 -0.

END OF READ.

12.08.52 CLOCK TIME
37.680 SEC. CPTIME
30 SEC. PPTIME

SIMULATION OF TLM TEST CASE 13 (PHASE I)
TRANSIENT LIQUID MOTION...PHI=0 DEG, 25 % FILL

SUMMARY OF INPUT DATA FOR BODY 2 WHICH IS RIGID.

THE 6X6 INERTIA MATRIX IS ---

		(1)	(2)	(3)	(4)	(5)	(6)
1	1	1.000E-04	0.	-0.	0.	-0.	0.
2	1	0.	1.000E-04	-0.	0.	0.	-0.
3	1	-0.	-0.	1.000E-04	-0.	0.	0.
4	1	0.	0.	-0.	1.000E-05	0.	0.
5	1	-0.	0.	0.	0.	1.000E-05	0.
6	1	0.	-0.	0.	0.	0.	1.000E-05

FOR BODY 2 THE P-O HINGE NO. AND THE EULER ROTATION TYPE APPEAR IN THE FOLLOWING INTEGER ARRAY WHICH IS FOLLOWED BY AN ARRAY CONTAINING EULER ANGLES (1,2,3), AND POSITION VECTOR COMPONENTS (4,5,6) THAT POSITION THE HINGE TRIAD WRT THE BODY TRIAD

		(1)	(2)
1	1	2	1
2	1	3	1

		(1)	(2)	(3)	(4)	(5)	(6)
1	1	0.	0.	0.	0.	0.	1.920E+00
2	1	0.	0.	0.	0.	0.	0.

12.08.52 CLOCK TIME
37.736 SEC. CPTIME
30 SEC. PPTIME

STMULATTON OF TLM TEST CASE 13 (PHASE T)
TRANSIENT LIQUID MOTION...PHI=0 DEG, 25 % FILL

CARD INPUT MATRIX MXYZ (1 X 4) BODY 3 (FLUTD) -0

1 1 4.03000000E-03 -0. -0. -0.

END OF READ.

SIMULATION OF TLM TEST CASE 13 (PHASE I)
TRANSIENT LTOUTD MOTION...PHI=0 DEG, 25 % FILL

12.08.53 CLOCK TIME
37.804 SEC. CPTIME
30 SEC. PPTIME

CARD INPUT MATRIX INERT (1 X 6)

-0

1 1 1.00000000E-04 1.00000000E-04 1.00000000E-04 -0,

END OF READ.

12.08.53 CLOCK TIME
37.849 SEC. CPTIME
30 SEC. PPTIME

SIMULATION OF TLM TEST CASE 13 (PHASE I)
TRANSIENT LIQUID MOTION...PHI=0 DEG, 25 % FILL

SUMMARY OF INPUT DATA FOR BODY 3 WHICH IS PIGID.

THE 6X6 INERTIA MATRIX IS ---

		(1)	(2)	(3)	(4)	(5)	(6)
1	1	1.000E-04	0.	-0.	0.	-0.	0.
2	1	0.	1.000E-04	-0.	0.	0.	-0.
3	1	-0.	-0.	1.000E-04	-0.	0.	0.
4	1	0.	0.	-0.	4.090E-03	0.	0.
5	1	-0.	0.	0.	0.	4.090E-03	0.
6	1	0.	-0.	0.	0.	0.	4.090E-03

FOR BODY 3 THE P-O HINGE NO. AND THE EULER ROTATION TYPE APPEAR IN THE FOLLOWING INTEGER ARRAY WHICH IS FOLLOWED BY AN ARRAY CONTAINING EULER ANGLES (1,2,3), AND POSITION VECTOR COMPONENTS (4,5,6) THAT POSITION THE HINGE TRIAD WRT THE BODY TRIAD

		(1)	(2)
1	1	3	1

		(1)	(2)	(3)	(4)	(5)	(6)
1	1	0.	0.	0.	0.	0.	0.

FOR BODY 3 THE SENSOR POINT NO. AND THE EULER ROTATION TYPE APPEAR IN THE FOLLOWING INTEGER ARRAY WHICH IS FOLLOWED BY AN ARRAY CONTAINING EULER ANGLES(1,2,3), AND POSITION VECTOR COMPONENTS (4,5,6) THAT POSITION THE SENSOR TRIAD WRT THE BODY TRIAD

		(1)	(2)
1	1	2	1

		(1)	(2)	(3)	(4)	(5)	(6)
1	1	0.	0.	0.	0.	0.	0.

THE FOLLOWING INTEGER ARRAY (INDEP) PRESCRIBES INDEPENDENT VARIABLES (1), AND DEPENDENT VARIABLES (0)

		(1)	(2)	(3)	(4)	(5)	(6)	(7)	(8)	(9)	(10)	(11)	(12)	(13)	(14)	(15)	(16)	(17)	(18)	(19)	(20)
1	1	1	1	1	1	1	0	0	0	0	0	0	0	0	0	0	1	1	1	1	1
1	21	1	1	1	1	1	1	1	1	1	1	1	1	1	1						

12.08.54 CLOCK TIME
38.391 SEC. CPTIME
30 SEC. PPTIME

SIMULATION OF TLM TEST CASE 13 (PHASE I)
TRANSIENT LIQUID MOTION...PHI=0 DEG, 25 % FILL

AT SIMULATION TIME, T = 0 *

THE STATE VECTOR Y =

		(1)	(2)	(3)	(4)	(5)	(6)	(7)	(8)	(9)	(10)
1	1	0.	0.	0.	0.	0.	0.	0.	0.	0.	0.
1	11	0.	0.	0.	0.	0.	0.	0.	0.	0.	0.
1	21	0.	0.	0.	0.	0.	0.	0.	0.	0.	0.
1	31	0.	0.	0.	0.						

AT SIMULATION TIME, T = 0 *

THE STATE VECTOR TIME DERIVATIVE YDT =

		(1)	(2)	(3)	(4)	(5)	(6)	(7)	(8)	(9)	(10)
1	1	0.	0.	0.	0.	8.369E+00	-3.443E+01	-4.301E+00	0.	0.	0.
1	11	1.093E-01	-3.443E+01	-4.301E+00	0.	0.	0.	1.093E-01	-3.443E+01	0.	0.
1	21	0.	0.	0.	0.	0.	0.	0.	0.	1.900E+02	1.900E+02
1	31	0.	0.	0.	0.						

AT SIMULATION TIME, T = 0 *

THE BETAS (EULER ANGLES, POSITION COORDINATES) ARE

		(1)	(2)	(3)
1	1	0.	0.	0.
2	1	0.	0.	0.
3	1	0.	0.	0.
4	1	0.	0.	0.
5	1	0.	0.	0.
6	1	0.	0.	0.

AT SIMULATION TIME, T = 0 *

THE BETA TIME DERIVATIVES ARE

		(1)	(2)	(3)
1	1	0.	0.	0.
2	1	0.	0.	0.
3	1	0.	0.	0.
4	1	0.	0.	0.
5	1	0.	0.	0.
6	1	0.	0.	0.

AT SIMULATION TIME, T = 0 *

THE DELTAS (CONTROL SYSTEM VARIABLES) ARE

		(1)	(2)	(3)	(4)	(5)	(6)	(7)
1	1	0.	0.	0.	0.	0.	0.	0.

AT SIMULATION TIME, T = 0 *

THE DELTA TIME DERIVATIVES ARE

		(1)	(2)	(3)	(4)	(5)	(6)	(7)
1	1	0.	1.900E+02	1.900E+02	0.	0.	0.	0.

AT SIMULATION TIME, T = 0 *

FOR BODY 1 THE VELOCITIES ARE

```
  1    1     0.          0.          0.          0.          0.          0.
FOR BODY  1   THE CORRESPONDING MOMENTA ARE
              ( 1)        ( 2)        ( 3)        ( 4)        ( 5)        ( 6)
  1    1     0.          0.          0.          0.          0.          0.
FOR BODY  1   ITS CONTRIBUTION TO TOTAL ANGULAR AND LINEAR MOMENTUM IS
              ( 1)        ( 2)        ( 3)        ( 4)        ( 5)        ( 6)
  1    1     0.          0.          0.          0.          0.          0.
ITS CONTRIBUTION TO TOTAL KINETIC AND POTENTIAL ENERGIES IS     0.              0.


      AT SIMULATION TIME, T = 0          * * * * * * * * * * * * * * * * * * * * * * * * * * * * * * * * * * * *
FOR BODY  2   THE VELOCITIES ARE
              ( 1)        ( 2)        ( 3)        ( 4)        ( 5)        ( 6)
  1    1     0.          0.          0.          0.          0.          0.
FOR BODY  2   THE CORRESPONDING MOMENTA ARE
              ( 1)        ( 2)        ( 3)        ( 4)        ( 5)        ( 6)
  1    1     0.          0.          0.          0.          0.          0.
FOR BODY  2   ITS CONTRIBUTION TO TOTAL ANGULAR AND LINEAR MOMENTUM IS
              ( 1)        ( 2)        ( 3)        ( 4)        ( 5)        ( 6)
  1    1     0.          0.          0.          0.          0.          0.
ITS CONTRIBUTION TO TOTAL KINETIC AND POTENTIAL ENERGIES IS     0.              0.


      AT SIMULATION TIME, T = 0          * * * * * * * * * * * * * * * * * * * * * * * * * * * * * * * * * * * *
FOR BODY  3   THE VELOCITIES ARE
              ( 1)        ( 2)        ( 3)        ( 4)        ( 5)        ( 6)
  1    1     0.          0.          0.          0.          0.          0.
FOR BODY  3   THE CORRESPONDING MOMENTA ARE
              ( 1)        ( 2)        ( 3)        ( 4)        ( 5)        ( 6)
  1    1     0.          0.          0.          0.          0.          0.
FOR BODY  3   ITS CONTRIBUTION TO TOTAL ANGULAR AND LINEAR MOMENTUM IS
              ( 1)        ( 2)        ( 3)        ( 4)        ( 5)        ( 6)
  1    1     0.          0.          0.          0.          0.          0.
ITS CONTRIBUTION TO TOTAL KINETIC AND POTENTIAL ENERGIES IS     0.              0.


      AT SIMULATION TIME, T = 0          * * * * * * * * * * * * * * * * * * * * * * * * * * * * * * * * * * * *
THE INTERCONNECTION CONSTRAINT FORCES(LAMBDAS) ARE
              ( 1)        ( 2)        ( 3)        ( 4)        ( 5)        ( 6)        ( 7)        ( 8)        ( 9)        (10)
  1    1     0.          0.          4.480E-04 -1.412E-01  0.          0.         -4.301E-04  0.          4.469E-04 -1.408E-01


      AT SIMULATION TIME, T = 0          * * * * * * * * * * * * * * * * * * * * * * * * * * * * * * * * * * * *
THE TOTAL ANGULAR MOMENTUM VECTOR IS
              ( 1)        ( 2)        ( 3)
  1    1     0.          0.          0.
THE TOTAL LINEAR MOMENTUM VECTOR IS
              ( 1)        ( 2)        ( 3)
  1    1     0.          0.          0.

THE TOTAL ANGULAR MOMENTUM =  0.
THE TOTAL LINEAR MOMENTUM  =  0.
THE TOTAL KINETIC ENERGY   =  0.
THE TOTAL POTENTIAL ENERGY =  0.
THE TOTAL ENERGY (T + V)   =  0.
```

15.40.53 CLOCK TIME
229.442 SEC. CPTIME
64 SEC. PPTIME

SIMULATION OF TLM TEST CASE 13 (PHASE I)
TRANSIENT LIQUID MOTION...PHI=0 DEG, 25 % FILL

AT SIMULATION TIME, T = 1.6000E+00* *
THE STATE VECTOR Y =

		(1)	(2)	(3)	(4)	(5)	(6)	(7)	(8)	(9)	(10)
1	1	2.009E-15	0.	0.	0.	1.329E+01	-5.509E+01	-1.751E-01	0.	0.	0.
1	11	-1.329E+01	-5.517E+01	-1.751E-01	0.	0.	0.	-1.329E+01	-5.524E+01	0.	0.
1	21	1.660E-15	0.	1.072E+01	-4.407E+01	0.	-5.316E+00	1.100E-01	-9.421E-02	2.947E+02	1.901E+02
1	31	-2.765E+01	0.	-5.363E-02	2.092E-01						

AT SIMULATION TIME, T = 1.6000E+00* *
THE STATE VECTOR TIME DERIVATIVE YDT =

		(1)	(2)	(3)	(4)	(5)	(6)	(7)	(8)	(9)	(10)
1	1	0.	0.	0.	0.	8.306E+00	-3.447E+01	4.177E+00	0.	0.	0.
1	11	9.569E+00	-3.678E+01	4.177E+00	0.	0.	0.	9.569E+00	-3.241E+01	0.	0.
1	21	2.009E-15	0.	1.329E+01	-5.509E+01	0.	-1.751E-01	-7.234E-02	4.373E+00	9.000E+01	1.532E+02
1	31	1.004E+01	0.	-5.520E-02	1.103E-01						

AT SIMULATION TIME, T = 1.6000E+00* *
THE BETAS (EULER ANGLES, POSITION COORDINATES) ARE

		(1)	(2)	(3)
1	1	0.	0.	0.
2	1	0.	0.	0.
3	1	1.660E-15	-5.316E+00	0.
4	1	0.	0.	0.
5	1	1.072E+01	0.	0.
6	1	-4.407E+01	0.	1.100E-01

AT SIMULATION TIME, T = 1.6000E+00* *
THE BETA TIME DERIVATIVES ARE

		(1)	(2)	(3)
1	1	0.	0.	0.
2	1	0.	0.	0.
3	1	2.009E-15	-1.751E-01	0.
4	1	0.	0.	0.
5	1	1.329E+01	0.	0.
6	1	-5.509E+01	0.	-7.234E-02

AT SIMULATION TIME, T = 1.6000E+00* *
THE DELTAS (CONTROL SYSTEM VARIABLES) ARE

		(1)	(2)	(3)	(4)	(5)	(6)	(7)
1	1	-9.421E-02	2.947E+02	1.901E+02	-2.765E+01	0.	-5.363E-02	2.092E-01

AT SIMULATION TIME, T = 1.6000E+00* *
THE DELTA TIME DERIVATIVES ARE

		(1)	(2)	(3)	(4)	(5)	(6)	(7)
1	1	4.373E+00	9.000E+01	1.532E+02	1.004E+01	0.	-5.520E-02	1.103E-01

AT SIMULATION TIME, T = 1.6000E+00* *
FOR BODY 1 THE VELOCITIES ARE

```
  1    1    2.009E-15  0.          0.          0.          1.329E+01 -5.509E+01
FOR BODY  1   THE CORRESPONDING MOMENTA ARE
             ( 1)        ( 2)        ( 3)        ( 4)        ( 5)        ( 6)
  1    1    2.303E-14  0.          0.          0.          1.157E+01 -4.793E+01
FOR BODY  1   ITS CONTRIBUTION TO TOTAL ANGULAR AND LINEAR MOMENTUM IS
             ( 1)        ( 2)        ( 3)        ( 4)        ( 5)        ( 6)
  1    1   -3.838E+00  0.          0.          0.          1.157E+01 -4.793E+01
ITS CONTRIBUTION TO TOTAL KINETIC AND POTENTIAL ENERGIES IS     1.33683744E+03 0.


      AT SIMULATION TIME, T = 1.6000E+00* * * * * * * * * * * * * * * * * * * * * * * * * * * * * * * * * *
FOR BODY  2   THE VELOCITIES ARE
             ( 1)        ( 2)        ( 3)        ( 4)        ( 5)        ( 6)
  1    1   -1.751E-01  0.          0.          0.         -1.329E+01 -5.517E+01
FOR BODY  2   THE CORRESPONDING MOMENTA ARE
             ( 1)        ( 2)        ( 3)        ( 4)        ( 5)        ( 6)
  1    1   -1.751E-05  0.          0.          0.         -1.329E-04 -5.517E-04
FOR BODY  2   ITS CONTRIBUTION TO TOTAL ANGULAR AND LINEAR MOMENTUM IS
             ( 1)        ( 2)        ( 3)        ( 4)        ( 5)        ( 6)
  1    1   -4.654E-04  0.          0.          0.          1.300E-04 -5.524E-04
ITS CONTRIBUTION TO TOTAL KINETIC AND POTENTIAL ENERGIES IS     1.61035693E-02 0.


      AT SIMULATION TIME, T = 1.6000E+00* * * * * * * * * * * * * * * * * * * * * * * * * * * * * * * * * *
FOR BODY  3   THE VELOCITIES ARE
             ( 1)        ( 2)        ( 3)        ( 4)        ( 5)        ( 6)
  1    1   -1.751E-01  0.          0.          0.         -1.329E+01 -5.524E+01
FOR BODY  3   THE CORRESPONDING MOMENTA ARE
             ( 1)        ( 2)        ( 3)        ( 4)        ( 5)        ( 6)
  1    1   -1.751E-05  0.          0.          0.         -5.436E-02 -2.259E-01
FOR BODY  3   ITS CONTRIBUTION TO TOTAL ANGULAR AND LINEAR MOMENTUM IS
             ( 1)        ( 2)        ( 3)        ( 4)        ( 5)        ( 6)
  1    1   -1.742E-01  0.          0.          0.          5.328E-02 -2.262E-01
ITS CONTRIBUTION TO TOTAL KINETIC AND POTENTIAL ENERGIES IS     6.60140326E+00 0.


      AT SIMULATION TIME, T = 1.6000E+00* * * * * * * * * * * * * * * * * * * * * * * * * * * * * * * * * *
THE INTERCONNECTION CONSTRAINT FORCES(LAMBDAS) ARE
             ( 1)        ( 2)        ( 3)        ( 4)        ( 5)        ( 6)        ( 7)        ( 8)        ( 9)        (10)
  1    1    0.          0.          5.520E-02 -1.103E-01  0.          0.          4.177E-04  0.         -4.342E-04 -1.230E-01


      AT SIMULATION TIME, T = 1.6000E+00* * * * * * * * * * * * * * * * * * * * * * * * * * * * * * * * * *
THE TOTAL ANGULAR MOMENTUM VECTOR IS
             ( 1)        ( 2)        ( 3)
  1    1   -4.012E+00  0.          0.
THE TOTAL LINEAR MOMENTUM VECTOR IS
             ( 1)        ( 2)        ( 3)
  1    1    0.          1.162E+01 -4.815E+01

THE TOTAL ANGULAR MOMENTUM =  4.01220241E+00
THE TOTAL LINEAR MOMENTUM  =  4.95340732E+01
THE TOTAL KINETIC ENERGY   =  1.40351435E+03
THE TOTAL POTENTIAL ENERGY =  0.
THE TOTAL ENERGY (T + V)   =  1.40351435E+03
```

15.40.53 CLOCK TIME
223.828 SEC. CPTIME
64 SEC. PPTIME

SIMULATION OF TLM TEST CASE 13 (PHASE I)
TRANSIENT LIQUID MOTION...PHI=0 DEG, 25 % FILL

SUMMARY OF PLOTTING INFORMATION

TRANSIENT LIQUID MOTION PLOTS

NSET = 2
NRPLOT = 161 NCPLOT = 132
KPPLOT = 500 KCPLOT = 16

ISET = 1
JVPL = 1 26 27 28 60 61 62 71 72 73 77 78 79

NCI = 1 NCD = 2 3 -0 NGRID = 1
TIME RADIAN TEST13-1974 BETA 2/1

NCI = 1 NCD = 4 -0 -0 NGRID = 1
TIME INCHES TEST13-1974 BETA 3/2

NCI = 1 NCD = 5 6 -0 NGRID = 1
TIME RAD/SC TEST13-1974 BETADT 2/1

NCI = 1 NCD = 7 -0 -0 NGRID = 1
TIME IN/SEC TEST13-1974 BETADT 3/2

NCI = 1 NCD = 8 9 10 NGRID = 1
TIME POUNDS TEST13-1974 FORCES 2/1

NCI = 1 NCD = 11 12 13 NGRID = 1
TIME POUNDS TEST13-1974 FORCES 3/2

ISET = 2
JVPL = 1 29 62 63 64 65 66 67 68 69

NCI = 1 NCD = 2 3 -0 NGRID = 1
TIME IN/SEC TEST13-1974 ALPHAD

NCI = 1 NCD = 4 -0 -0 NGRID = 1
TIME IN/SC2 TEST13-1974 ALPHADD

NCI = 1 NCD = 5 6 -0 NGRID = 1
TIME DEG TEST13-1974 THETA,PHI

```
NCI  =    1      NCD  =    7    -0   -0      NGRID =
TIME      DEG/SC                    TEST13-1974 PHIDT

NCI  =    1      NCD  =    8     9   10      NGRID =    1
TIME      POUNDS                    TEST13-1974 LIQ. FORCES FX,FY,FZ
```

TIME SHEET

CURRENT TIME OF DAY IN H,M,S = 15.43.55.

TOTAL CPTIME USED TO NOW = 234.363 SECONDS.
TOTAL PPTIME USED TO NOW = 81 SECONDS.

END OF INPUT DATA HAS BEEN REACHED.

SAMPLE PLOTS ---- PROGRAM LAMPS3

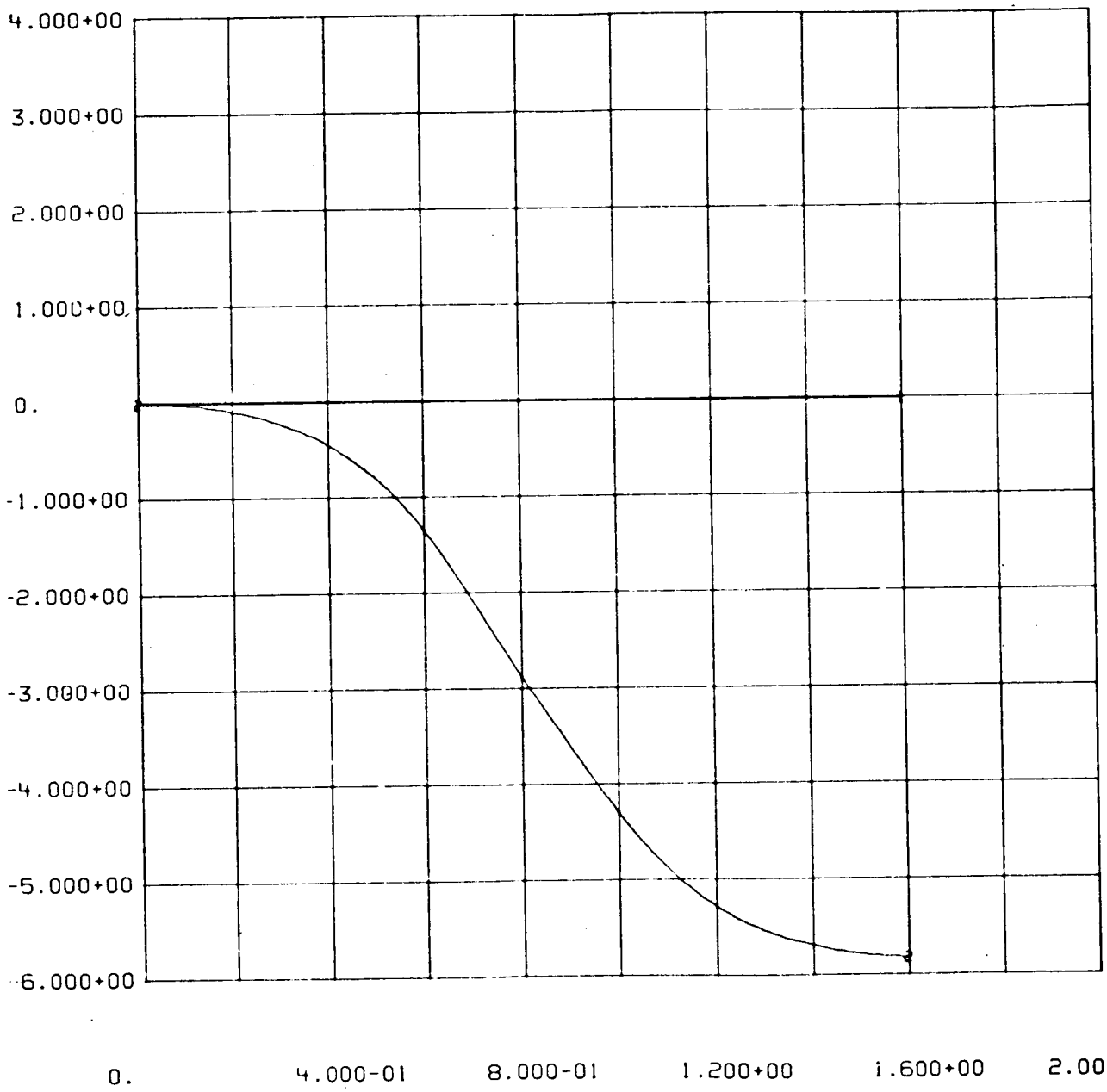

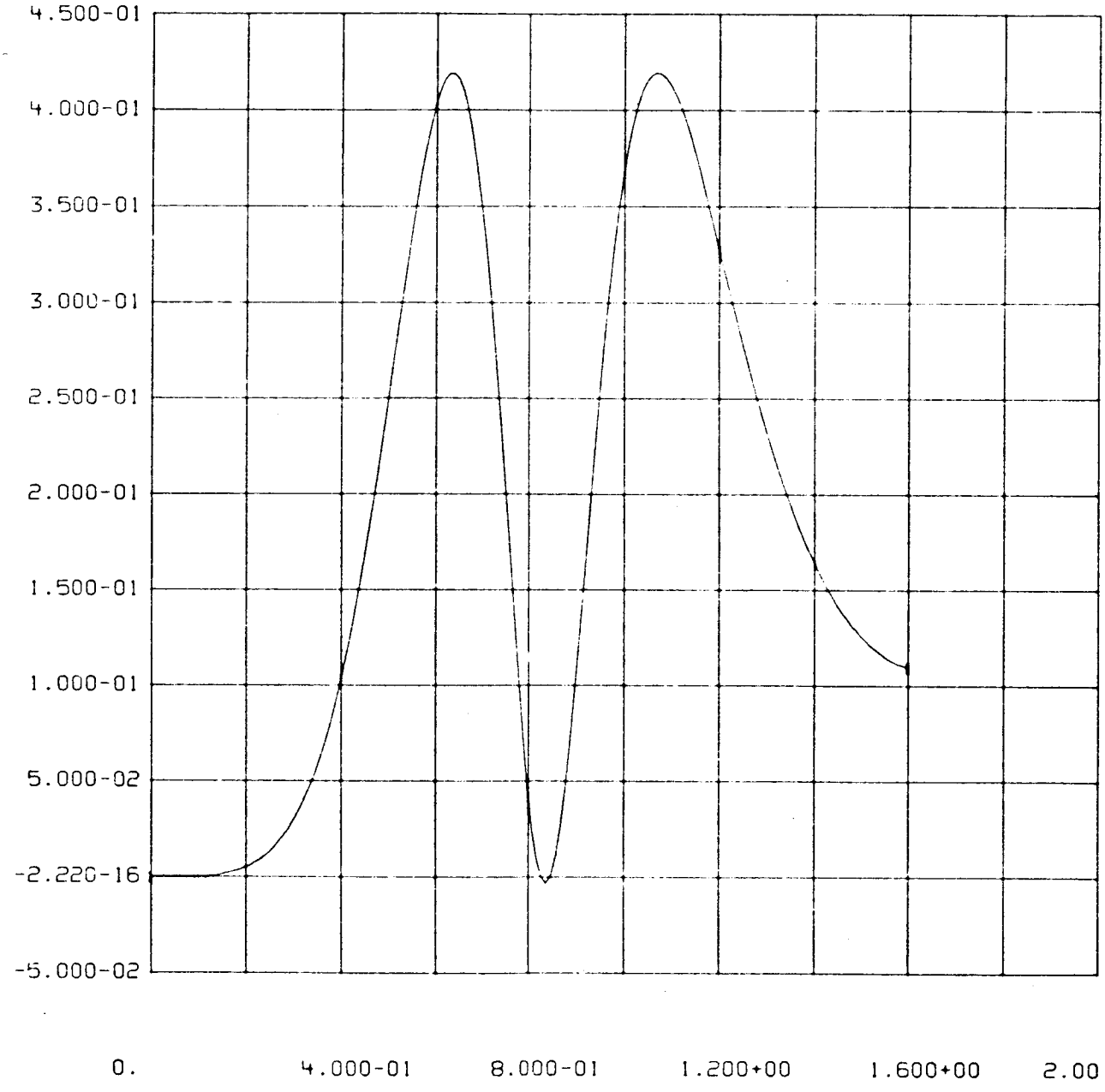
4.500-01
4.000-01
3.500-01
3.000-01
2.500-01
2.000-01
1.500-01
1.000-01
5.000-02
-2.220-16
-5.000-02
0.
4.000-01
8.000-01
1.200+00
1.600+00
2.00
INCHES
VS
TIME
1
TLM13
02FE76
TEST13-1974 BETA 3/2

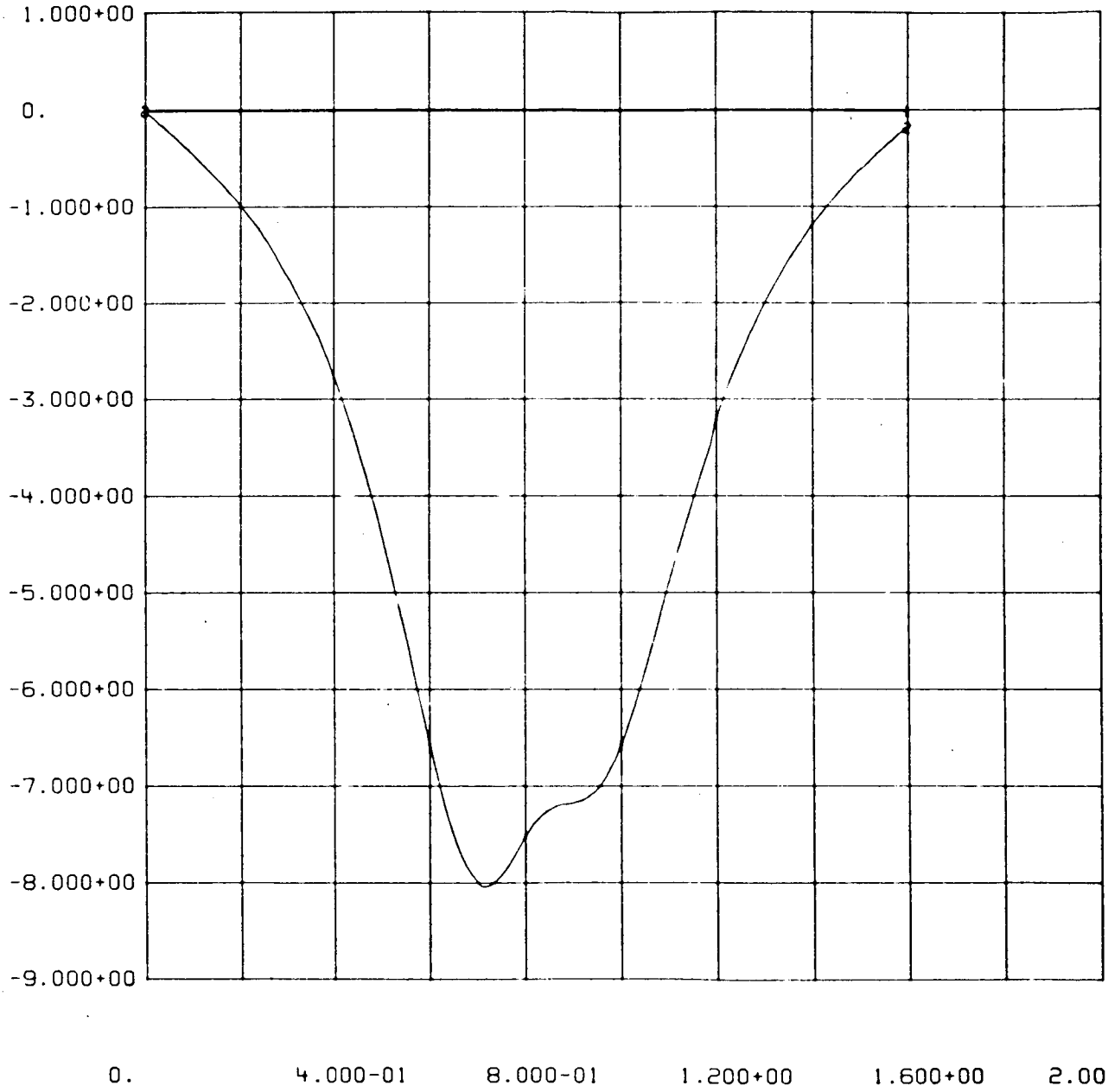

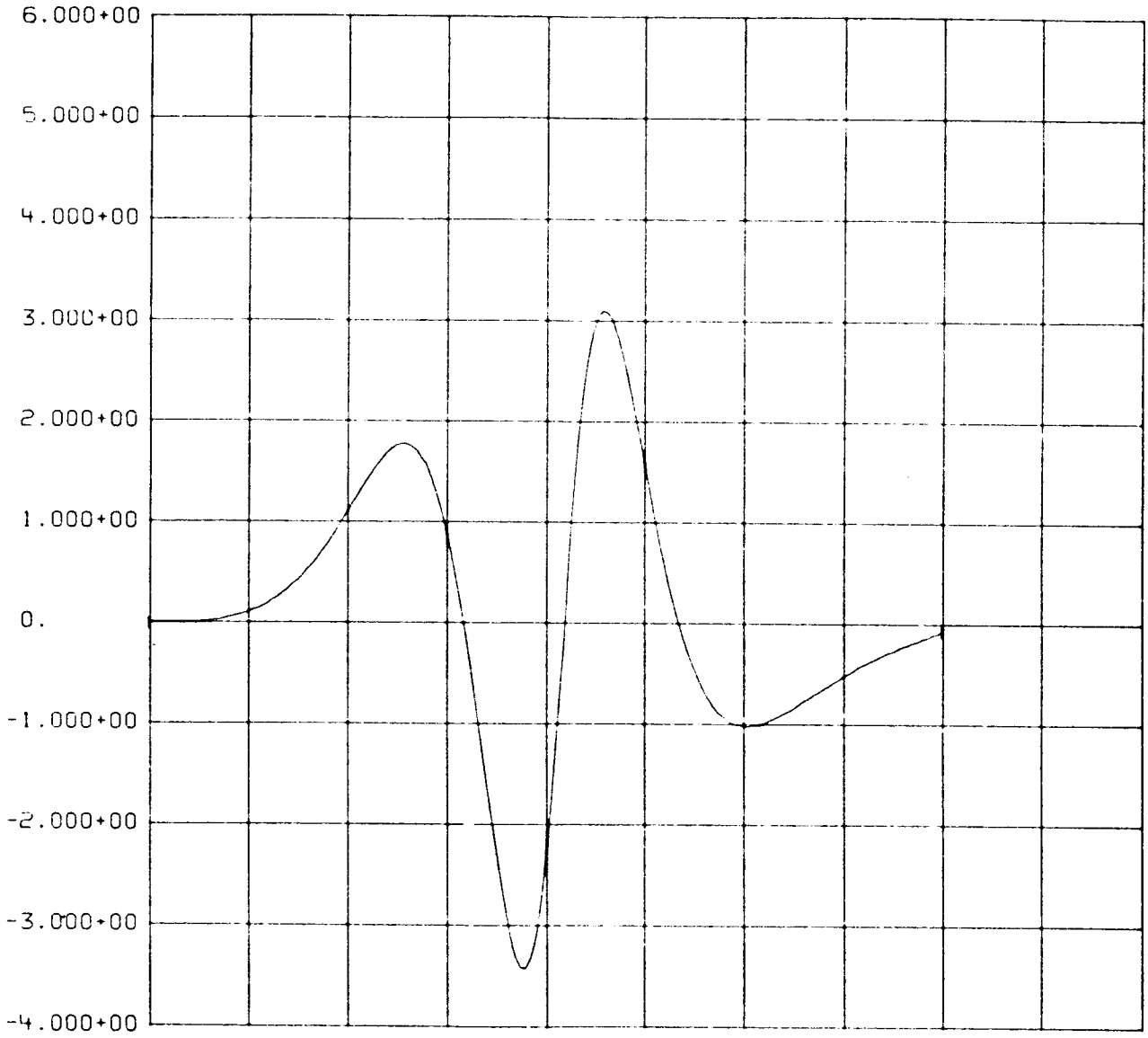
6.000+00
5.000+00
4.000+00
3.000+00
2.000+00
1.000+00
0.
-1.000+00
-2.000+00
-3.000+00
-4.000+00
0.
4.000-01
8.000-01
1.200+00
1.600+00
2.00
IN/SEC
VS
TIME
1
TLM13
02FE76
TEST13-1974 BETADT 3/2

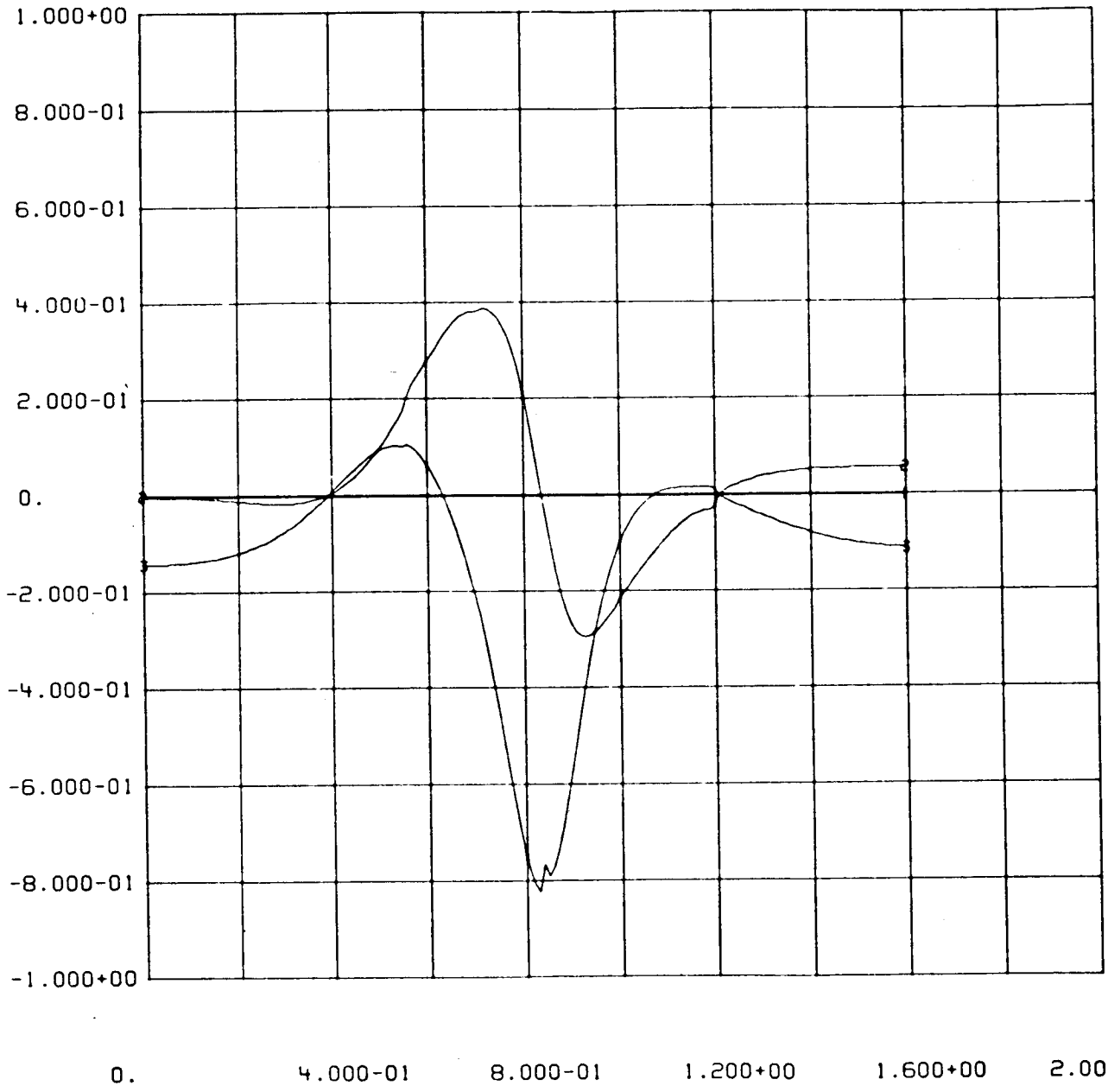

POUNDS VS TIME

1 TLM13 02FE76 TEST13-1974 FORCES 2/1

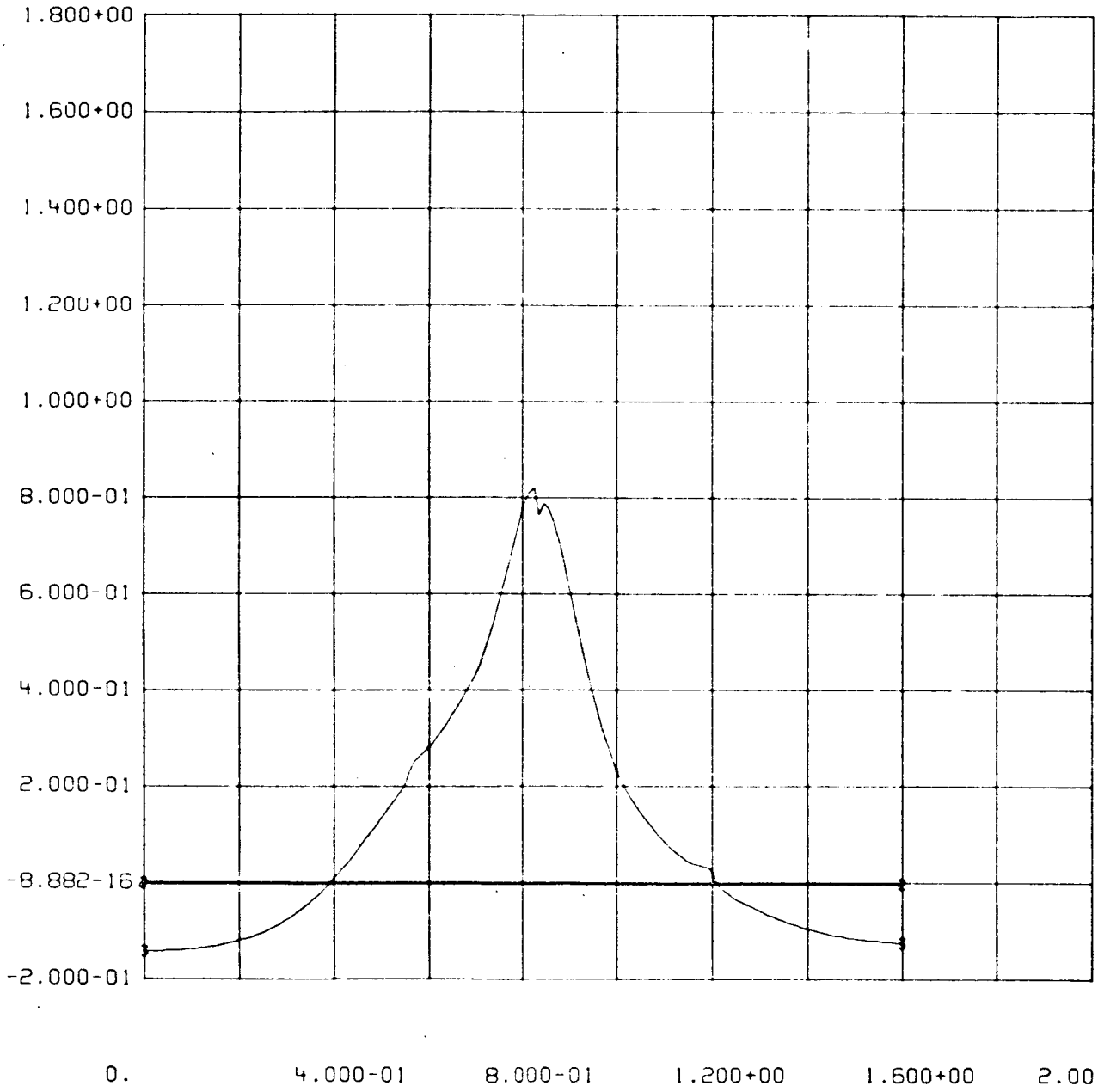

POUNDS VS TIME

1 TLM13 02FE76 TEST13-1974 FORCES 3/2

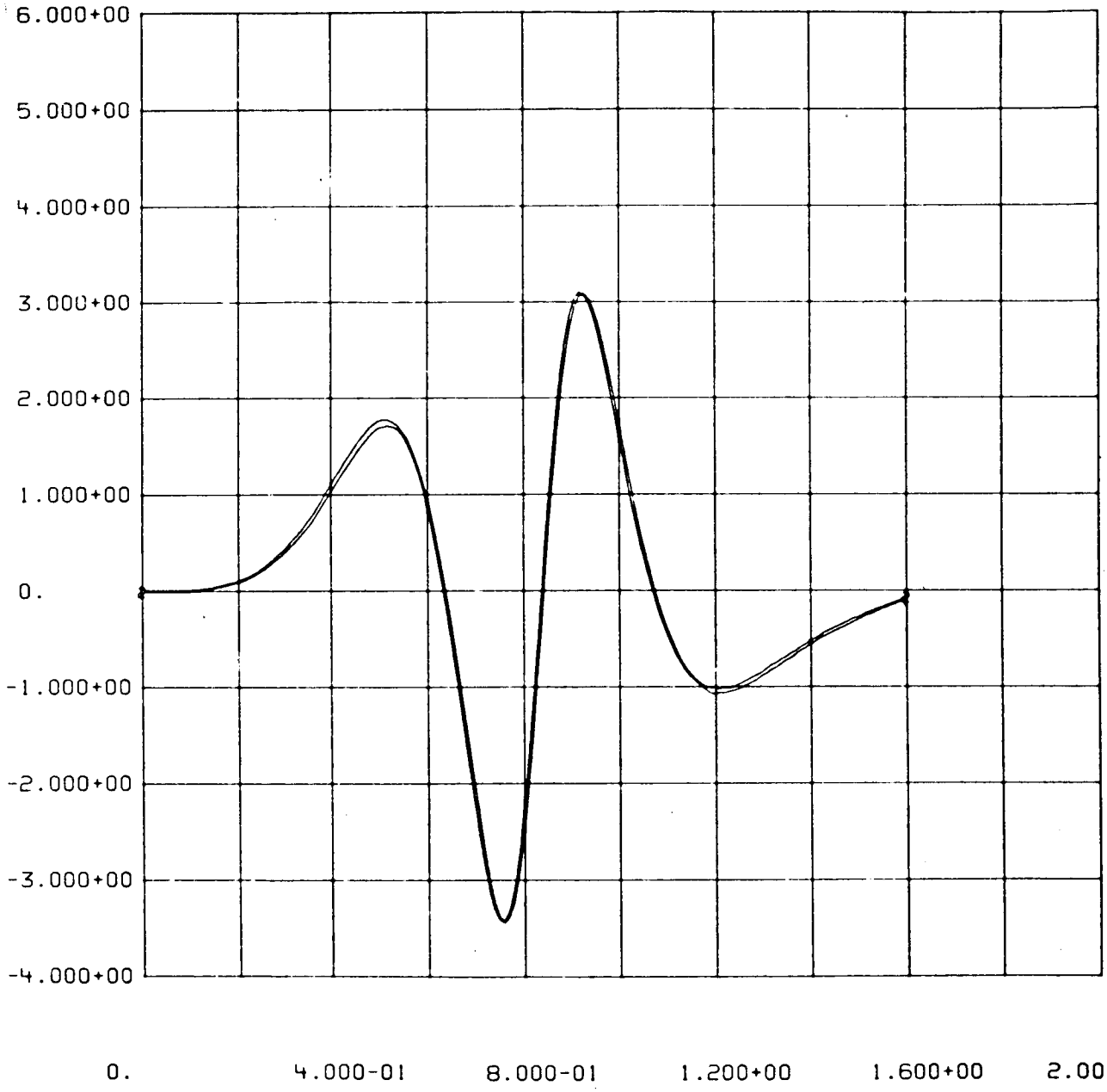
6.000+00
5.000+00
4.000+00
3.000+00
2.000+00
1.000+00
0.
-1.000+00
-2.000+00
-3.000+00
-4.000+00
0.
4.000-01
8.000-01
1.200+00
1.600+00
2.00
IN/SEC
VS
TIME
1
TLM13
02FE76
TEST13-1974 ALPHAD

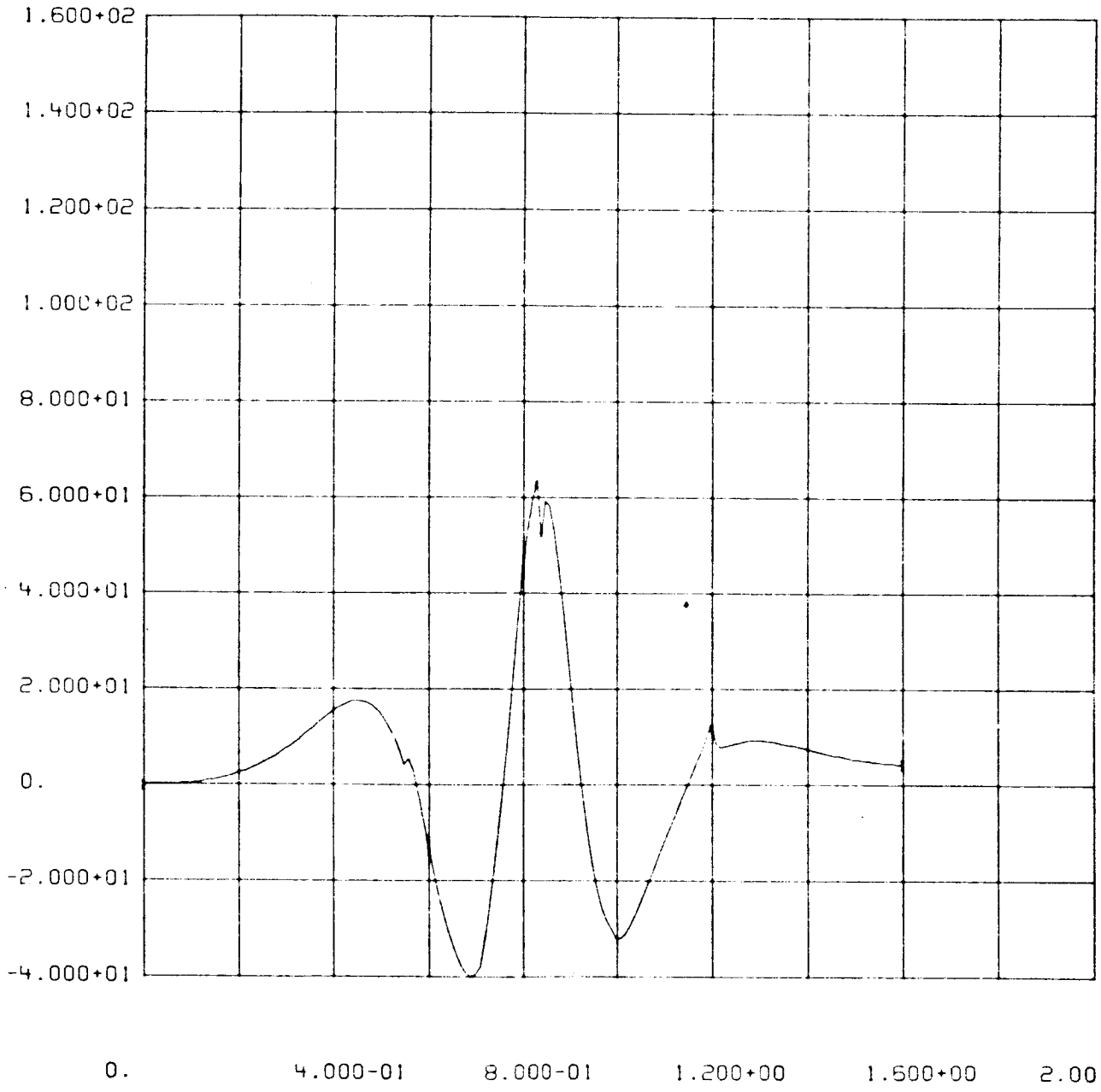
1.600+02
1.400+02
1.200+02
1.000+02
8.000+01
6.000+01
4.000+01
2.000+01
0.
-2.000+01
-4.000+01
0.
4.000-01
8.000-01
1.200+00
1.600+00
2.00
IN/SC2
VS
TIME
1
TLM13
02FE76
TEST13-1974 ALPHADD

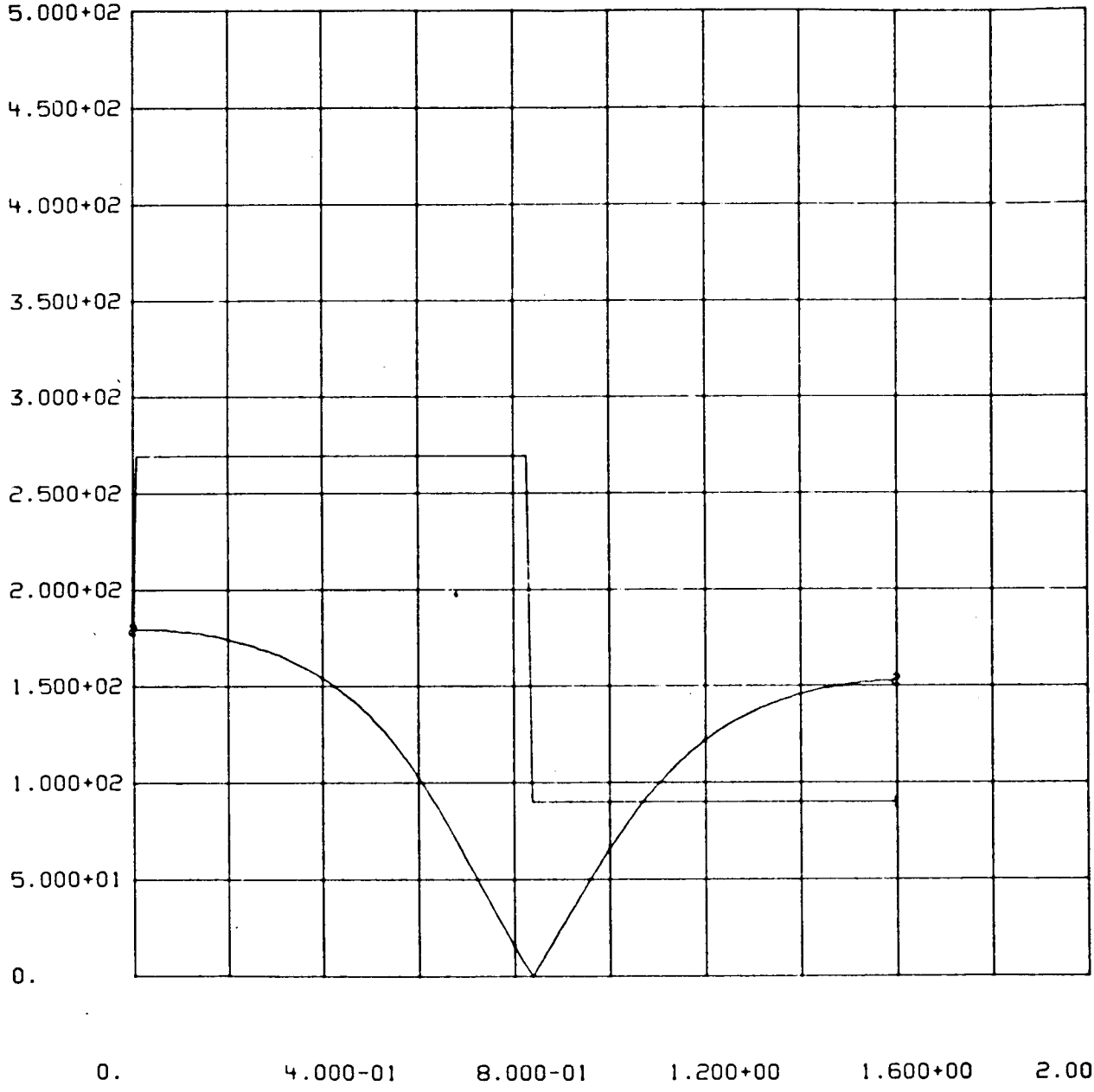

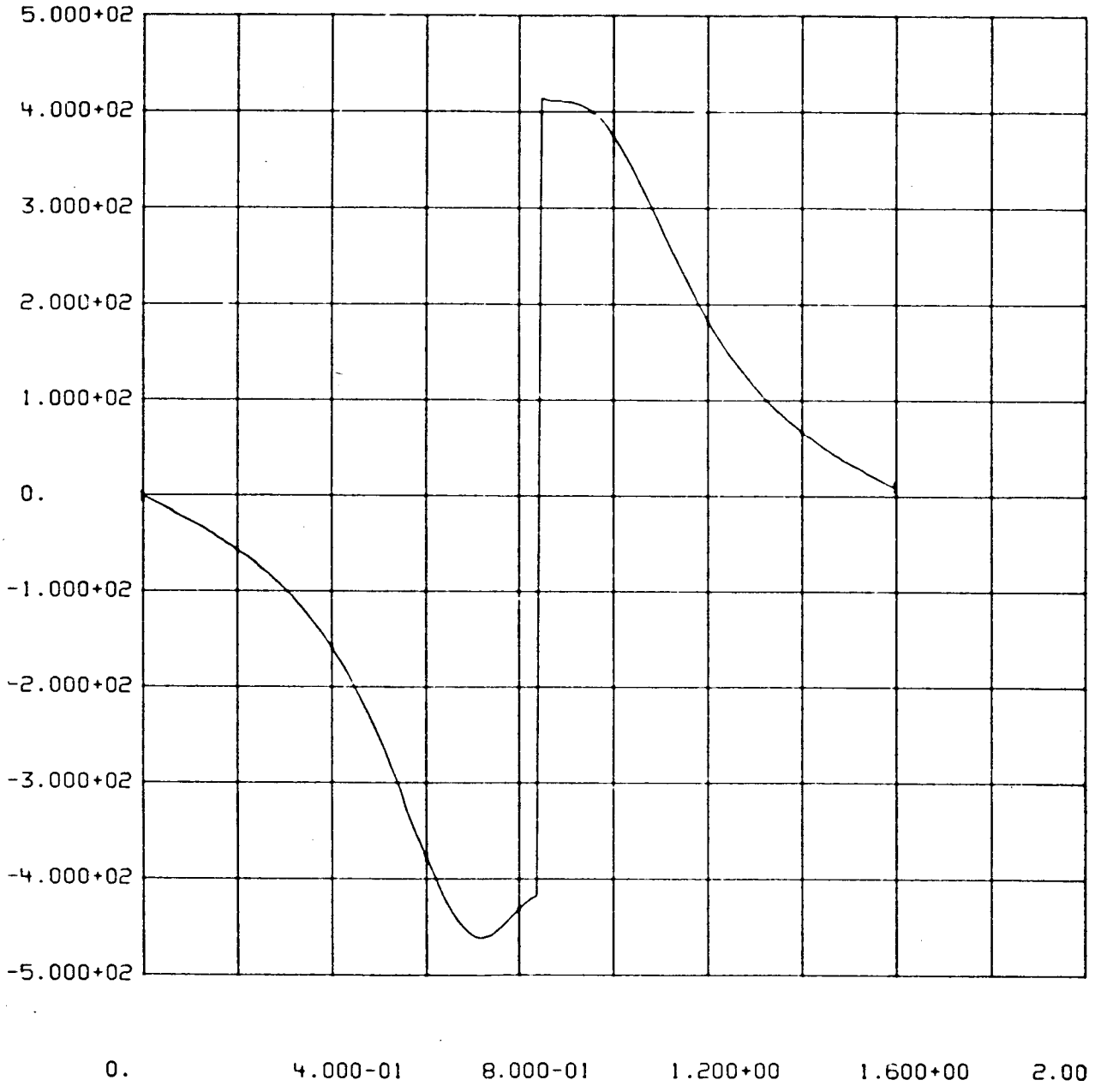
5.000+02
4.000+02
3.000+02
2.000+02
1.000+02
0.
-1.000+02
-2.000+02
-3.000+02
-4.000+02
-5.000+02
0.
4.000-01
8.000-01
1.200+00
1.600+00
2.00
DEG/SC
VS
TIME
1
TLM13
02FE76
TEST13-1974 PHIDT

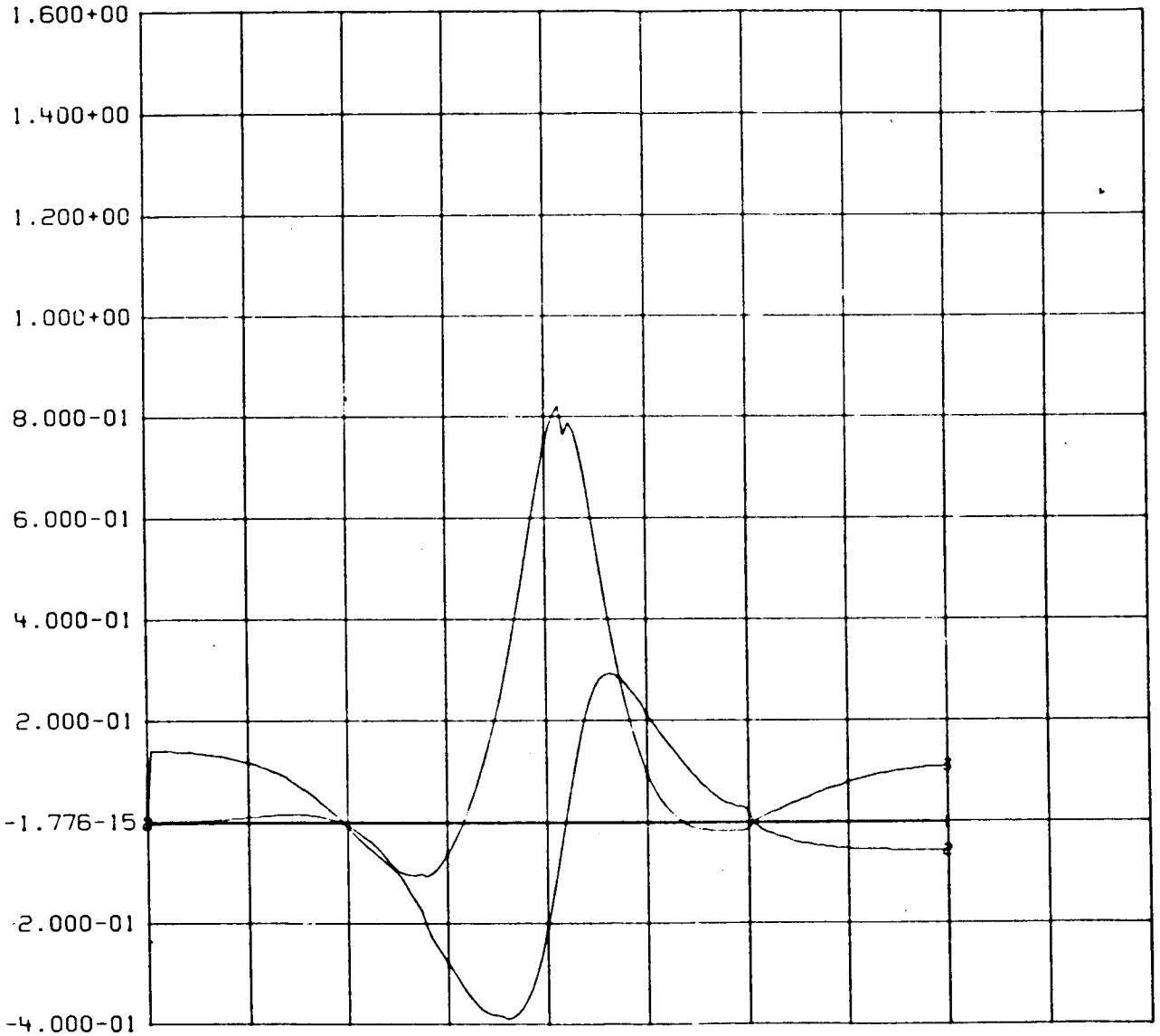

POUNDS VS TIME

1 TLM13 02FE76 TEST13-1974 LIQ. FORCES FX,FY,FZ

COMPARISON OUTPUT FORCES PROGRAM LAMPS

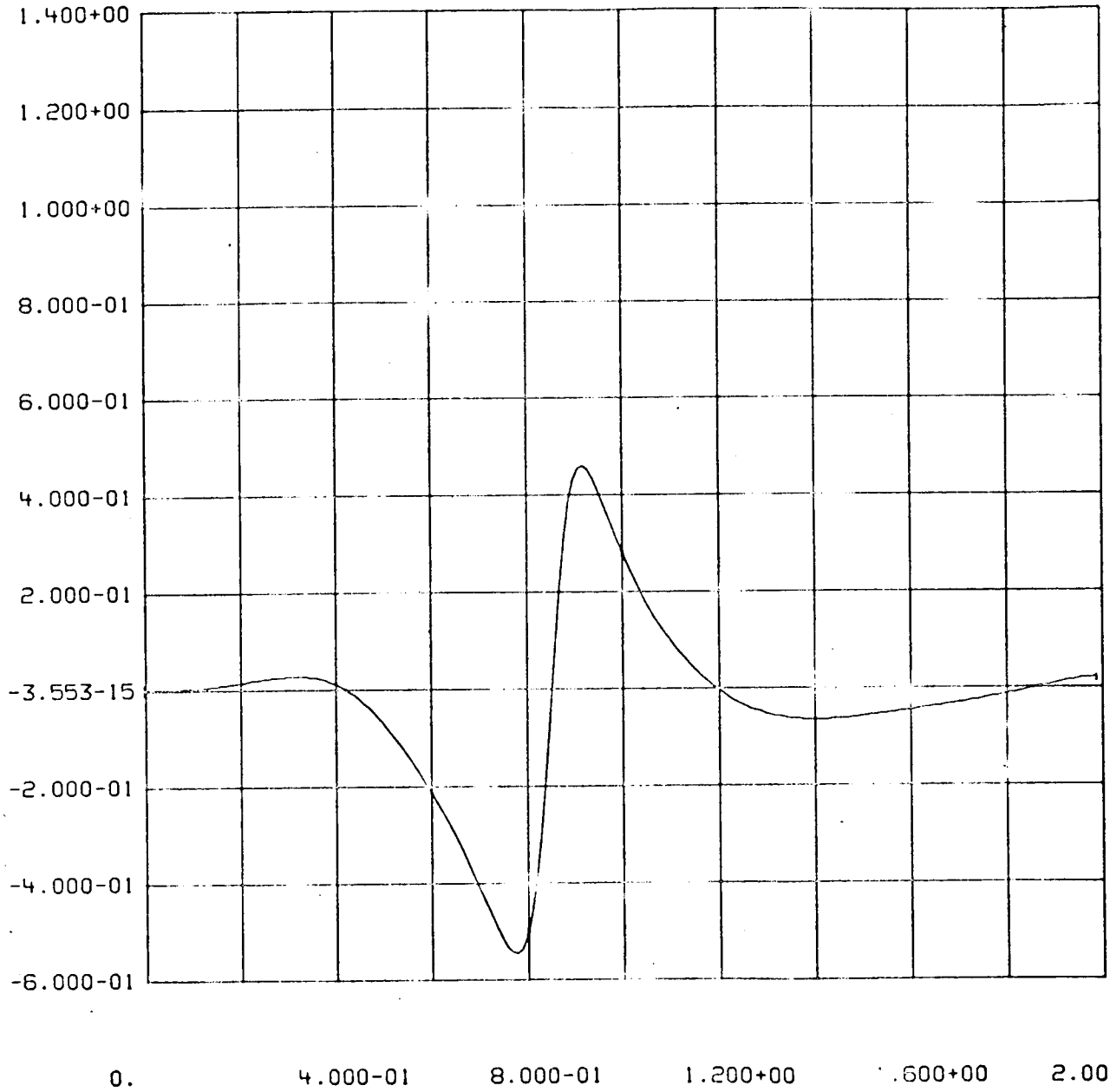

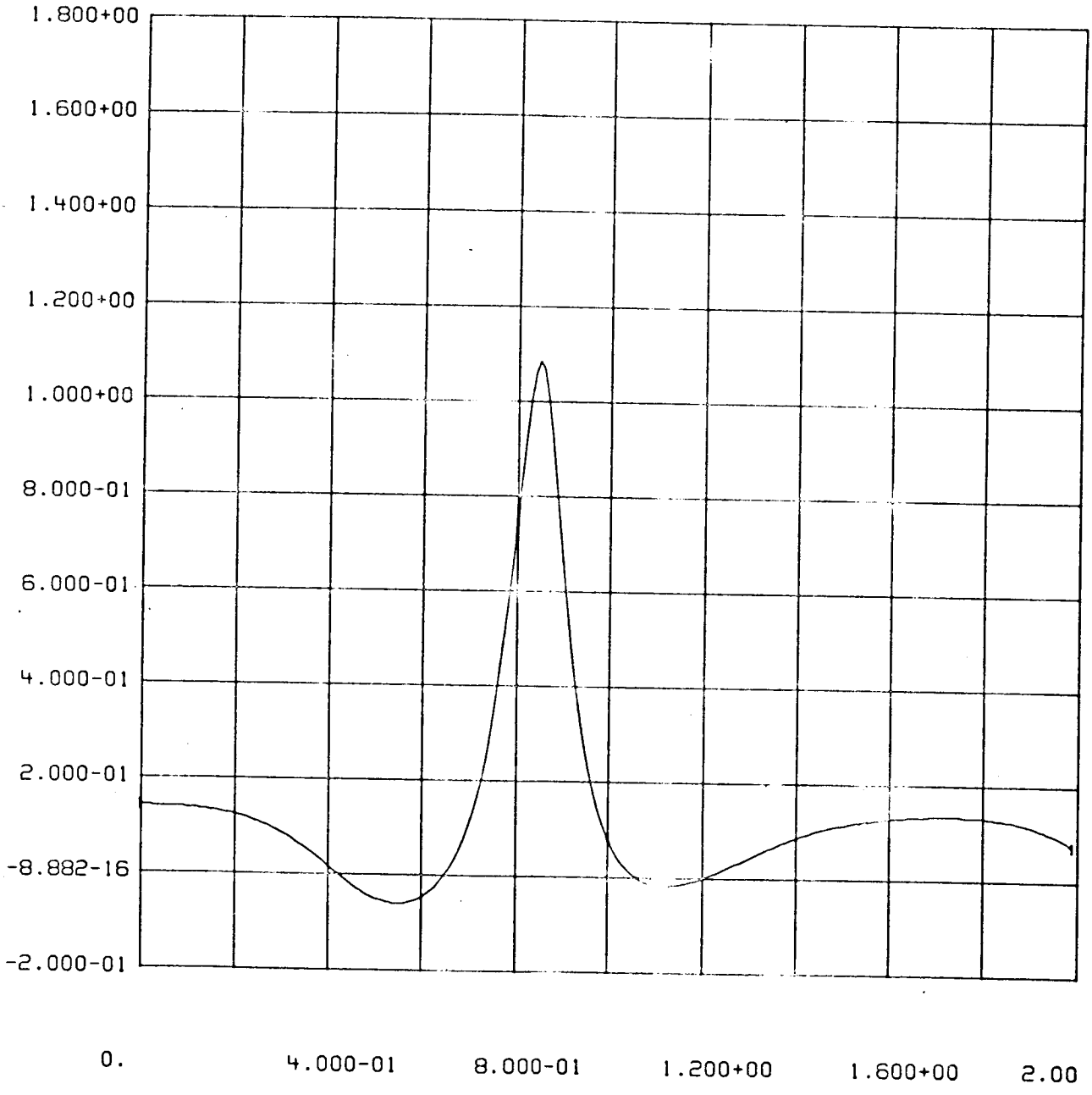
1.800+00
1.600+00
1.400+00
1.200+00
1.000+00
8.000-01
6.000-01
4.000-01
2.000-01
-8.882-16
-2.000-01
0.
4.000-01
8.000-01
1.200+00
1.600+00
2.00
FZ
VS
SEC
1
TEST13
26JA76
LARGE AMPLITUDE SLOSH SIMULATION

APPENDIX B - TEST RESULTS

This appendix presents (Figures B-1 through B-12) the reduced test data for all 23 tests. Shown in these figures are plots of the tank Y and Z forces vs time.

Table B-1 summarizes the test conditions for each case. Values of axial acceleration (AZI) were calculated based on test time, drop capsule and drag shield masses, and drop capsule travel distance. Lateral accelerations (AYI) were scaled from high speed photographs taken during testing.

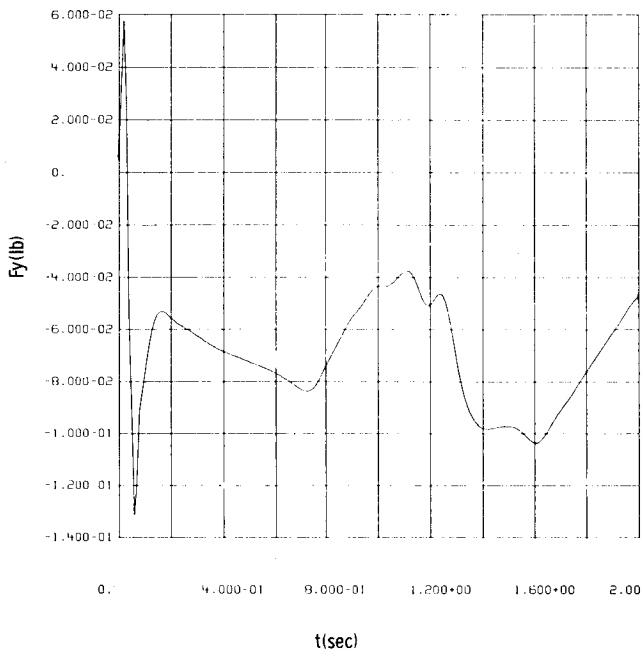

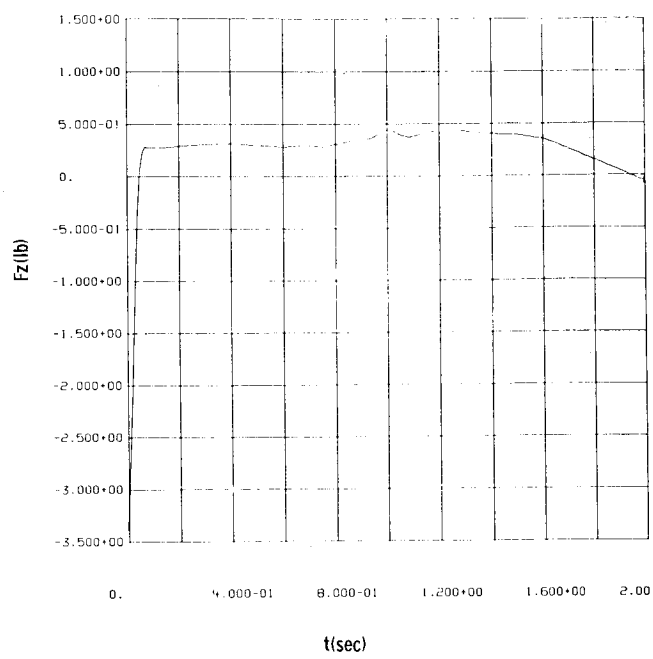

Test 1 - baseline tank ; 25 % fill ; $\theta x = 0^{\circ}$; Aa= 0.086

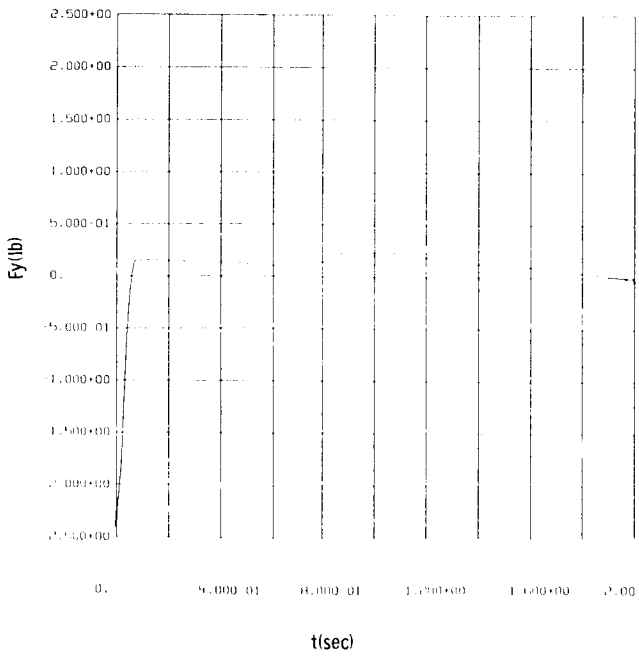

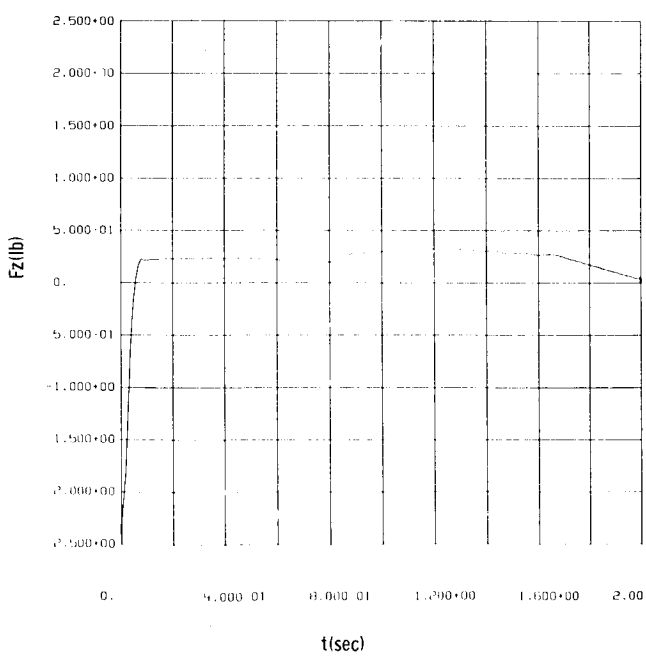

Test 2 - baseline tank ; 25 % fill ; $\theta x = 45^{\circ}$; Aa= 0.084

Figure B-1

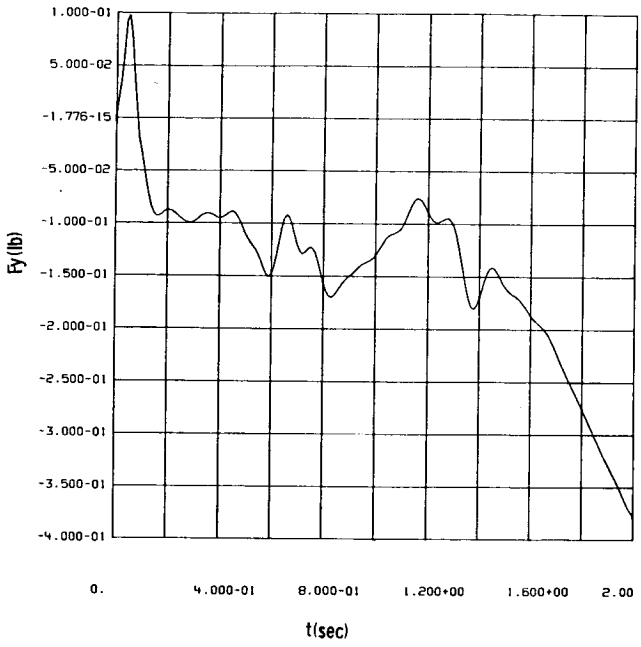

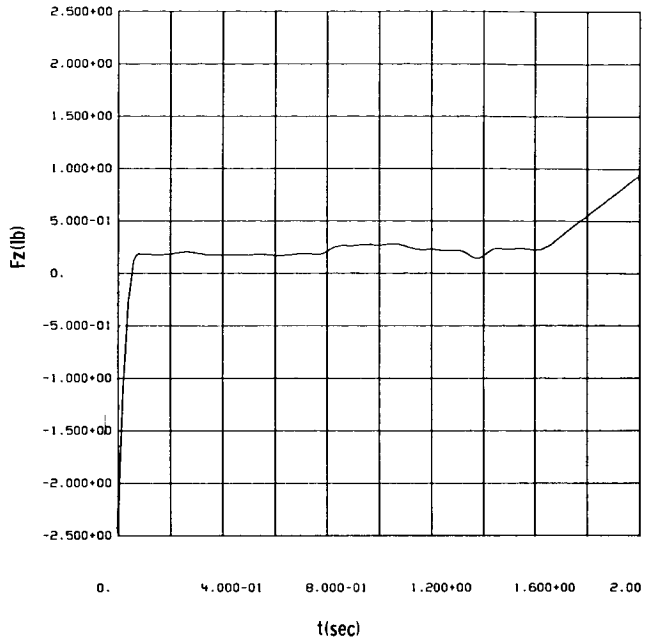

Test 3 - baffles tank ; 10 % fill ; $\theta x = 0^{\circ}$; Aa= 0.084

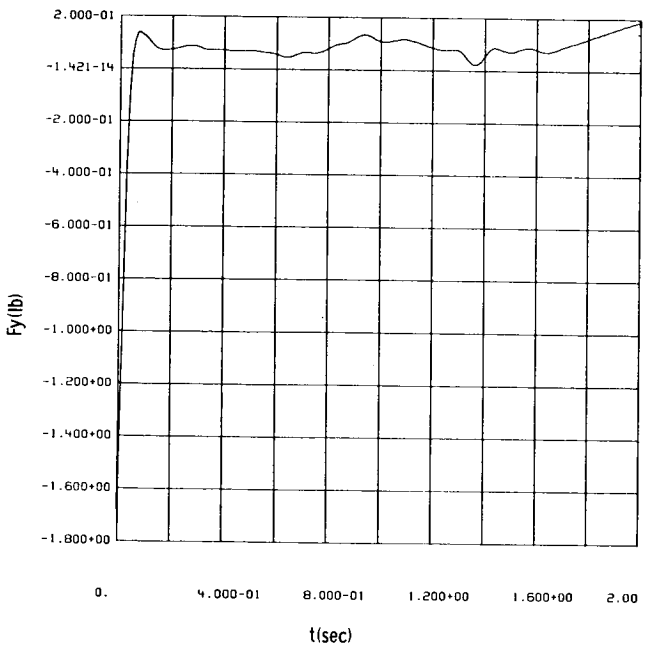

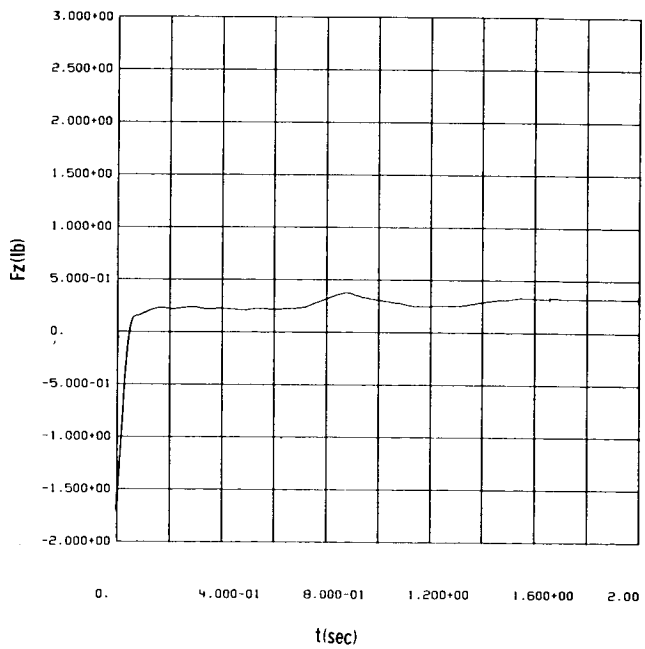

Test 4 - baffles tank ; 10 % fill ; $\theta x = 45^{\circ}$; Aa= 0.082

Figure B-2

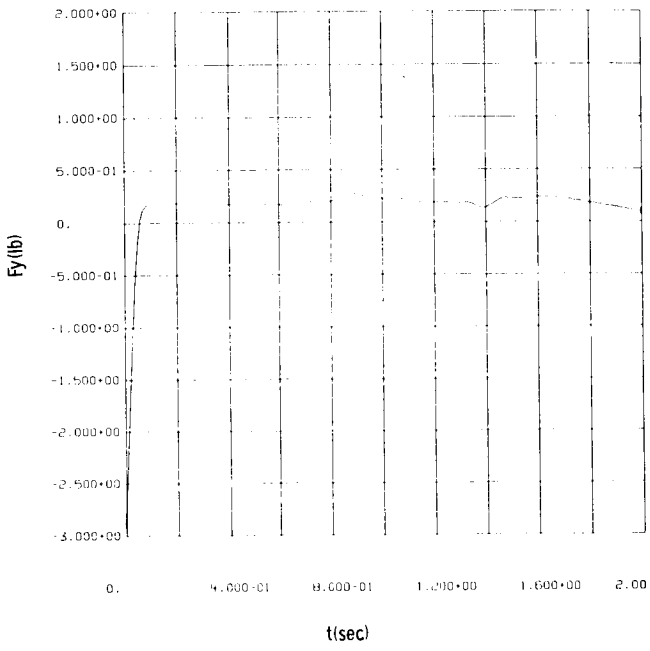

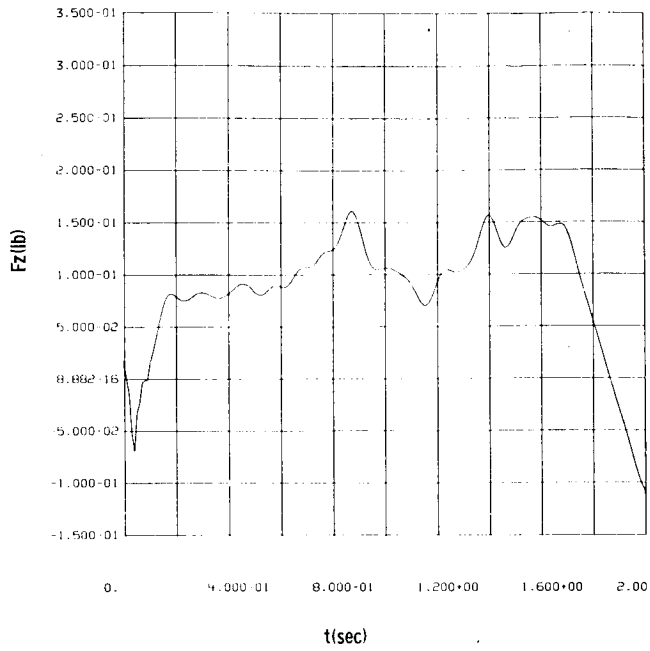

Test 5 - baffles tank ; 10 % fill ; $\theta x = 90^{\circ}$; Aa= 0.080

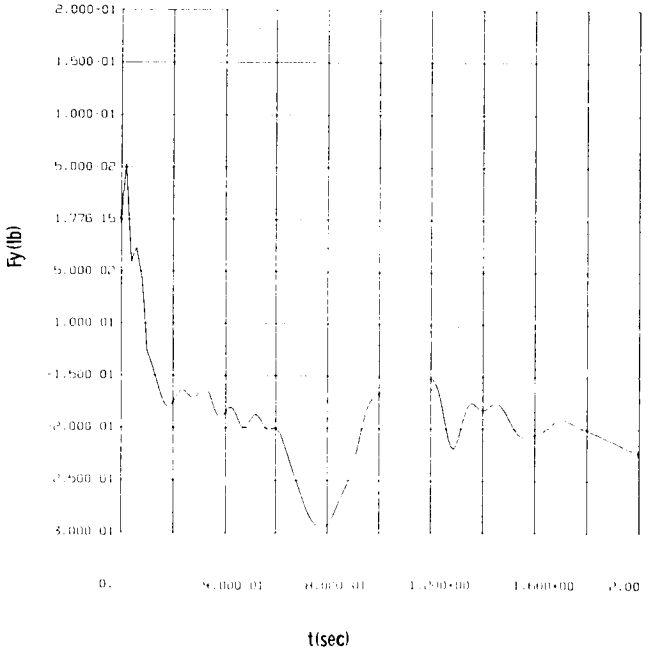

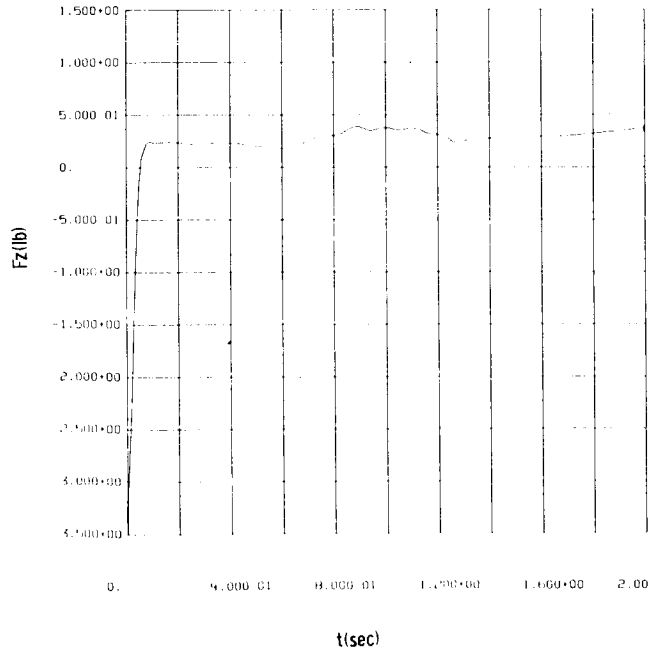

Test 6 - baffles tank ; 25 % fill ; $\theta x = 0^{\circ}$; Aa= 0.074

Figure B-3

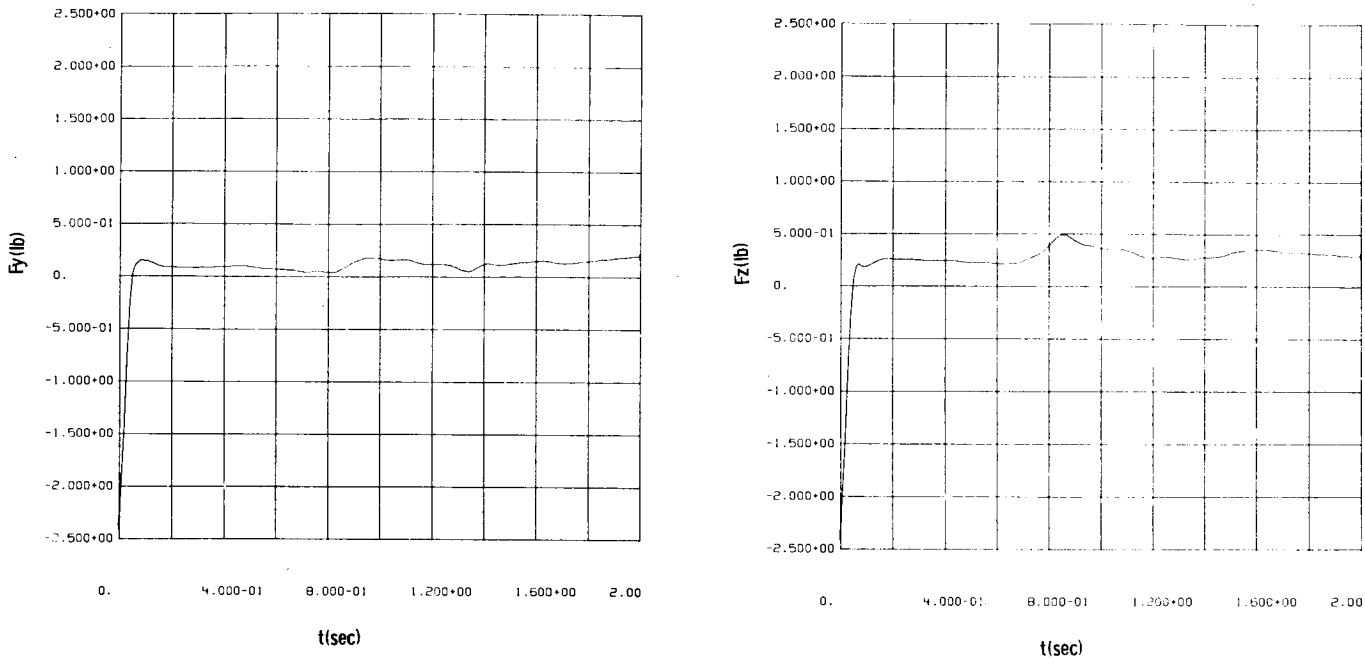

Test 7 - baffles tank ; 25 % fill ; $\theta x = 45^\circ$; Aa= 0.075

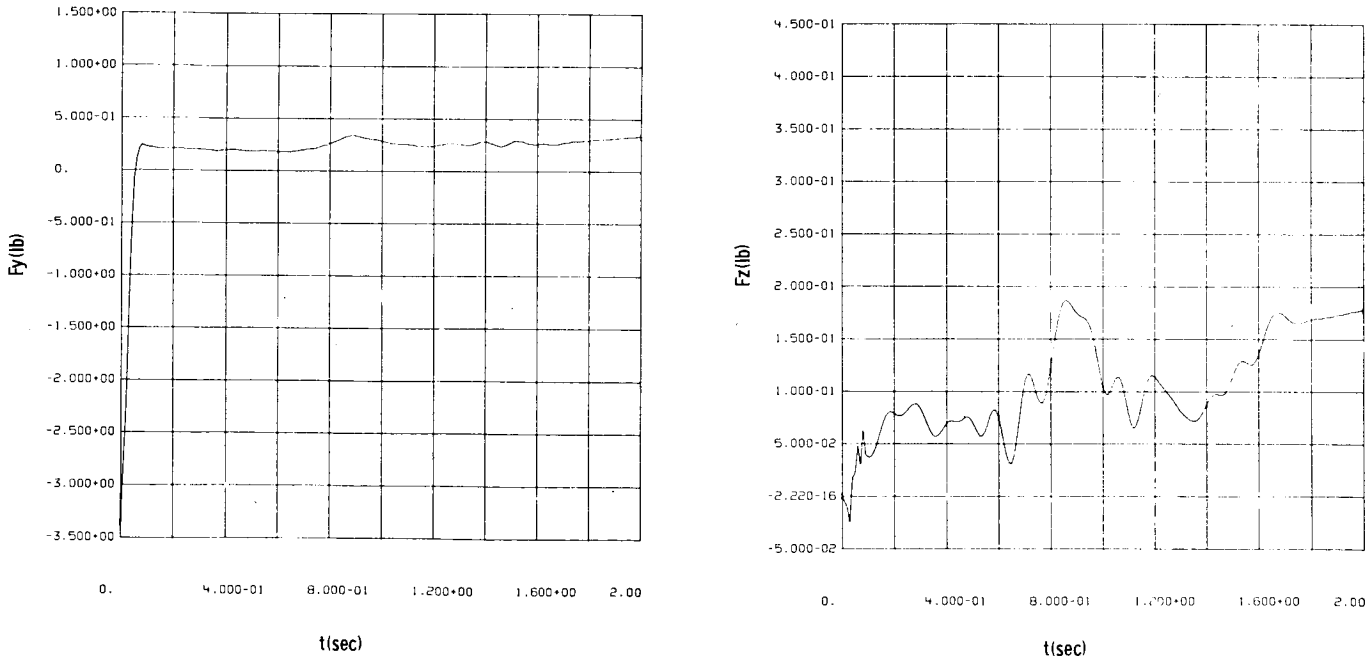

Test 8 - baffles tank ; 25 % fill ; $\theta x = 90^\circ$; Aa= 0.075

Figure B-4

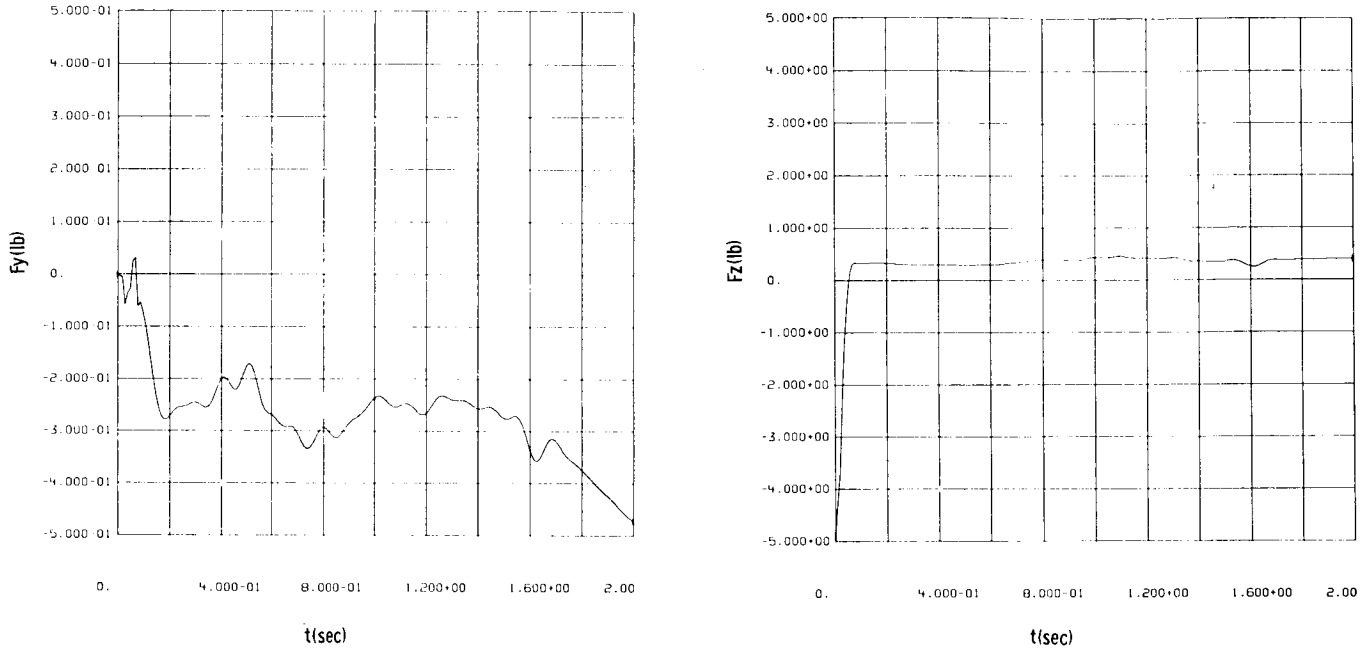

Test 9 - baffles tank ; 50 % fill ; $\theta x = 0^{\circ}$; Aa= 0.072

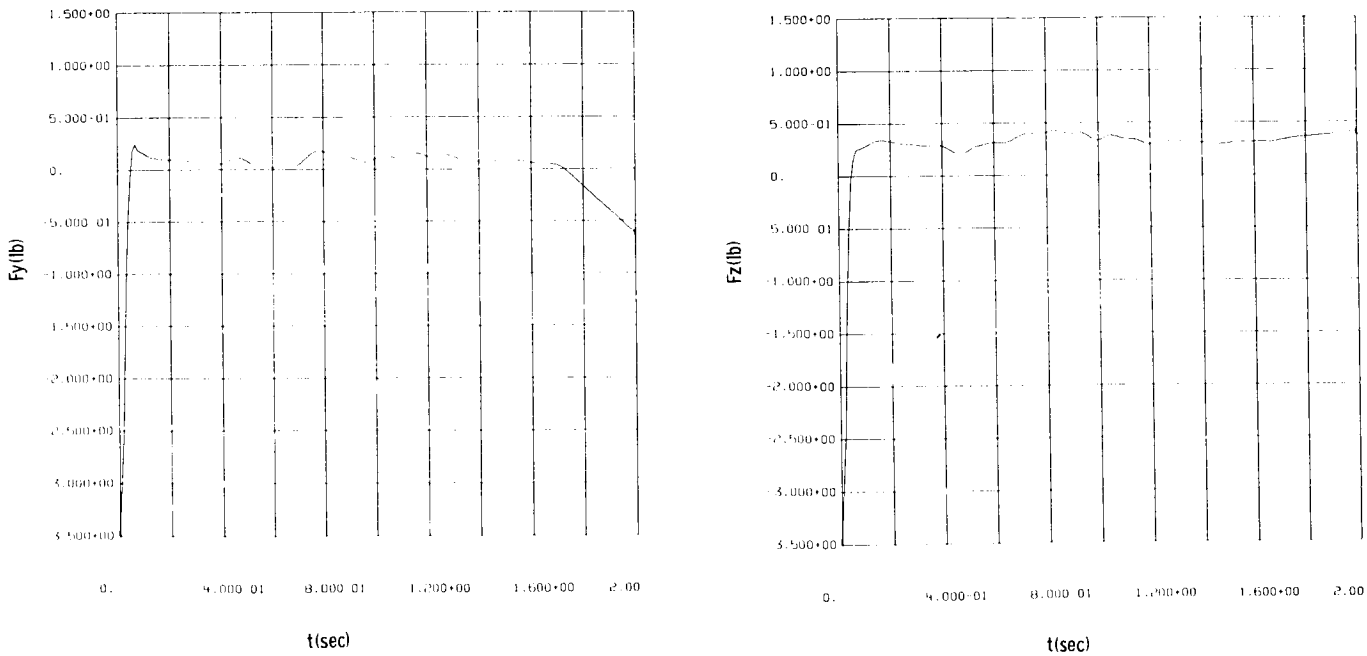

Test 10 - baffles tank ; 50 % fill ; $\theta x = 45^{\circ}$; Aa= 0.073

Figure B-5

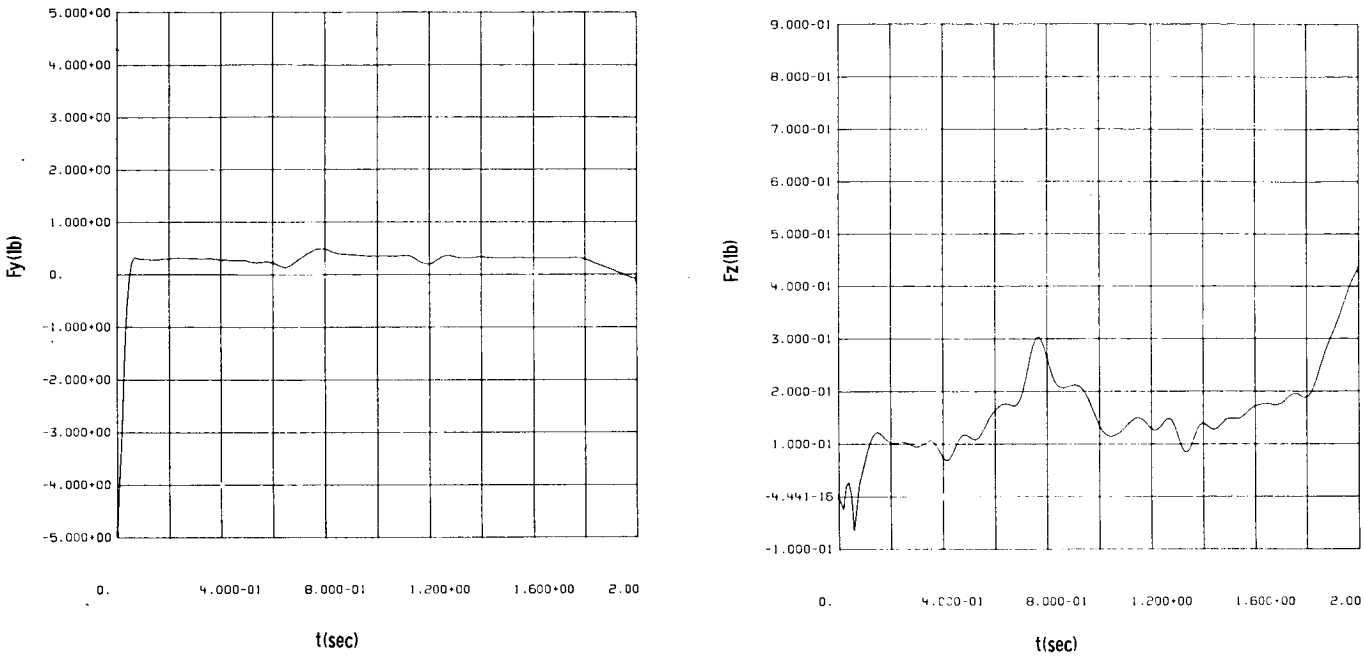

Test 11 - baffles tank ; 50 % fill ; $\theta x = 90^\circ$; Aa=0.068

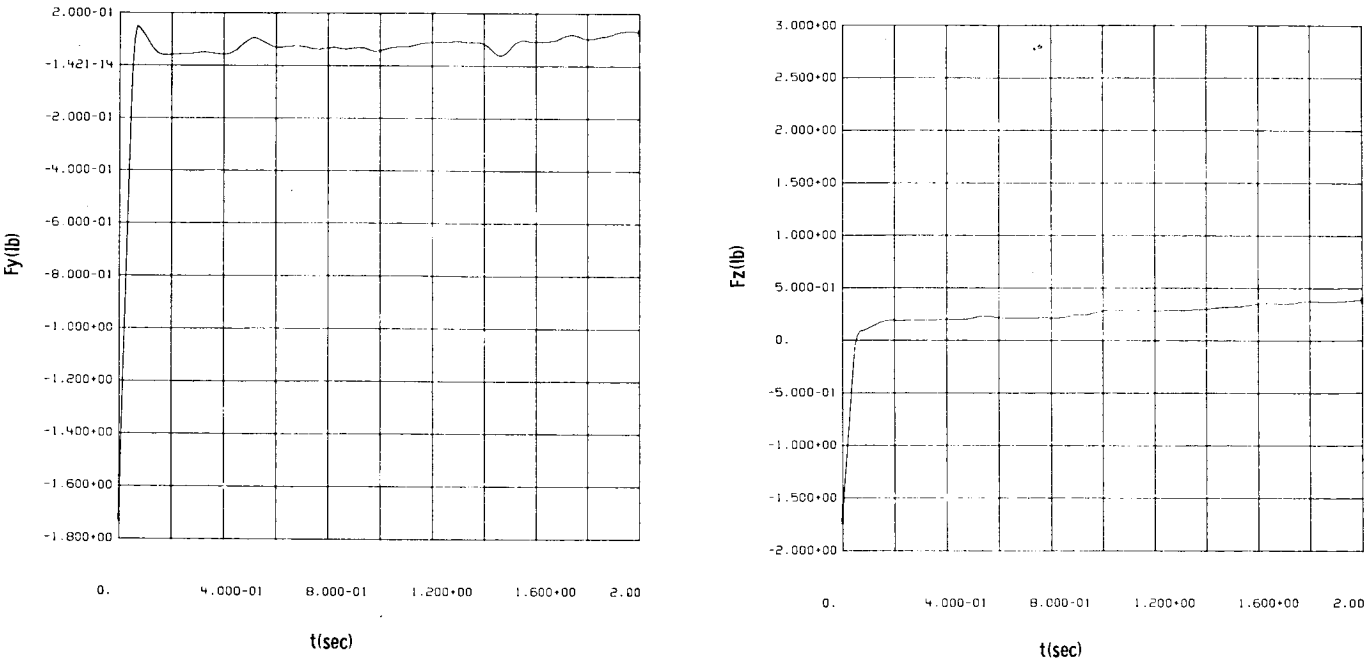

Test 12 - baffles tank ; 10 % fill ; $\theta x = 45^\circ$; Aa= 0.042

Figure B-6

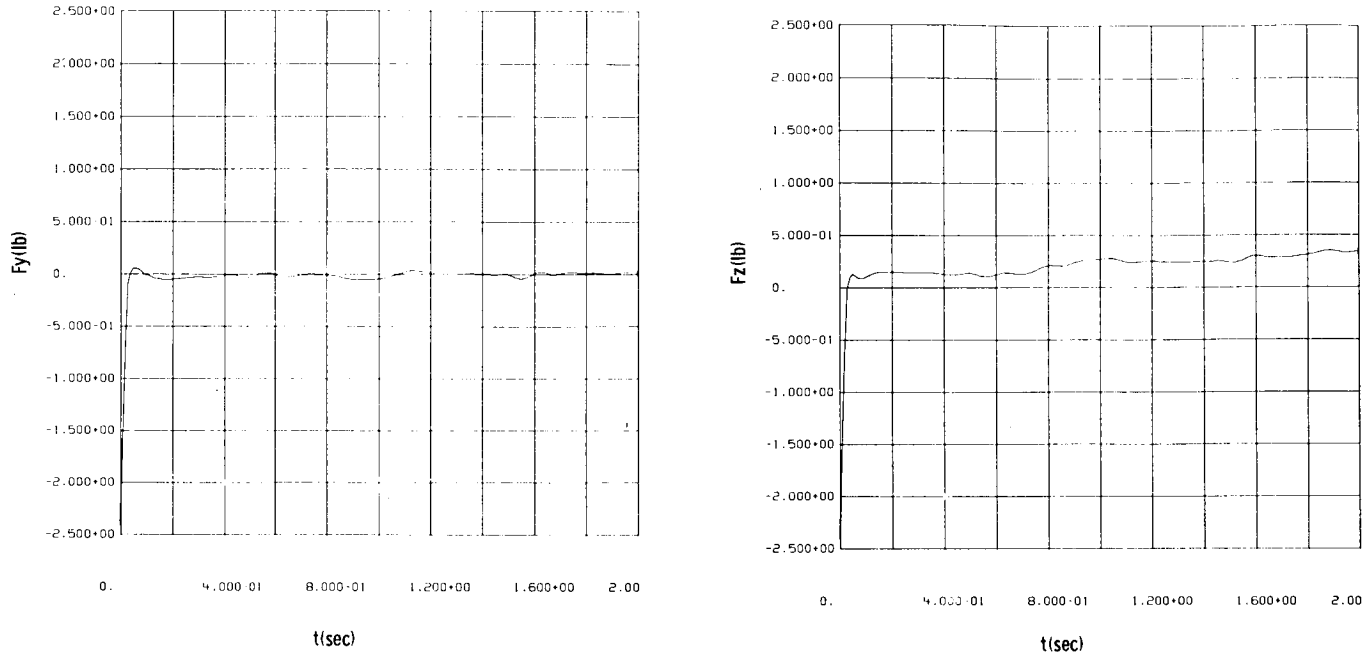

Test 13 - baffles tank ; 25 % fill ; $\theta x = 45^{\circ}$; Aa= 0.042

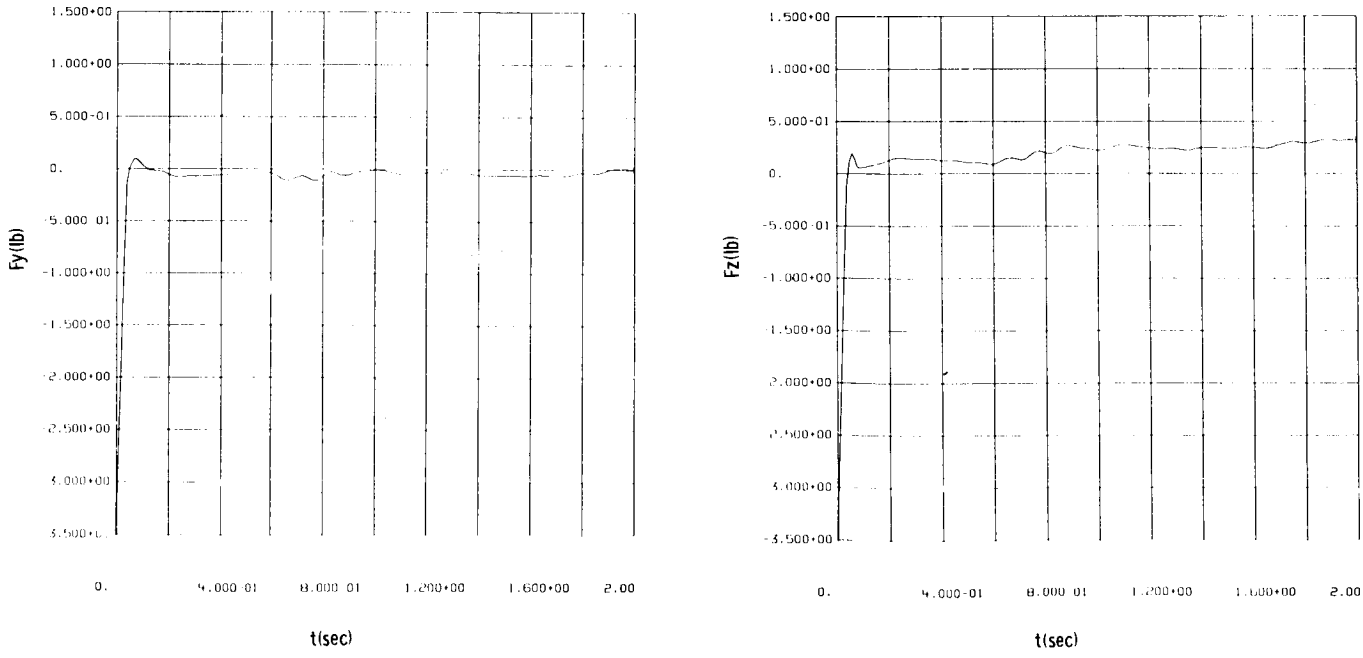

Test 14 - baffles tank ; 50 % fill ; $\theta x = 45^{\circ}$; Aa= 0.042

Figure B-7

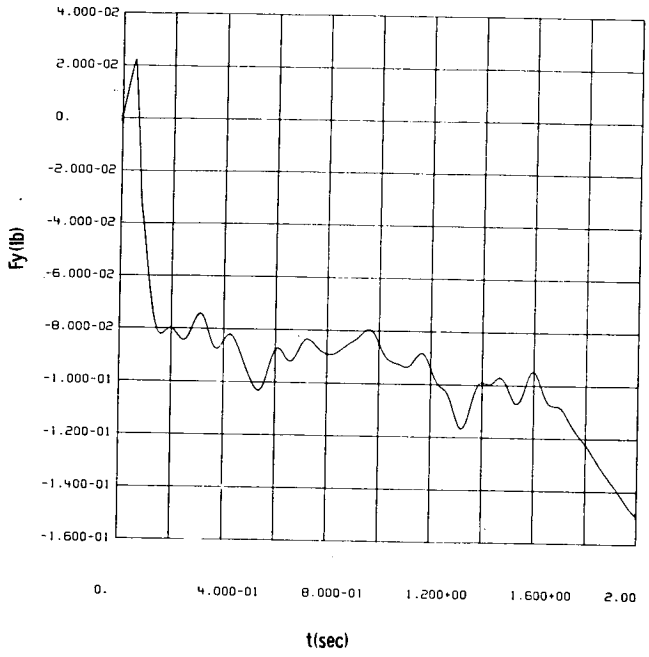

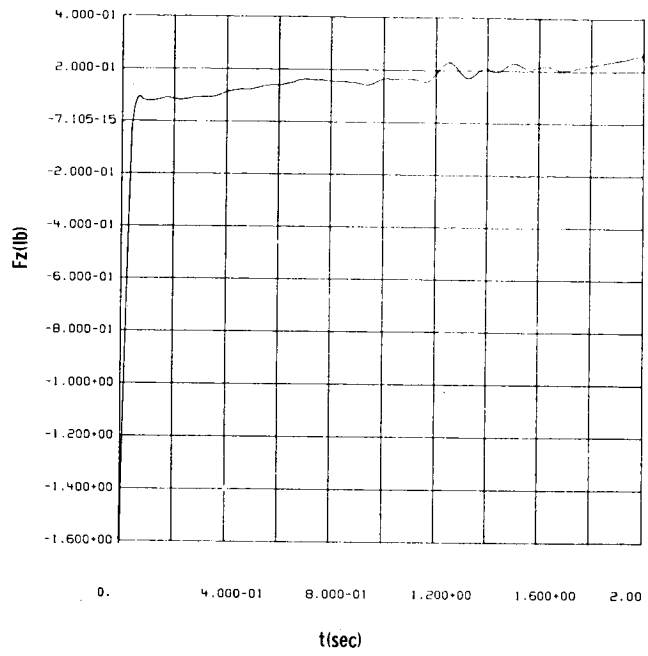

Test 15 - small tank ; 25 % fill ; $\theta x = 0^\circ$; Aa= 0.075

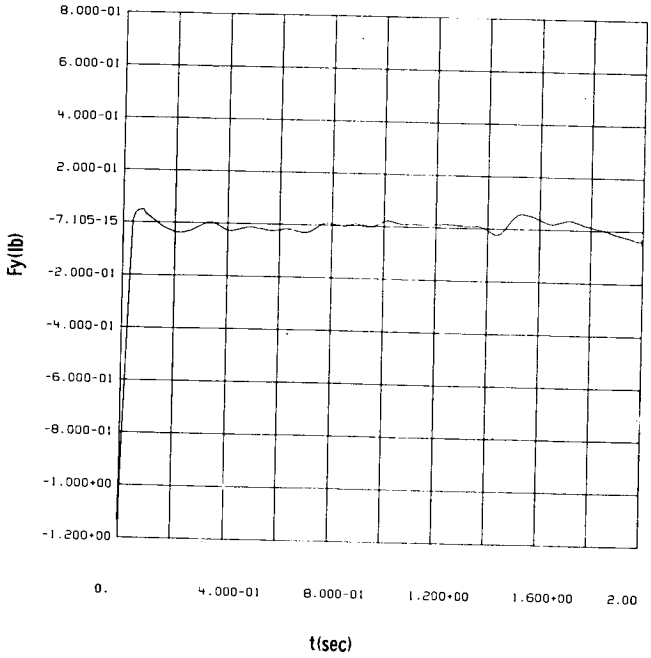

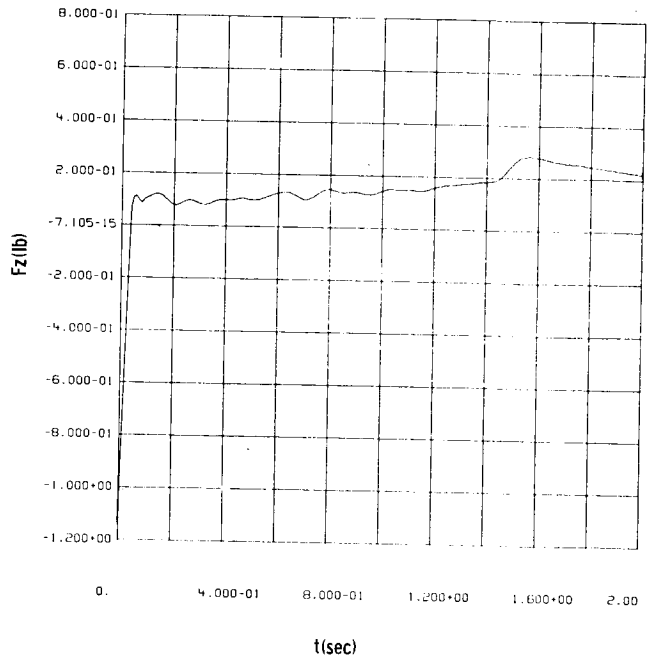

Test 16 - small tank ; 25 % fill ; $\theta x = 45^\circ$; Aa= 0.074

Figure B-8

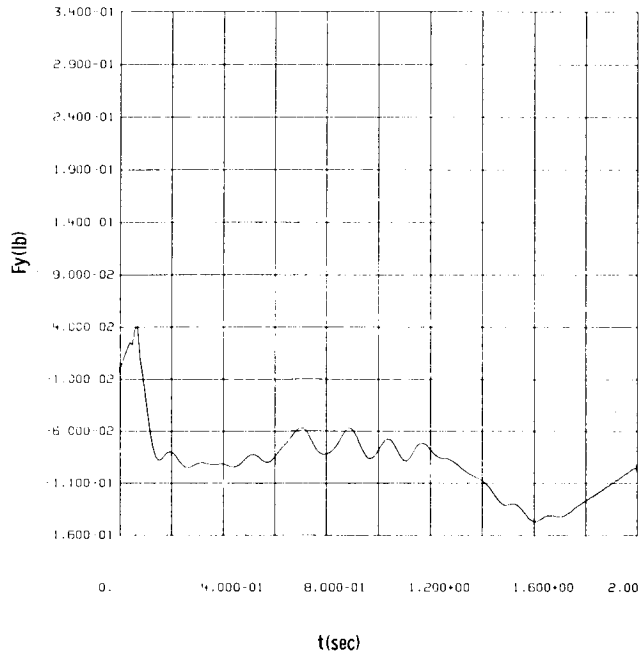

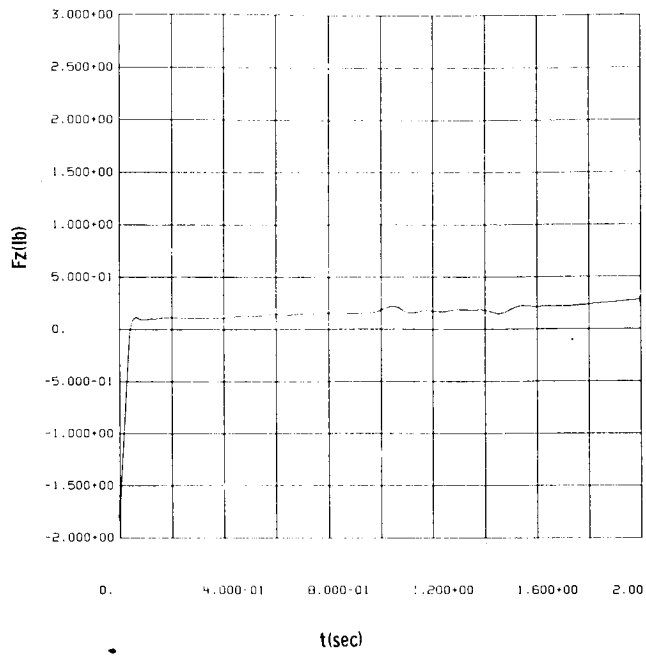

Test 17 - small tank ; 50 % fill ; $\theta x = 0^\circ$; Aa= 0.074

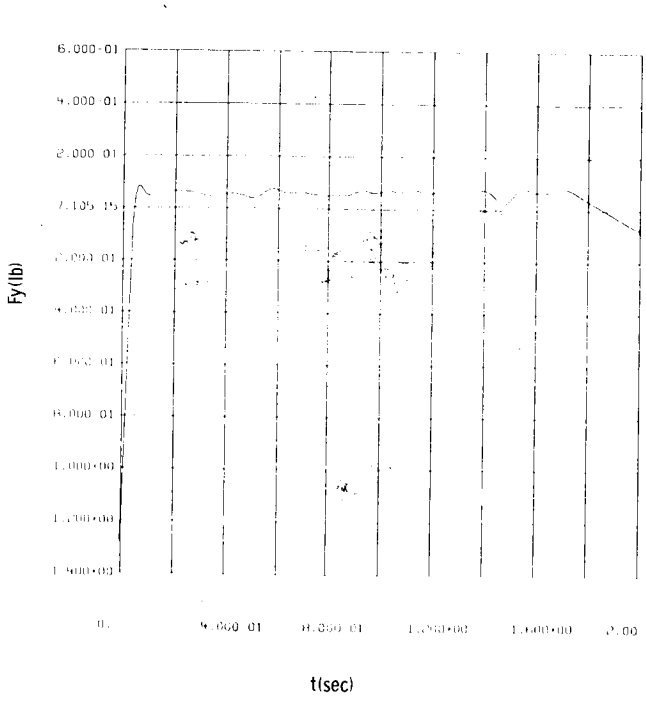

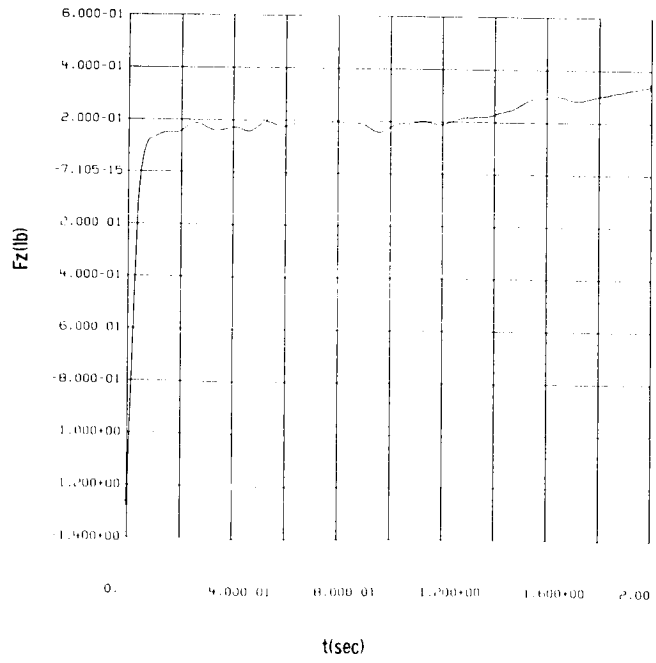

Test 18 - small tank ; 50 % fill ; $\theta x = 45^\circ$; Aa= 0.074

Figure B-9

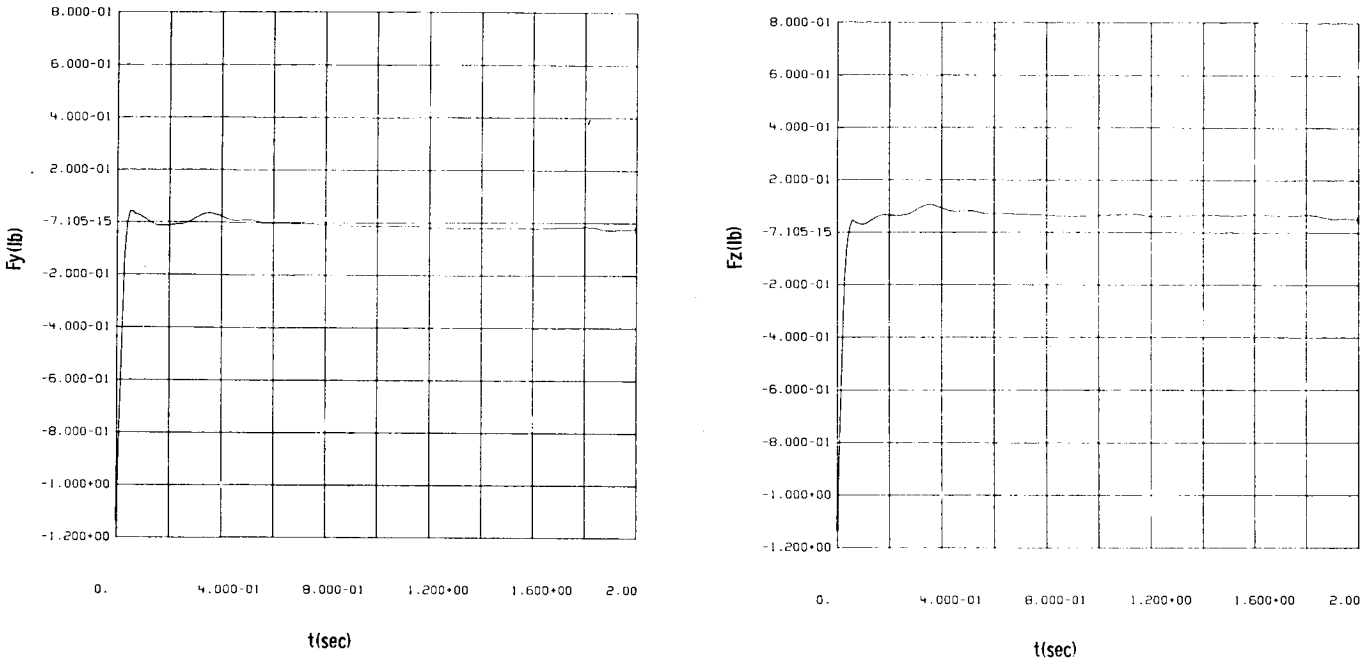

Test 19 - small tank ; 25 % fill ; $\theta x = 45^\circ$; Aa= 0.043

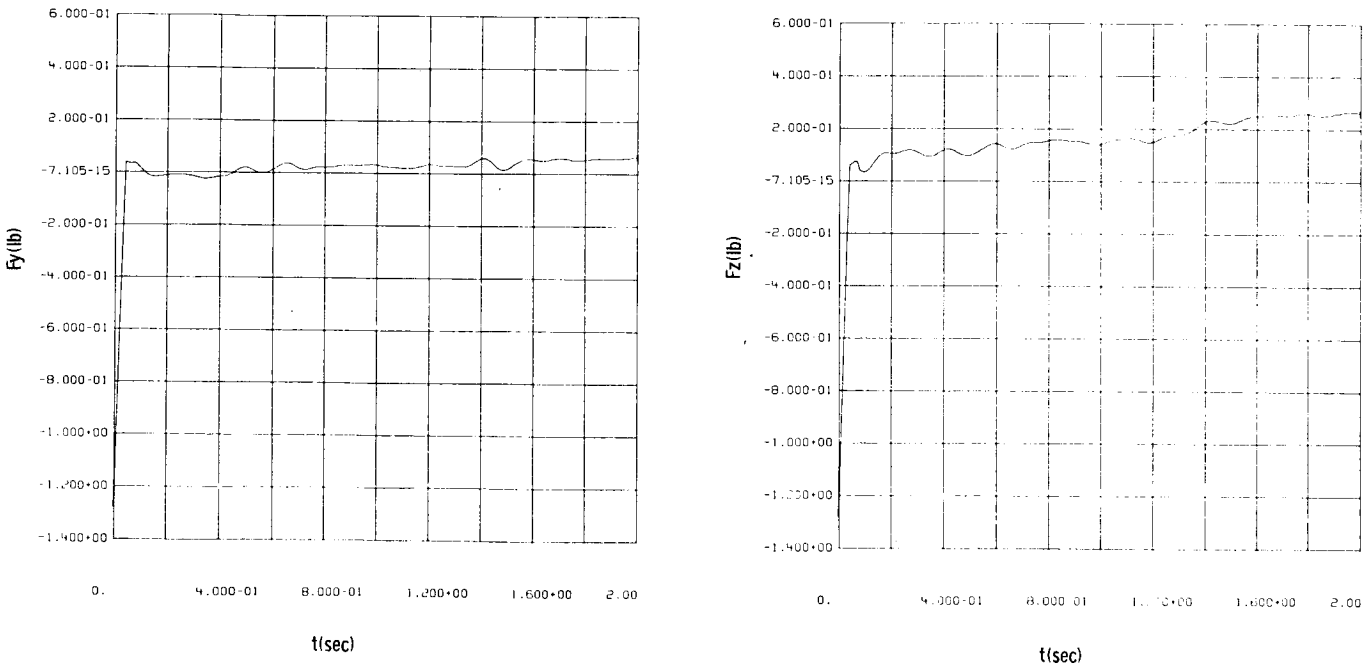

Test 20 - small tank ; 50 % fill ; $\theta x = 45^\circ$; Aa= 0.043

Figure B-10

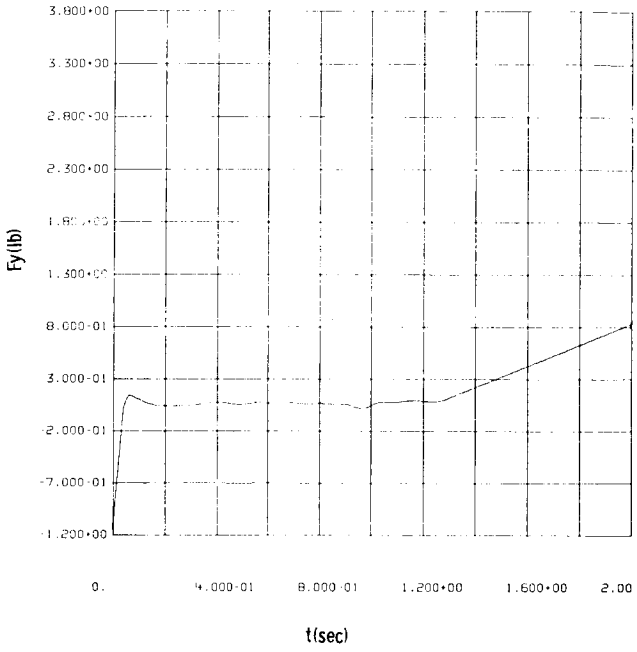

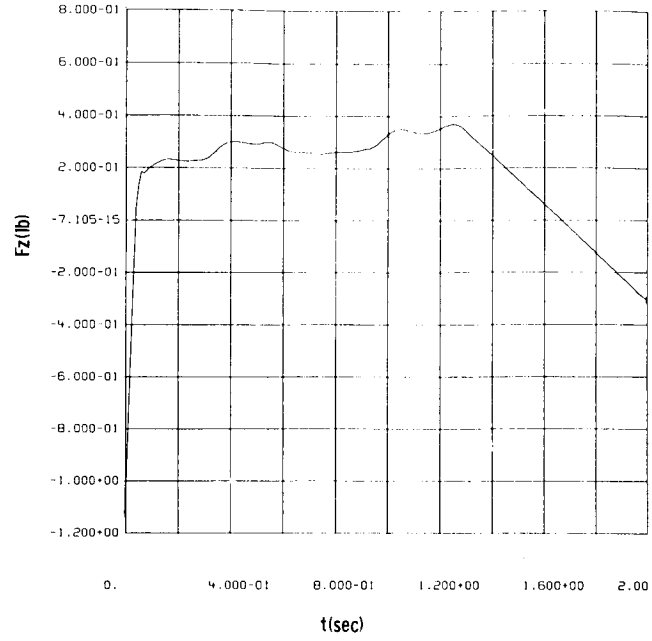

Test 21 - small tank ; 25 % fill ; ϕx= 45° ; Aa= 0.074

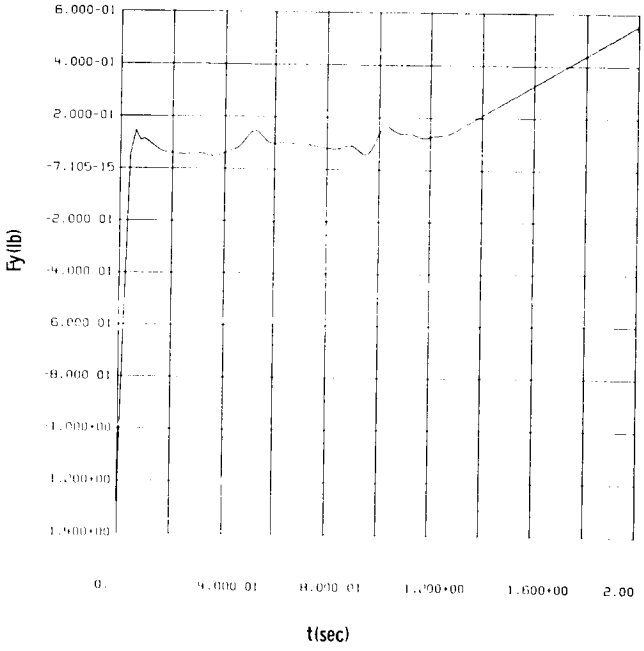

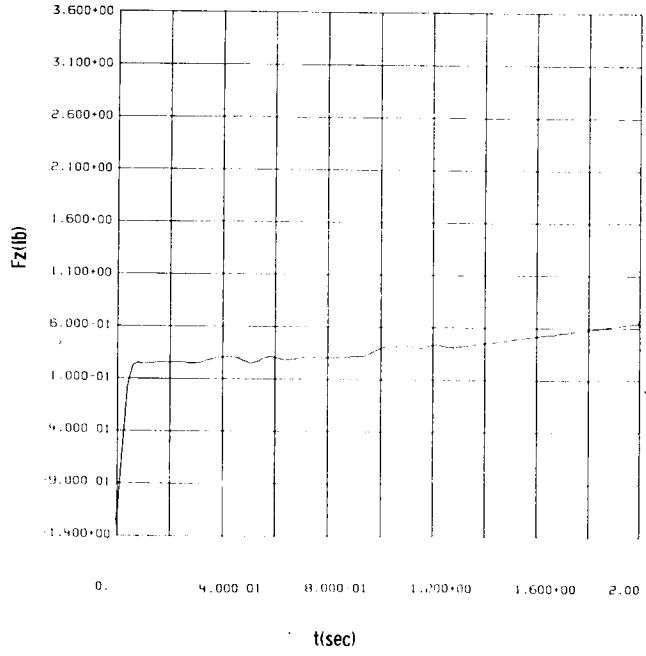

Test 22 - small tank ; 50 % fill ; ϕx= 45° ; Aa= 0.074

Figure B-11

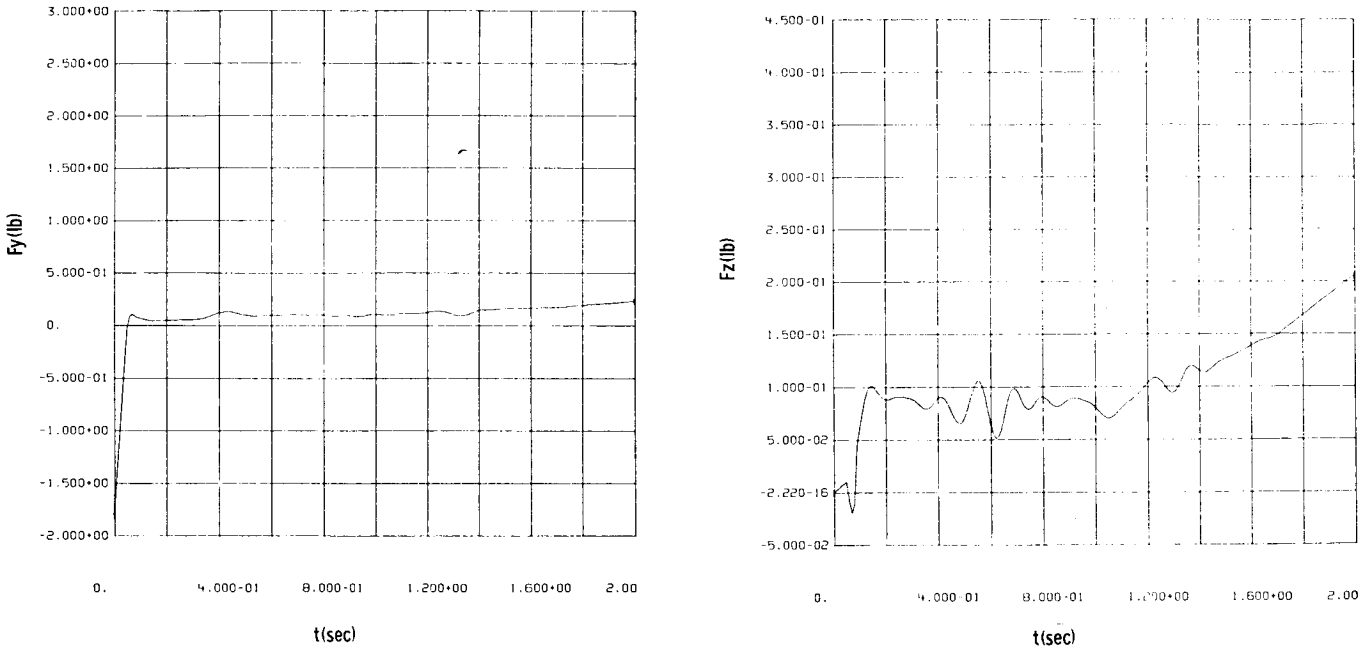

Test 23 - small tank ; 50 % fill ; $\theta x = 90^{\circ}$; Aa= 0.072

Figure B-12

TABLE B-1. AXIAL AND LATERAL ACCELERATION TABLE

TEST #	TANK CONFIGURATION	θX (DEG)	% FILL	TIME (SEC)	AZI (IN/SEC^2)	AYI (IN/SEC^2)
1	Baseline	0.0	25.	0.0	386.04	0.0
				0.07	-33.20	0.0
				1.64	-33.20	0.0
2	Baseline	45.0	25.	0.0	386.04	0.0
				0.08	-32.25	0.0
				1.66	-32.25	0.0
3	Baffled	0.0	10.	0.0	386.04	9.72
				0.08	-32.25	9.72
				1.66	-32.25	9.72
4	Baffled	45.0	10.	0.0	386.04	10.12
				0.07	-31.79	10.12
				1.67	-31.79	10.12
5		90.0	10.	0.0	386.04	10.39
				0.09	-30.89	10.39
				1.69	-30.89	10.39
6		0.0	25.	0.0	386.04	10.43
				0.09	-28.38	10.43
				1.75	-28.38	10.43
7		45.0	25.	0.0	386.04	9.91
				0.07	-28.78	9.91
				1.74	-28.78	9.91
8		90.0	25.	0.0	386.04	7.78
				0.08	-28.98	7.78
				1.735	-28.98	7.78
9		0.0	50.	0.0	386.04	7.931
				0.08	-27.68	7.931
				1.768	-27.68	7.931

TABLE B-1. (continued)

TEST #	TANK CONFIGURATION	θX (DEG)	% FILL	TIME (SEC)	AZI (IN/SEC^2)	AYI (IN/SEC^2)
10	Baffled	45.0	50.	0.0	386.04	6.53
				0.07	-27.99	6.53
				1.76	-27.99	6.53
11		90.0	50.	0.0	386.04	7.87
				0.07	-26.12	7.87
				1.81	-26.12	7.87
12		45.0	10.	0.0	386.04	8.73
				0.06	-16.40	8.73
				2.05	-16.40	8.73
13		45.0	25.	0.0	386.04	7.24
				0.08	-16.21	7.24
				2.06	-16.21	7.24
14		45.0	50.	0.0	386.04	7.77
				0.07	-16.40	7.77
				2.05	-16.40	7.77
15	Small	0.0	25.	0.0	386.04	10.34
				0.07	-28.78	10.34
				1.74	-28.78	10.34
16		45.0	25.	0.0	386.04	8.990
				0.08	-28.71	8.990
				1.742	-28.71	8.990
17		0.0	50.	0.0	386.04	8.051
				0.07	-28.585	8.051
				1.745	-28.585	8.051
18		45.0	50.	0.0	386.04	8.63
				0.08	-28.386	8.63
				1.750	-28.386	8.63

TABLE B-1. (continued)

TEST #	TANK CONFIGURATION	θX (DEG)	% FILL	TIME (SEC)	AZI (IN/SEC^2)	AYI (IN/SEC^2)
19	Small	45.0	25.	0.0	386.04	8.50
				0.06	-16.498	8.50
				2.045	-16.498	8.50
20		45.0	50.	0.0	386.04	8.52
				0.07	-16.595	8.52
				2.040	-16.595	8.52
21		45.0	25.	0.0	386.04	20.96
				0.08	- 28.386	20.96
				1.28	- 28.386	20.96
22		45.0	50.	0.0	386.04	21.12
				0.08	- 28.386	21.12
				1.295	- 28.386	21.12
23		90.0	25.	0.0	386.04	7.96
				0.08	-27.606	7.96
				1.77	-27.606	7.96